수의학박사학위논문

Morphological Feature of a Novel Tissue, Primo-Vascular System

최근 발견된 조직인 프리모순환계통의
형태학적 특성

2017년 2월

서울대학교 대학원
수의학과 수의생명과학 전공
(수의약리학)
임 채 정

Doctoral Thesis

Morphological Features of a Novel Tissue, Primo-Vascular System

Chae Jeong Lim

Academic advisor: Pan Dong Ryu, D.V.M, Ph.D

Graduate School

Seoul National University

February 2017

ABSTRACT

The primo-vascular system (PVS) is a newly identified vascular network that was first reported in the 1960s by Bong-Han Kim, who claimed that the PVS corresponds to classical acupuncture meridians. The PVS has been observed in various tissues mainly in laboratory animals; however, its detailed structures, functions, and relations to the acupuncture meridians are not yet well understood. In this study, I have investigated the gross morphological and cytological properties of the organ surface PVS (osPVS) and subcutaneous PVS (scPVS) of rat abdomen by staining the PVS with various dyes including Hemacolor, trypan blue, toluidine blue, and acridine orange.

The major findings of this study are as follows: (1) osPVS, which consists of primo-node (PN) and primo-vessel (PV), has an inner space ductule (20–50 μm) and a unique cellular composition (90.3%, white blood cells; 5.9%, red blood cells; 3.8%, mast cells); (2) scPVS is present in the abdominal subcutaneous tissue, as revealed by Hemacolor staining, and has major characteristics in common with the osPVS in terms of morphology and cellular/structural feature; (3) The distribution and the high density of mast cells in scPVS are closely related with acupuncture meridian and its acupoints (i.e., conception vessel meridian); (4) the extracellular matrix of os- and scPVS revealed extensive fibers and microparticles (0.5–2 μm) covered with nanoparticles (10–100 nm) in a markedly different manner from those of the lymphatic vessels; (5) osPVS had increased size (2.1-times), number per rat

(2.2-times), and ratio of immature red blood cells (2.1-times) in heart failure rats compared to Sham rats, indicating the occurrence of erythropoiesis in the osPVS tissue.

Taken together, the results showed the usefulness of Hemacolor staining on the PVS study, the identification of scPVS and its relation with the acupuncture meridians, the ultrastructural properties of os- and scPVS different from lymphatic vessels, and its potential function as a hematopoietic organ of osPVS. These new findings will help to identify various PVS types in the body and further elucidate their pathophysiological roles in healthy and diseased states.

Keyword: Hemacolor staining, subcutaneous tissue layer, mast cell, red blood cell, extracellular matrix, heart failure, hematopoiesis

Student Number: 2010-21651

CONTENTS

LIST OF FIGURES AND TABLES

BACKGROUND

CHAPTER I

CHAPTER II

CHAPTER III

CHAPTER IV

ABBREVIATIONS

PVS	Primo-vascular system
PN	Primo-node
PV	Primo-vessel
H&E	Hematoxylin and eosin
osPVS	Organ surface primo-vascular system
scPVS	Subcutaneous primo-vascular system
scPN	Subcutaneous primo-node
scPV	Subcutaneous primo-vessel
WBC	White blood cell
RBC	Red blood cell
MC	Mast cell
CLSM	Confocal laser scanning microscopy
EM	Electron microscopy
SEM	Scanning electron microscopy
TEM	Transmission electron microscopy
CV	Conception vessel
ECM	Extracellular matrix
HF	Heart failure

BACKGROUND

1. Discovery of the Bonghan system

A novel vascular tissue was first claimed in 1962 by Bong-Han (BH) Kim that corresponded with the anatomical entity of the ancient acupuncture meridians (Kim, 1962). The tissue was named the Bonghan system (BHS), and was composed of Bonghan ducts (BHD) and Bonghan corpuscles (BHC) containing Bonghan liquor. Kim reported a series of research articles on the relation between BHS and the acupuncture meridians (Kim, 1962; Kim, 1963; Kim, 1965a; Kim, 1965b). The BHD compose a bundle structure comprised of several subducts (Figure 1A). Kim reported that the BHS existed throughout the entire body, including in the superficial layer of the skin, on the surfaces of abdominal organs, and inside the blood and lymphatic vessels (Kim, 1963) (Figure 1B). Kim claimed that the intravascular BHS functions as a hematopoietic organ (Kim, 1965a; Kim, 1965b). Additionally, Kim claimed that "sanal" (Bonghan microcell of 1–2 μm size), which circulated through the Bonghan liquor in BHS, played an important role in the regeneration of damaged tissues (Kim, 1965b; Soh, 2009) (Figure 1C). However, Kim's findings have not been reproduced until recently, mainly because the detailed experimental methods and materials were not available.

2. Rediscovery of Bonghan system (primo-vascular system)

In the early 2000s, Dr. Soh's group rediscovered part of the Kim's findings

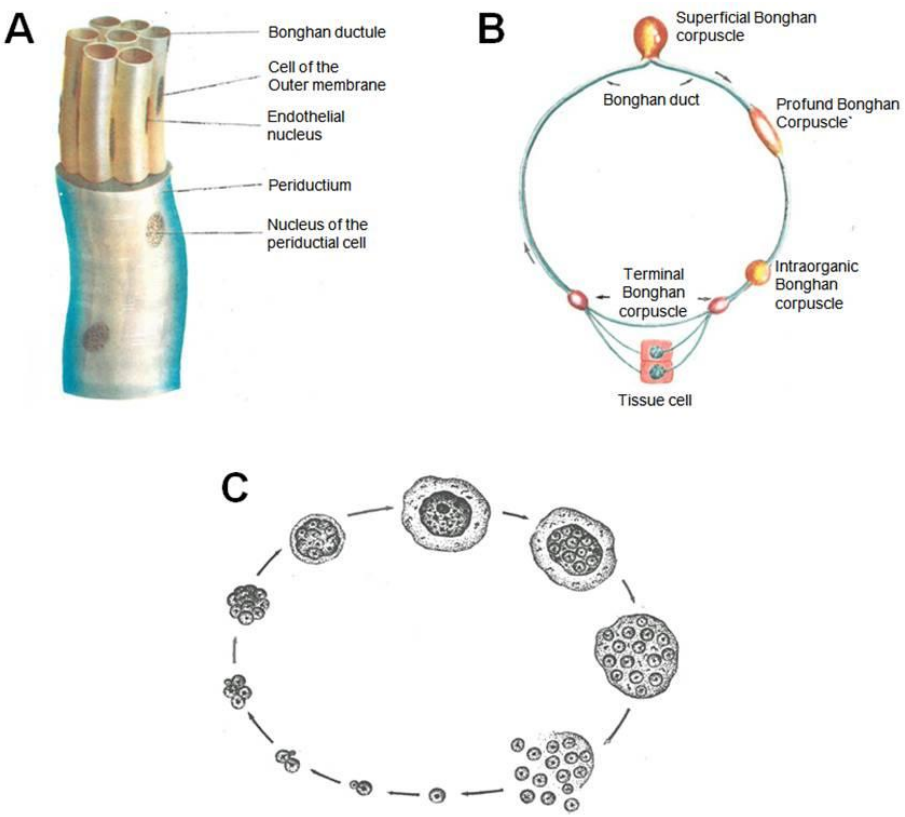

Figure 1. Schematic diagram of the Bonghan system and sanal. (A) A Bonghan duct consisting of a bundle of several small subducts. **(B)** The circulatory Bonghan system. **(C)** Bonghan sanal-cell cycle. (Kim et al, 1965a).

Table 1. Flow of various studies on the primo-vascular system

Year	Species	Methods	Findings	References
2004	Rat	Acridine orange staining	PVS inside a blood vessel	Lee et al., 2004
2005	Rabbit	Feulgen reaction	PVS on the abdominal organ	Shin et al., 2005
2006	Rat	Alcian blue staining	PVS inside a lymphatic vessel	Lee et al., 2006
2009	Rat	TEM	Primo-microcells	Baik et al., 2009
2010	Mice	Trypan blue staining	PVS around tumor nodules	Yoo et al., 2010
2012	Rat	Alcian blue staining	PVS above the pia mater of brain and spine	Lee et al., 2012
2014	Human	Trypan blue staining	PVS inside blood vessel in the placenta	Lee et al., 2014a
2014	Mice	SEM, TEM, and immunostaining	Stem cells in PVS	Lee et al., 2014
2015	Rat	Hemacolor staining	PVS in the abdominal subcutaneous tissue	Lim et al., 2015
2016	Rat	Fluorescent nanoparticles	PVS in the abdominal wall	Jang et al., 2016

using special dyes such as trypan blue (Lee et al., 2009b; Lee et al., 2010), alcian blue (Lee et al., 2006; Yoo et al., 2008), and acridine orange (Lee et al., 2004) to visualize the BHS, and it was subsequently renamed the primo-vascular system (PVS). The PVS has been observed in several animal species, including rats, rabbits, and pigs (Jia et al., 2011; Moon et al., 2012). It has also been consistently identified in various sites including the serosal surfaces of the internal organs (i.e., large intestine, small intestine, and liver) in the peritoneal cavity (Shin et al., 2005), inside the vascular and lymphatic vessels ((Lee et al., 2006; Yoo et al., 2008), and in the central nervous systems including in brain ventricles (Moon et al., 2013) and the spinal cord (Lim et al., 2011) (Table 1). Among these sites, the organ surface PVS (osPVS) has been often used as a specimen for various studies, as it is semitransparent, freely movable, and relatively easy to recognize with careful gross examination without staining (Lim et al., 2013).

3. Properties of the primo-vascular system

The biggest difficulty in the current PVS studies is that there are no biomarkers (i.e., antibodies) with which to specify PVS tissue. Therefore, as a second-best solution, establishing reliable criteria for the identification of the PVS is required. Reliable criteria for the identification of PVS could be summarized as follows based on the previous studies. First, the PVS primarily consists of vessel parts and node parts, and the vessels are often sub-branched from each node (Shin et al., 2005; Soh, 2009). Second, endothelial cells with rod-shaped

nuclei (revealed by DNA-specific fluorescent staining) are distributed in a linearly aligned manner along the longitudinal axis of the PVS (Lee et al., 2004; Yoo et al., 2008). Third, the PVS contains various immune cells, including mast cells (MCs, majority) and white blood cells (WBCs), such as eosinophils, neutrophils, lymphocytes, and monocytes (Kwon et al., 2012; Lee et al., 2007). Fourth, the PVS is composed of a bundled structure of several small subducts or ductules that contain immune cells, which is morphologically different from that of the lymphatic vessel with a single lumen (Kwon et al., 2012; Shin et al., 2005).

4. Purposes

According to BH Kim, PVS has the anatomical structure of the acupuncture meridian, and plays a role in hematopoiesis (Kim et al., 1963; Kim et al., 1965b). Current studies have mainly confirmed the presence of the PVS tissue; however, Kim's claim regarding the function of PVS remained unknown. In addition, easy methods for identification of PVS are not well studied.

Thus, I studied: 1) to test Hemacolor regents, a simple and rapid staining system used in hematology and clinical cytology to determine whether the staining can suit PVS studies (Chapter I); 2) the PVS in the skin or hypodermis, where the putative acupoints are located, and its correlations with the acupuncture meridians (Chapter II); 3) the ultrastructural features of PVS at the extracellular matrix level according to electron microscopy (Chapter III); the potential erythropoiesis in the PVS from rats with heart failure (Chapter IV).

CHAPTER I

Gross morphological features of the organ surface primo-vascular system revealed by Hemacolor staining

ABSTRACT

The primo-vascular system (PVS), which consists of primo-vessels (PVs) and primo-nodes (PNs), is a novel thread-like structure identified in many animal species. Various observational methods have been used to clarify its anatomical properties. Here, I used Hemacolor staining to examine the gross morphology of organ surface PVS in rats. I observed a sinus structure (20–50 μm) with a remarkably low cellularity within PNs and PVs, and several lines of ductules (3–5 μm) filled with single cells or granules (~1 μm) in PV. Both sinuses and ductules were linearly aligned along the longitudinal axis of the PVS. Such morphology of the PVS was further confirmed by acridine orange staining. In PN slices, there was a honeycomb-like structure containing the granules with pentagonal lumens (~10 μm). Both PVs and PNs were densely filled with WBCs, RBCs and putative mast cells (MCs), which were 90.3%, 5.9%, and 3.8% of the cell population, respectively. Granules in putative MCs showed spontaneous vibrating movements. In conclusion, the results show that Hemacolor, a simple and rapid staining system, can reveal the gross morphological features reported previously. These findings may help to elucidate the structure and function of the PVS in normal and disease states in future studies.

INTRODUCTION

The primo-vascular system (PVS) is a novel anatomical network and new circulatory system. In the 1960s, Bong-Han Kim claimed that the PVS represented the meridian system and acupuncture points (Kim, 1963). However, studies on the PVS have long been hampered because their isolation and identification have not been feasible. Recently, Dr. Soh's group developed several techniques for detecting a PVS and characterized the distribution, structures, and functions of the PVS (Soh, 2009; Stefanov et al., 2012).

The PVS has been observed in small laboratory animals, such as mice, rats, and rabbits (Jia et al., 2011). It has been consistently identified in various tissues including the surfaces of internal organs (Choi et al., 2011; Han et al., 2010a; Lee et al., 2009a; Shin et al., 2005), blood vessels (Lee et al., 2004; Yoo et al., 2008), and lymphatic vessels (Lee et al., 2006) using special dyes, such as trypan blue (Lee et al., 2009b; Lee et al., 2010), acridine orange (Lee et al., 2004), and alcian blue (Lee et al., 2006; Yoo et al., 2008). The organ surface PVS has been primarily used in various PVS studies, as it is semitransparent, freely movable, and relatively easy to recognize with careful gross examination.

A bundle structure composed of several subducts (~10 μm) and sinuses of various diameters in primo-vessels (PVs) were revealed by various electron microscopic studies (Lee et al., 2007). Follicle-like formations containing clusters of immune cells and several small channels or ductules (7–15 μm) were observed inside or near the formation in primo-nodes (PNs) (Ogay et al., 2009a).

In addition, a bundle structure of several ductules (10–20 μm) exhibiting characteristic rod-shaped in whole PVs and a tissue formation containing several lumen (6–10 μm) were showed in cross-sections of PVs (Ogay et al., 2009a).

At the cellular level, the PVS contains various types of immune cells, such as macrophages, mast cells (MCs), and eosinophils, which implies the system's potential role in immune responses (Kwon et al., 2012; Lee et al., 2007; Ogay et al., 2009a; Sung et al., 2010). In addition, PVS cells have been categorized into four major types based on current-voltage (I-V) relations recorded from the cells in PN slices (Choi et al., 2011). Some PVS cells are much larger and rounder (10–20 μm) with granules, whereas others are much smaller and rounder or appear similar to red blood cells (RBCs) (Choi et al., 2011; Lee et al., 2004).

In previous studies, diverse staining methods and light and electron microscopy (EM) have been used to identify the PVS and characterize its structure (Soh, 2009). For example, trypan blue has been used to detect the PVS *in situ* (Lee et al., 2009; Lee et al., 2010). Various DNA-specific staining dyes and confocal laser scanning microscopy (CLSM) analysis have been used to identify rod-shaped nuclei, the hallmark of PVs (Lee et al., 2006; Soh, 2009). Hematoxylin and eosin (H&E) staining has been mainly used for PVS cytology (Ogay et al., 2009), whereas EM has been used for the ultrastructural characterization of the PVS (i.e., ductules, bundle structure) (Lee et al., 2007; Ogay et al., 2009a). However, trypan blue staining is limited in elucidating the

cytology and anatomical structure in the PVS although it is simple to use. In addition, long processing times (about 24 hours) and/or sophisticated instruments like EM and CLSM are needed in the other methods. Thus, it would be desirable to determine rapid and simple methods to identify and morphologically characterize the PVS. In this study, I tested Hemacolor reagents, a rapid staining system used in hematology and clinical cytology (Keisari, 1992; Walter et al., 2011), to determine whether the staining can be suitable for PVS studies, in combination with a recently developed PVS slice preparation technique (Choi et al., 2011; Han et al., 2010a).

MATERIALS AND METHODS

Isolation of organ surface PVS

Male Sprague-Dawley rats weighing 282 ± 13 g (n = 23; Orient Bio Inc., Gyeonggi-do, Korea) were housed in a temperature-controlled environment (20–26 °C) with a relative humidity range of 40–70% under a 12 h light/dark cycle; they received water and standard rodent chow *ad libitum*. All animal experiments were carried out in accordance with the guidelines of the Laboratory Animal Care Advisory Committee of Seoul National University. The rats were anesthetized with an anesthetic cocktail (Zoletil, 25 mg/kg; xylazine, 10 mg/kg) administered by intramuscular injection. The abdomen of each rat was incised, and the PVS was sampled under a stereomicroscope (OSM-1, Dongwon, Korea) from the surface of the abdominal organs, according to the methods reported previously (Lee et al., 2009; Shin et al., 2005). Briefly, I identified the organ surface PVS tissue based on established standard: milky-colored, semitransparent, and slightly flexible tissue composed of nodes and vessels.

PVS slice preparation

I prepared the PVS slices according to the published protocol (Choi et al., 2011; Han et al., 2010a). Briefly, the intact PVS tissues that were isolated from the surface of internal organs were taken in a Ca^{2+} -free Krebs solution supplied

with O_2 (95%)-CO_2 (5%) and maintained in an ice-cooled Krebs solution (0–4 °C). Meanwhile, 4% low-melting agarose (Lonza, Rockland, ME, USA) dissolved at 70 °C was poured into a cubic frame (25 × 25 × 25 mm). When the agarose solution was chilled to 34–37 °C, the PVS was embedded into the frame and then cooled on ice until the viscous solution was completely solidified. The agarose block was then taken out of the frame and firmly affixed to the bottom of a slicing chamber using instant glue before it was sectioned at a thickness of 200 μm using vibrating microtome (1000 Plus, Vibratome, St. Louis, MO, USA). The resulting slice were incubated for 20–30 min in the oxygenated Krebs solution composed of (in mM) NaCl (120.35), $NaHCO_3$ (15.5), glucose (11.5), KCl (5.9), $CaCl_2$ (2.5), NaH_2PO_4 (1.2), and $MgSO_4$ (1.2) followed by staining at 31 °C (Spencer et al., 2005).

Staining methods for the identification of PVS cells

Hemacolor staining, a system of three solutions (solution 1, methanol fixative; solution 2, eosin stain; solution 3, methylene blue stain), was performed for the rapid cellular identification of PVS cell's WBCs and RBCs. The overall staining procedure of the PVS is as follows: either a PVS slice (200 μm) or the whole PVS tissue was transferred into a drop of Hank's balanced salt solution (HBSS; Sigma, St. Louis, MO, USA) on slide glass and air-dried completely without water for 1–3 min. The slide glass was then dipped into and taken out of the solution 1 ten times for 10 sec. This staining process was repeated for solution 2 and 3 and completed within 30 sec. Each stained PVS sample was

kept in a drop of phosphate buffer solution (pH 7.2) for 20 sec, dipped into a distilled water three times for 10 sec, completely air-dried for 3–5 min, and then mounted with Canada balsam (Sigma). Using a stereomicroscope, low (100x and 200x) and high (1000x) magnification digital images were obtained from the Hemacolor-stained PVS cells. I took the pictures of the PVS tissues containing a micromeasure with a minimal unit of 0.01 mm and measured the luminal diameter of the tissues from the digital images. H&E staining, a method widely used for the morphological evaluation of various tissue types, was carried out to confirm the cellular composition of PVS cells and to determine their relative abundance. The PVS tissue was initially fixed overnight in 10% neutral buffered formalin routinely processed, embedded in paraffin, and cross-sectioned at 3 μm. The resulting PVS sections were stained with H&E as a part of the routine intake procedure. To identify DNA and RNA components in the PVS cells, each PVS sample was stained with 0.1% acridine orange solution for 15 min and then observed under a confocal laser scanning microscope (CLSM; LSM710, Carl Zeiss, Germany) in line with wavelengths excitation and the emission of acridine orange (Darzynkiewicz et al., 1987; Lee et al., 2004; Okuthe, 2013). To stain mast cells (MCs) in the PVS, the sample was stained with 1% toluidine blue solution for 3 min (Cerri et al., 2010).

Mechanical separation and isolation of single PVS cells

For the cytological evaluation of the cellular component in the PVS, single PVS cells were prepared from intact PVS tissues as well as PVS slices on a slide

glass by sprinkling the Krebs solution using a 1 mL syringe. Here, the motive power of isolating the PVS cells is solely the impact by the Krebs droplet, and trituration action was not applied to the PVS samples. The isolated cells were transferred to a slide glass followed by staining with Hemacolor in accordance with the procedure described above.

Digital video recording of putative MC movement of the PVS

One of the PVS slices in the incubation chamber was transferred to a recording chamber (0.7 mL) and was fixed with a grid of nylon threads supported by a donut-shaped silver wire weight while being perfused (3 mL/min) with oxygenated Krebs solution at 30–33 ℃ (Choi et al., 2011; Han et al., 2010a). The movement of putative MC granules was observed by light microscope with differential interference contrast (BX50WI, Olympus, Tokyo, Japan) and recorded by a USB digital CCD camera series 150III.

PVS cell counting and data analysis

To determine the cellular composition of the PVS, individual PVS cells were counted from 25 rectangular fields (125 × 95 μm) in the images of H&E-stained PVS slices at 1000x magnification. Caution is needed when selecting these sample areas because H&E-stained PVS slices (3 μm in thickness) are very thin, and there may be some areas without cells in the edges of the slices. Considering this fact, I consistently avoided parts without cells in the PVS slices and selected only the fields filled with WBCs, RBCs, and putative MCs.

Thus, I selected the representative PVS fields that showed uniform distribution of various cells. The sizes of PNs, PVs, and individual cells were measured using imageJ software (developed at the US National Institute of Health). All the data values were expressed as mean ± standard errors, and the number of specimens or cells was represented by *n*.

RESULTS

General characteristics

The results of this study were obtained from the evaluation of the 33 organ surface PVS tissues from 23 rats. The PNs were collected mainly from the serosal surface of the small and large intestines (58.1%), and liver (35.5%) with or without PVs attached. Figure 1A shows a representative PVS tissue on the surface of the small intestine composed of two PNs connected by a PV of typical size. Figure 1B shows another example of PVS on the surface of the liver with an enlarged PN, which was even thicker than that of normal PNs. The average size of PNs was 1.26 ± 0.11 mm (major axis, 0.52–2.57 mm) and 0.73 ± 0.06 mm (minor axis, 0.34–1.50 mm, n = 27), and the average thickness of PVs was 0.25 ± 0.03 mm (n = 19).

Hemacolor staining of the whole PVS

To visualize the cells in the PVS, I stained the PVS with Hemacolor, a rapid staining dye widely used in hematology and clinical cytology (Keisari et al., 1992; Walter et al., 2011). In this study, PVS cells stained by Hemacolor refer to the cells within the inside of the walls of the cells, such as WBCs, RBCS, and MCs, and do not include the cells that compose the cell walls of the PVS. Figure 2A shows a PVS sample isolated from the surface of internal organ in Krebs solution for staining. Figure 2B is a representative stereoscopic image of

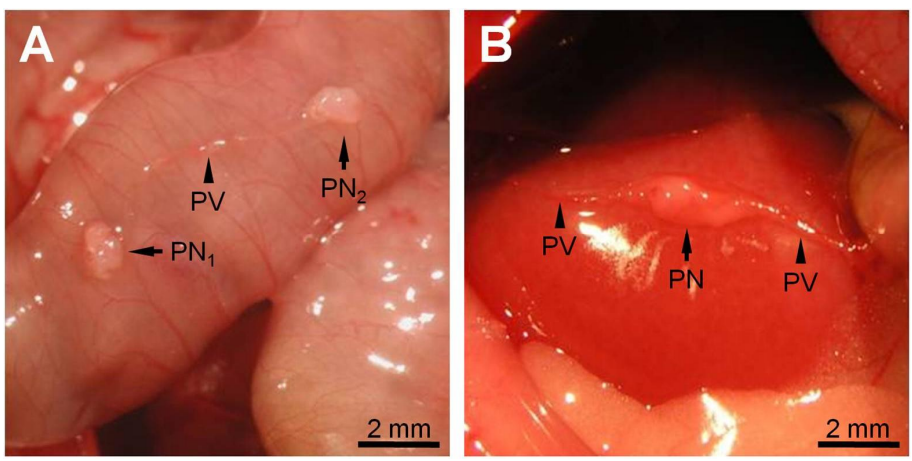

Figure 1. Intact PVS tissue identified on the surface of the abdominal organs in rat. (A) Representative example of a PVS tissue composed of two PNs (arrows) and a PV (arrowhead) on the surface of the small intestine (PN_1, 1.22 × 0.86 mm; PN_2, 1.17 × 0.77 mm; PV, 0.19 mm). **(B)** PVS tissue composed of an enlarged PN (arrow) and a typical PV (arrowheads) on the surface of the liver (PN, 2.57 × 1.11 mm; PV, 0.17 mm).

the whole PVS stained with Hemacolor. The outer parts of the PNs and PVs were densely filled with cells, but the inner parts appearing as a white space (circles in Figure 2B) were filled with little cells. The inner space showing low cellularity was continuous along the longitudinal axis of the PVS and had various luminal diameters depending on the location in the PVS. In general, the diameter of the space in PNs was larger than in PVs (30–50 vs. 20–30 μm), and there were two spaces in PNs (circles of PN_1 and PN_2 in Figure 2B). The inner space could be identified by its different cellular composition and high number of granules (Figures 2E and 2F). Hemacolor-stained PVS cells were classified into the following three major groups based on their morphological properties: small round cells (majority), large granular cells, and small yellowish cells. The PN and PV cells differed, in that the PN cells were mostly round in shape and were distributed uniformly and randomly (Figure 2C). However, most PV cells, including large granular cells and small round cells were elliptical, and were arranged in parallel along with longitudinal axes of the PVs (Bottom inset in Figure 2B and Figure 2D). In PVs, the staining properties of three major cell types are similar to those in PNs. The major cells of the PVS were also located in the inner space within PVs (Figure 2E). In particular, there were a number of granules (~1 μm in diameter) in the inner space within PVs (Figure 2F).

To further confirm the morphological features of whole PVS tissue, I stained the tissue sample with acridine orange, which is DNA (green staining) and RNA (red staining)-specific dye (Darzynkiewicz et al., 1987; Okuthe, 2013), under a similar experimental condition to that in Figure 2. The cellular morphology observed in acridine orange-stained PVS tissue is similar to that

Figure 2. Images of the whole tissue and cells of the PVS stained by Hemacolor. (A) The unstained whole PVS sample in Krebs solution. **(B)** Typical unsectioned longitudinal image of a whole PVS tissue composed of PNs and a PV. Note the continuous inner space structures (circles) along the longitudinal axis of the PVS. There are two spaces (circles, PN_1, 30–50 μm; PN_2, 10–50 μm) in the PNs and one space (circle, bottom inset, 20–30 μm) in the PV. PVS cells at the edges were more abundant than in the middle of the PV. **(C)** Distribution of the cells in the inner region (marked as "(C)" in (B)) of the PNs. Note that most PN cells (arrow, large granular cells; arrowhead, small round cells) are round, and placed evenly and randomly. **(D)** Distribution of the cells in the inner region (marked as "(D)" in (B)) of the PV. Note that most PV cells (arrow, large granular cells; arrowhead, small round cells) are elliptical and horizontally arranged along the long axis of the PV. **(E and F)** Distribution of the cells in the inner spaces (marked as "(E)" and "(F)" in (B)) of the PV. Note that the inner space (arrows) also contains numerous PVS cells (arrowhead, small round cells; open arrowhead, small yellowish cells; dotted circle, granules).

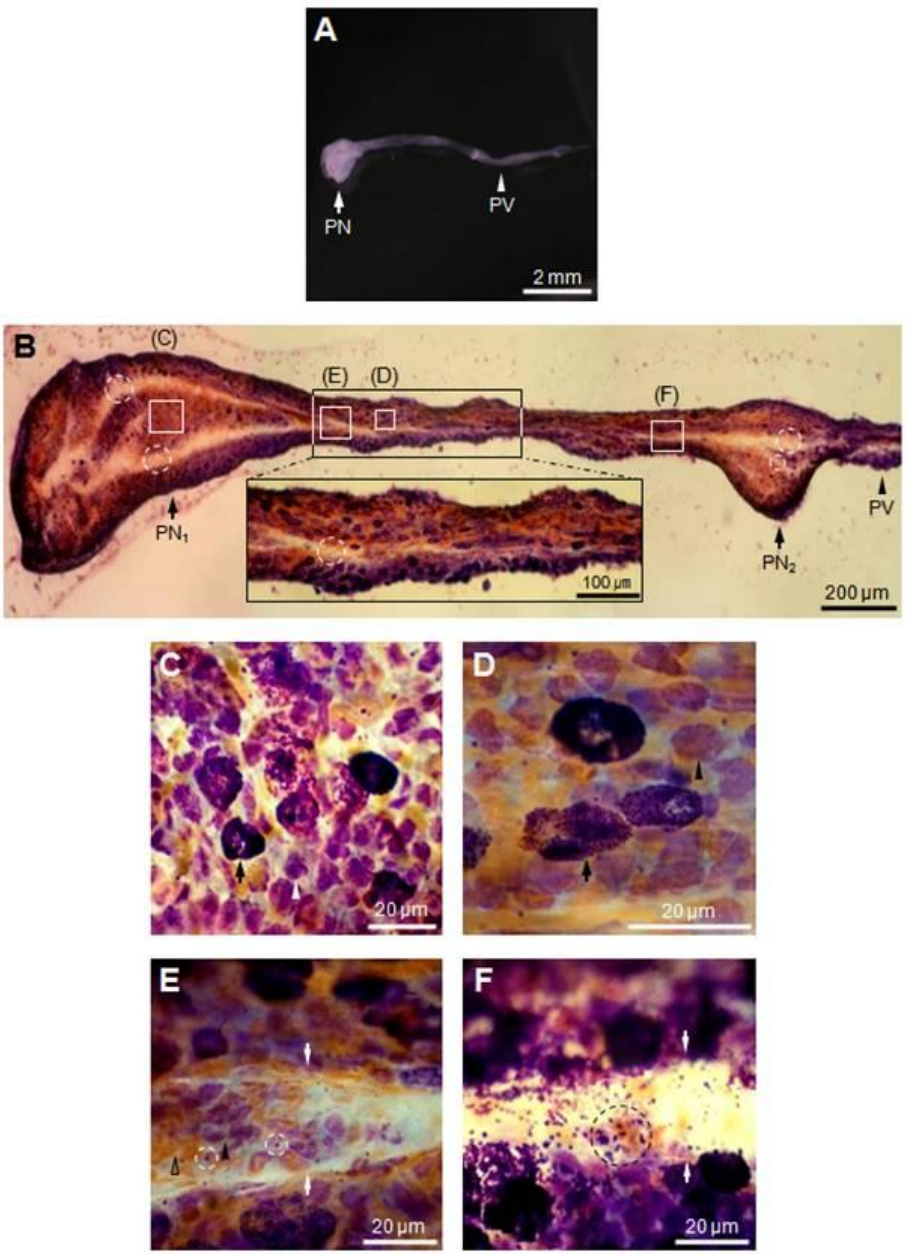
A
PN
PV
2 mm
B
(C)
(E)
(D)
(F)
PN1
PV
PN2
100 µm
200 µm
C
20 µm
D
20 µm
E
20 µm
F
20 µm

obtained using Hemacolor staining. Most PV cells were stained green as shown in Figure 3A, and arranged in parallel along the longitudinal axis of the PV (Bottom inset in Figure 3A and Figure 3D), whereas PN cells were distributed randomly (Figures 3B and 3C). Most small round cells were revealed by their green color (denoting DNA) as a results of acridine orange staining, and large granular cells were revealed in green (denoting DNA) and red (denoting RNA) in nuclei and granules, respectively (Figures 3C and 3D) (Darzynkiewicz et al., 1987; Okuthe, 2013). The granules were appeared dark brown at a low magnification (100x) (Figure 3A). As shown in Figures 2E and 2F, the inner space structure of the PV also revealed by acridine orange staining according to depth of optical sectioning (Figure 4).

Figure 5 shows a thin PV (30–40 μm) stained by Hemacolor. As shown in Figure 2, various PVS cells (large granular cells, small round cells, and small yellowish cells) and granules are linearly aligned within the narrow channels (3–5 μm) along the longitudinal axis of the PV.

To further characterize the morphology of the PVS, I stained a cross-section of a PN slice (200 μm) with Hemacolor. In general, the cellular density is higher in the outer part and lower in the inner part of the PN slice as shown in Figure 6A, which is similar to the findings in whole PVS tissue staining (Figure 2B). I observed a honeycomb-like structure in the inner space, and the diameter of the individual lumens in the honeycomb was ~10 μm (Figure 6B). In the honeycomb structure, granules were located within and on the borderline of the each lumen. In addition, all three major cell groups were also found in the outer part of PN slices (Figure 6C). In addition, PNs were sectioned into thin slices

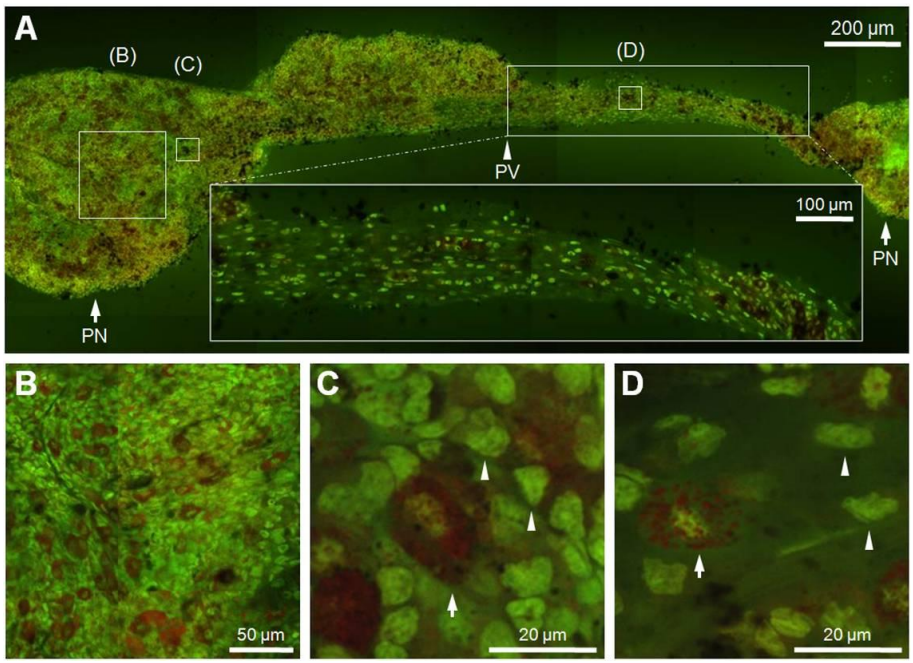

Figure 3. Confocal laser scanning microscopic images of whole PVS tissue and cells stained by acridine orange. (A) Unsectioned longitudinal image of a whole PVS composed of two PNs connected by a PV. Note that the tissue is densely filled with cells stained with green (majority) or dark brown. Some cells are linearly aligned along the longitudinal axis of the PV (bottom inset). **(B)** PN cells with random distribution in the inner region (marked as "(B)" in (A)). **(C and D)** PN and PV cells at a high magnification (400x) (marked as "(C)" and "(D)" in (A)). Note the large cells (arrows) with granules stained red and small round cells (arrowheads) stained green in both the PNs and the PV.

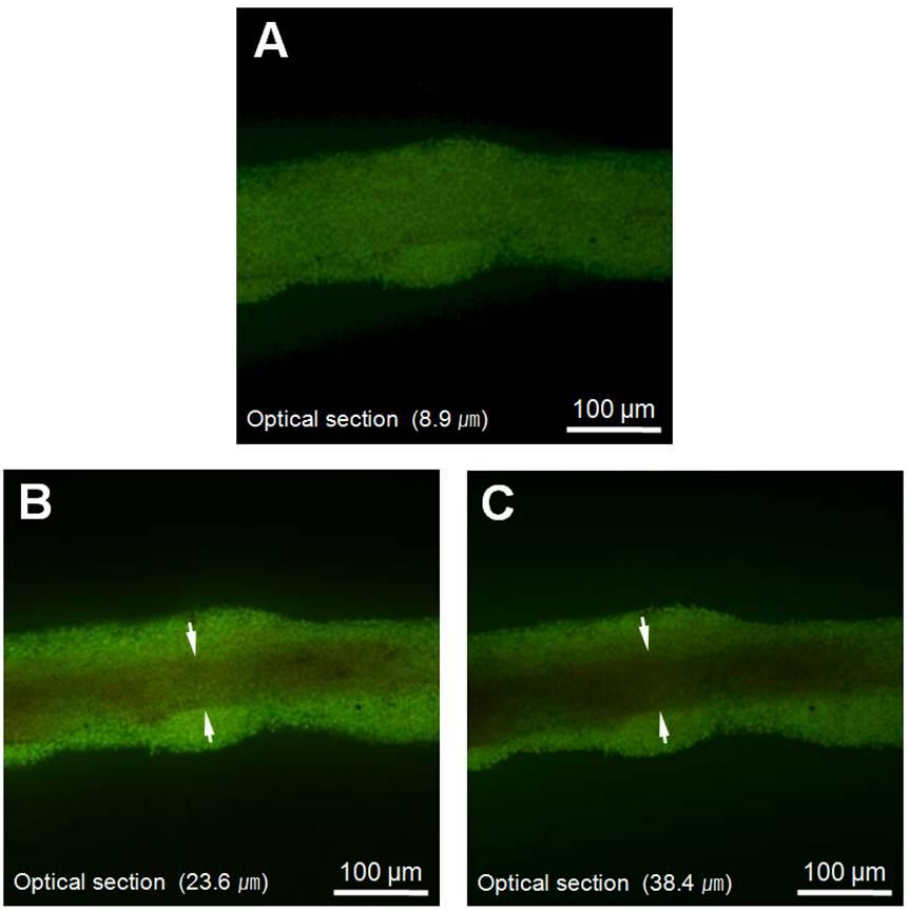

Figure 4. Unsectioned longitudinal confocal laser scanning microscopic image of a whole PV showing an inner space according to depth of optical sectioning. (A) A whole PV stained by acridine orange staining. **(B and C)** The inner space structure (arrows) avoid of cells is become darker with increasing depth of optical section.

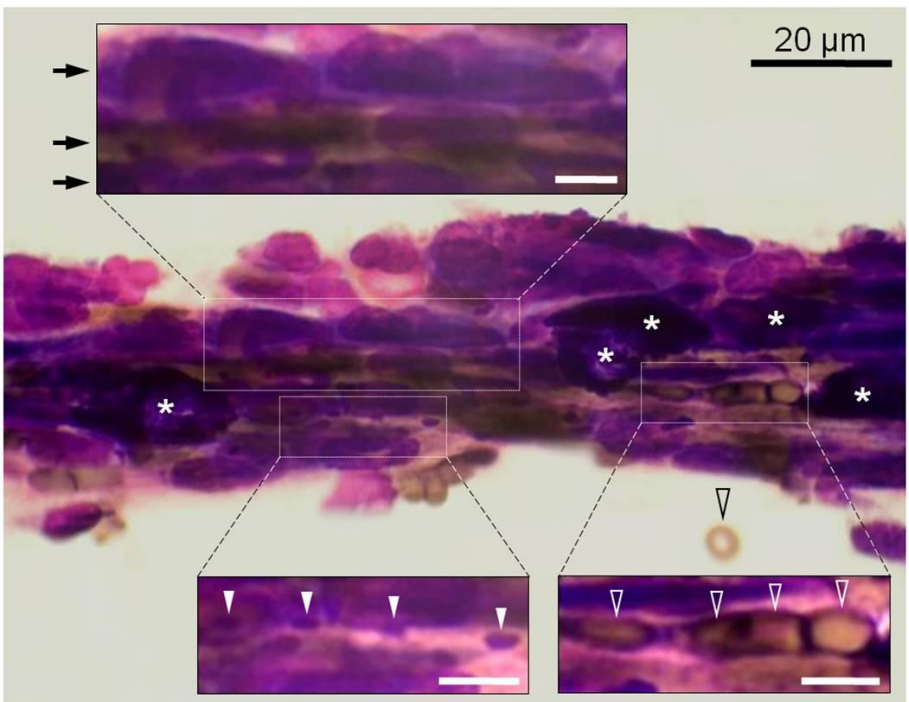

Figure 5. Longitudinal image of a thin PV stained with Hemacolor. Note the multiple linear arrangement of cells (arrows in the top inset), small yellowish cells (open arrowheads in the bottom right inset), granules (arrowheads in the bottom left inset), and large granular cells (asterisks). Scale bars in the insets are 5 µm.

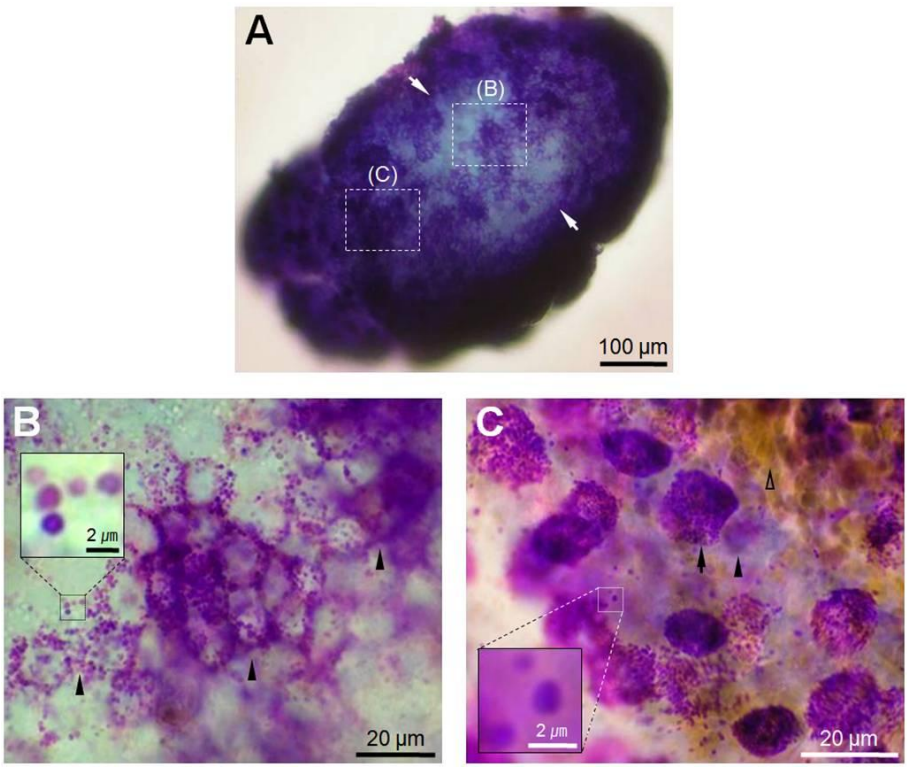

Figure 6. Honeycomb-like structure inside a PN slice (200 µm) stained with Hemacolor. (A) Cross-sectional image of the PN slice showing the inner space structure devoid of cells (arrows). **(B)** The image of the inner space in the PN slice at a higher magnification. Note the honeycomb structure (arrowheads, about 10 µm) and granules (inset) in the structure. **(C)** The image of the outer part of PN slice stained with Hemacolor. Note the large granular cell (arrow), small round cell, small yellowish cell (open arrowhead), and the granules (inset).

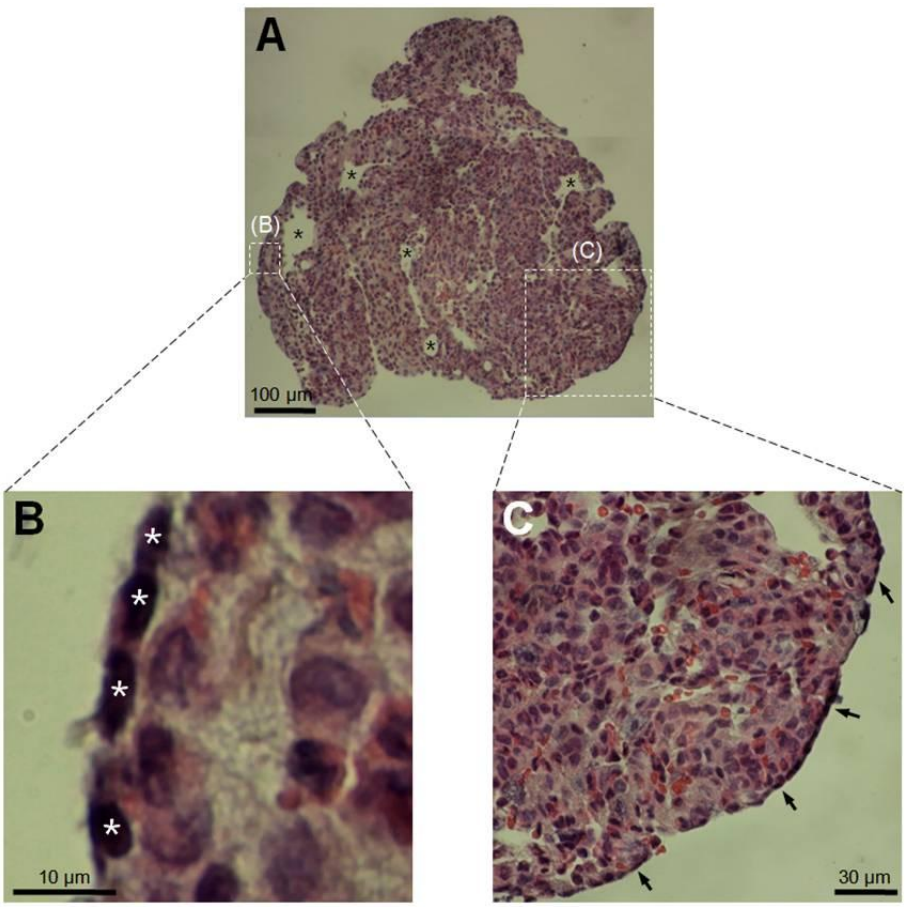

Figure 7. Mesothelial cells inside a PN slice (5 µm) stained with hematoxylin and eosin. (A) Cross-sectional image of the PN slice showing the sinus structures (asterisks). **(B and C)** Magnified views (marked as squares in (B) and (C)) of the PN slice (A). Note that the mesothelial cells (asterisks in (B) and arrows in (C)) are located along the outer surface of the PN slice.

(5 μm) and stained with H&E to identify cells in the outer part of the PN. Figure 7 illustrates that flattened mesothelial cells line the outer surface of the PN slices (5 μm) stained with H&E (Young and Heath, 2002). Several sinus structures (asterisks) were also shown in the PN slices.

Cytomorphology of PVS cells

Figure 8A shows a stereoscopic image of an unstained PN slice at a low magnification. At a higher magnification of the unstained PN slices (Figure 8a), the PNs are densely filled with round cells of various sizes; large round (arrow, 12–20 μm), biconcave (flat) disk-shaped (open arrowhead, 5–7 μm), and small round cells (arrowhead, 8–10 μm). Among these PVS cell groups, the small round cells were the most abundant. They were tightly packed like a cluster of grapes and evenly distributed in the area of the PN slices. Figures 8B and 8b illustrate the three groups of cells in the PN slice stained with H&E. In the Figure 8b, the large round cells were identified as putative MCs (arrow) based on their size and staining pattern in addition to their spherical nuclei and cytoplasm filled with intensely basophilic granules (Ross and Pawlina, 2005). The small round cells stained dark blue and with round to horseshoe-shaped or multilobed nuclei (neutrophils, monocytes, and lymphocytes) were identified as WBC group (Figure 8b, arrowhead). The biconcave-shaped cells without nucleus, yellow-stained cells by Hemacolor, were identified as RBCs (Figure 8b, open arrowhead) (Eroschenko, 2008; Ross and Pawlina, 2005).

The three cell groups in the Hemacolor-stained PN slice (Figures 8C and

Figure 8. Three major groups of PVS cells revealed by various kinds of staining. (A and a) Unstained cross-sectional image of a PN slice with a thickness of 200 μm. Note the PN cells resembling a large round cell (arrow, 12.69 μm), a biconcave (flat)-shaped cell (open arrowhead, 7.42 μm), and a small round cell (arrowhead, 9.42 μm). **(B–E)** Typical cross-sectional images of the PN slice stained by H&E (B), Hemacolor (C), acridine orange (D), and toluidine blue (E). **(b–e)** Three groups of PN cells at a higher magnification displaying putative MCs (arrows), RBCs (open arrowheads), and WBC groups (arrowheads) which correspond to the neutrophils with lobulated nuclei. Note that the Hemacolor-stained PN slice clearly revealed the granules within putative MCs and isolated granules ((c), dotted circle). (D) and (d) are fluorescent microscopic images of acridine orange staining. (A)–(E) and (a)–(e) are images of different PVS tissues photographed at the same magnification. **(F)** Collection of three major groups of cells isolated from PVS tissue stained with Hemacolor. The individual PVS cells shown in ((F)-a_1–a_4) belong to the WBC group. WBC groups are composed of a plasma cell ((F)-a_1)) with eccentrically placed nucleus, lymphocyte ((F)-a_2)) with dense-staining nuclei and sparse cytoplasm, eosinophil ((F)-a_3)) with eosinophilc cytoplasmic granules, and neutrophil ((F)-a_4)) with multilobed nuclei and a lack of stained granules. The cells in ((F)-b) appeared in the group of normal mature RBCs. The cells shown in ((F)-c_1–c_3) are putative MCs (c_1, typical (10–15 μm); c_2, large (> 20 μm); and c_3, elliptical type). **(G)** The cellular composition of the PVS. The PVS cells were counted from 25 fields (125 × 95 μm) in images of H&E staining of PVS (n = 8) at 1000x magnification.

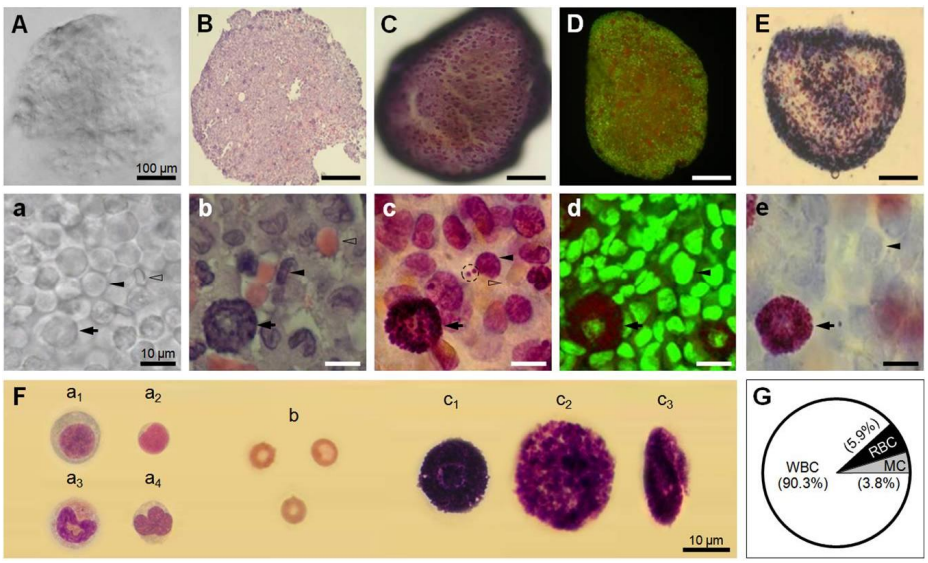
A
100 μm
B
C
D
E
a
10 μm
b
c
d
e
F
a1
a2
a3
a4
b
c1
c2
c3
10 μm
G
(5.9%)
RBC
WBC
(90.3%)
MC
(3.8%)

8c) had a staining pattern similar to those of H&E. In general, most PVS cells stained with Hemacolor were more clearly discernible than those stained with H&E under this experimental conditions. In particular, the images of putative MCs (Figure 8c, arrow) and isolated granules (Figure 8c, dotted circle)) were more sharply visualized by Hemacolor staining. In the case of RBCs, however, H&E showed a staining quality superior to Hemacolor (Figure 8b, open arrowhead).

Acridine orange staining also showed similar cytologic morphology of Hemacolor staining. The nuclei of the majority of WBCs stained by acridine orange were stained green (Denoting DNA; Figure 8d, arrowhead). In the putative MCs, the nuclei were stained green, whereas the granules were stained red (Figure 8, arrow), indicating the presence of DNA and RNA in nuclei and granules, respectively (Darzynkiewicz et al., 1987; Okuthe, 2013). Figures 8E and 8e illustrate the images of a PN slice stained with toluidine blue, which is known as a dye used to stain MCs (Cerri et al., 2010). The granules in these cells showed typical metachromatic staining, indicating that the large granular cells in the PVS were putative MCs.

To further characterize the morphology of single PVS cells, individual cells were isolated from the tissues and stained by Hemacolor. I identified the WBC group of PVS, including the plasma cell (Figure 8F-a_1) with an eccentrically placed nucleus, lymphocyte (Figure 8F-a_2) with dense-staining nuclei and sparse cytoplasm, eosinophil (Figure 8F-a_3) with eosinophilic cytoplasmic granules, neutrophil (Figure 8F-a_4) with multilobed nuclei and a lack of stained granules, and RBC (Figure 8F-b) with non-nucleated red-

staining and typical size (Eroschenko, 2008; Ross and Pawlina, 2005). Putative MC of PVS could be classified into typical (Figure 8F-c_1), large (Figure 8F-c_2), and elliptical types (Figure 8F-c_3) based on their morphological properties. Typical putative MCs had centrally placed nuclei and closely packed granules. As shown in Figure 2B, the elliptical type of putative MCs was more abundantly distributed in PVs than in PNs.

The relative composition of the three groups of PVS cells, determined from the images of H&E staining (Figure 8G), indicated that the proportions of WBCs, RBCs, and putative MCs were 90.3%, 5.9%, and 3.8%, respectively. The average total number of the cells per PVS field (125 × 95 μm) was 167.7 ± 4.12 (158–186) in eight PNs. The numbers of putative MCs, RBCs, and WBCs per field were 6.43 ± 0.89, 11.04 ± 3.23, and 148.81 ± 2.64, respectively.

The identification of putative mast cells and granules of PVS

In this study, putative MCs of the PVS contained granules of about 1 μm (inset in Figure 9A-a_4). The degranulation stage of putative MCs differed from cell to cell (Figure 9A-a_1–a_4). As shown in Figure 2F, the presence of typical putative MCs in the inner space of PVS was low, but degranulating putative MCs and isolated granules facing the inner space of the PVS were more abundant than in the outer area. I also observed that the granules in some putative MCs of the PVS had continuous and spontaneous movements. Degranulation of the putative MC in this study was not artificially triggered, and all occurred spontaneously. Figure 9B illustrates a representative still image of the granules in motion

within a live putative MC. In addition, I found that some of the isolated granules had spontaneous vibrating movements in random directions (Figure 9C). It is interesting that one granule appeared as two divided granules at one moment while moving (Figure 9C-0.6 sec). The average major axis of recorded MCs with vibrating granules were 15.34 ± 1.45 (11.66–20.5 μm). The diameter of the putative MCs containing the granules in motion was also comparable to that of typical MCs stained with dyes as shown in Figure 8F-c_1.

Figure 9. The properties of putative MCs of PVS and granules. (A) Classification of putative MCs of the PVS based on the degranulation condition. Note that the granules from a_1 (typical) to a_4 were increasingly degranulated; the granule size was about 1 μm (inset of a_4). **(B)** Continuous still image of granules in motion inside an MC. Note that arrowheads point to the granule that exhibits spontaneous vibrating movements on the right upper side. **(C)** Continuous still image of a granule with motility. Note that the granule displayed continuous vibrating movements, and appeared as two divided granules for a moment (0.6 sec). This microscopy was performed on a live putative MC without any staining, which is described in the materials and methods section. The crossing points (B) and (C) of the two dotted lines indicate the location of the granule at $t = 0$.

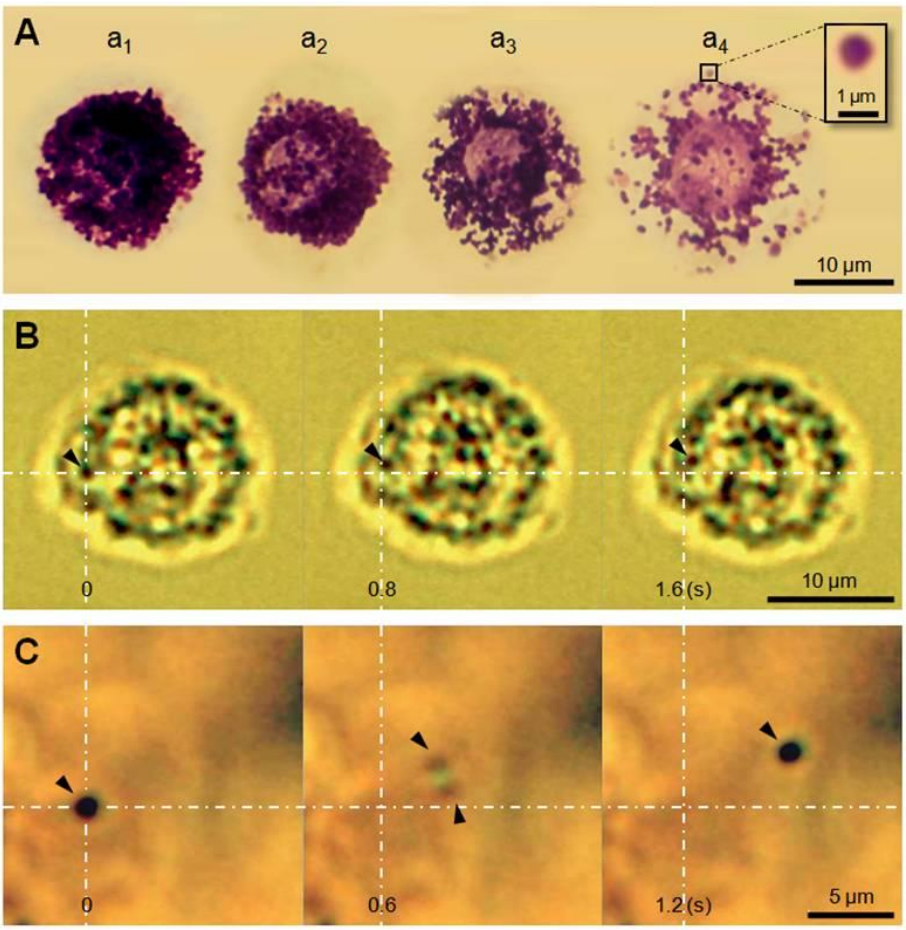
A
a1
a2
a3
a4
1 μm
10 μm
B
0
0.8
1.6 (s)
10 μm
C
0
0.6
1.2 (s)
5 μm

DISCUSSION

In this study, using Hemacolor staining, I confirmed the channel structures composed of a few sinuses (20–50 μm) within PNs and PVs, and several lines of ductules (3–5 μm) filled with single cells or granules (~1 μm) in PVs. In a PN slice, there was a honeycomb-like structure containing granules with pentagonal lumens (~10 μm). At the cellular level, the PVS was densely filled with WBCs (90.3%), RBCs (5.9%), and putative MCs (3.8%). Granules were also found within the putative MCs at various degranulation stages, and some granules showed spontaneous vibrating movements. The results of the present study indicate that Hemacolor is a promising staining system for the rapid identification and characterization of PVS cells and structures.

Hemacolor staining revealed that the PVS had an inner space structure with a lower cellular density. It is unlikely that this is an artifact formed by the slide glass suppressing the round tissue because the tissue was mounted with Canada balsam without pressing. In addition, the inner space was further confirmed by acridine orange staining of whole PV tissue (Figure 4). This inner space contained all three major cell groups of the PVS and granules (Figure 2). In some areas, RBCs and granules are the major contents of the inner space (Figures 2E and 2F). The inner space is similar to the “sinus” reported from previous studies using electron microscopy (Lee et al., 2007; Sung et al., 2008) in that the sinus contained immune cells and granules. The present study newly reveals that the sinuses are continuous inner channels along the PVS that

contain various PVS cells and granules. The detailed structures and functions of the sinuses in the PVS remain to be studied further.

The most salient finding in this study is the characterization of the gross morphology of the PVS using Hemacolor staining. In general, Hemacolor staining has been used to stain and identify blood cells, such as lymphocytes, monocytes, and erythrocytes, in a short time period (Keisari, 1992; Walter et al., 2011). I applied the Hemacolor staining method to the PVS for the first time and determined the most appropriate dying and staining times for the PVS. As a result, I was able to swiftly identify the cellular and structural features of the PVS. The major advantage of Hemacolor staining is that it takes just 5–10 minutes (drying time before staining: 1–3 min; Hemacolor staining for 30 sec; wash out for 30 sec; drying time after staining: 3–5 min) from the moment the whole PVS was sampled from the organ surface to the moment it was microscopically observed. In addition, by using Hemacolor staining in combination with PVS slice preparation, I was able to identify the longitudinal part of the PVS, as well as its cross-section, within 30 min. The PVS staining method is faster and simpler than the H&E staining method, while maintaining good quality to allow the identification of the internal structure and the cellular morphology of the PVS. H&E staining, a common method to identify the PVS, takes about one day to microscopically observe the stained samples (Ogay et al., 2009a; Soh, 2009). Due to the short dying process involved in Hemacolor staining, I may have observed the PVS in a more natural state than that seen with previous methods. In addition, the application of Hemacolor on the PVS allows the major features of putative MCs and isolated granules in the PVS to

be identified. Using Hemacolor staining, I confirmed all the previously reported immune cells stained with toluidine blue (Cerri et al., 2010), H&E, and Wright Giemsa staining (Kwon et al., 2012; Lee et al., 2007; Ogay et al., 2009a). This method also allowed us to demonstrate the detailed features of the cells composing the PVS and revealed the sinuses within the PVS, ductules in PVs, and various individual cells in tissue or in isolation. Therefore, the Hemacolor staining method, combined with slice preparation, is suitable for the study of the PVS due to its fast identification of the gross and cellular morphology of the PVS.

From Hemacolor staining of the whole PVS and PN slices, I found evidence for the presence of sub-ducts known as “ductules” in previous studies (Lee et al., 2007; Ogay et al., 2009a). The linear alignment of single cells and granules along the longitudinal axes of the PVs in this study (Figures 2B and 5) is in good agreement with the linearly-aligned elliptical or elongated cells with rod-shape nuclei in PVs (Shin et al., 2005; Soh, 2009), which have been considered a hall mark for the identification of the PVS (Soh, 2009). This observation also provides evidence supporting the notion that the PVS is a circulatory channel (Soh, 2009; Stefanov et al., 2012).

One of the novel findings of this study is the honeycomb-like structure inside the PN slice with pentagonal lumens of about 10 μn in the honeycomb (Figure 6B). The size of each lumen of the honeycomb structure (~10 μm) is comparable to that of the ductules (10 μm or 7–15 μm) reported in the PV (Lee et al., 2007; Ogay et al., 2009a). In terms of its size, it is likely that each lumen of the honeycomb-like structure inside the PN may function as a ductule, as

reported previously (Kim, 1963; Lee et al., 2007; Ogay et al., 2009a), and the channels for the flow of single cells or granules, as shown in Figure 5. The honeycomb-like structure in this study is similar to findings from prior cryo-scanning electron microscopic studies (Lee et al., 2007; Sung et al., 2008) in that individual lumens are tightly arranged in close contact, but distinctly different in that the size of the lumens is larger (~10 μm vs. 1–5 μm) and much more homogeneous than that in the previous studies (Lee et al., 2007; Sung et al., 2008). This discrepancy may arise from the differences in experimental conditions and/or the types of PVS tissue tested. Further research is needed to understand the honeycomb-like structure observed in this study and its relation with the ductules reported in previous studies (Lee et al., 2007; Sung et al., 2008) as well as the channels for the alignment of single cells or granules shown in this study (Figure 5).

As shown in Figure 7, mesothelial cells were identified in the outer surface of the PN slices (5 μm) stained with H&E. It is been known that mesothelial cells protectively cover and coat the surface of the visceral organs (i.e., liver, intestine, and omentum) and the parietal walls (i.e., pericardium, peritoneum) of cavities (Jones, 1987; Junqueira and carneiro, 2003; Simionescu et al., 1977), and that they are the front line of defense against chemical or bacteria (Yung et al., 2012) and synthesize lubricants to make a slippery surface that promotes movement between organs (Lua et al., 2016). Mesothelial cells in the PVS may have originated from the visceral organs in the abdominal cavity and also likely function as a protective barrier that covers the surface of the PVS. In addition, a recent study has reported that mesothelial cells are not only a

protective barrier on the liver but that they are also involved in the liver's development, injury, and regeneration (Lua et al., 2016); according to BH Kim's claim, PVS has a role in the regeneration of damaged tissues (Kim, 1965b). Thus, it may be assumed that the regeneration function of PVS is related to the mesothelial cells in PVS. Additional studies are required to fully elucidate the role of mesothelial cells in PVS. In addition, sinus structures were identified in the PN slice (5 μm) as in previous studies (Lee et al., 2007).

In this study, I classified PVS cells into three major groups on the basis of their cytologic morphology: WBCs, RBCs, and putative MCs comprising 90.3%, 5.9%, and 3.8% of the cell population, respectively. These overall findings were similar to those of recent studies using H&E staining and electron microscopy that showed the presence of numerous immune cells in the PVS, such as MCs, macrophages, and neutrophils (Kwon et al., 2012; Lee et al., 2007; Ogay et al., 2009a; Sung et al., 2010). I attempted to observe the PVS cells in tissue as well as the single cells in isolation from PVS tissue for more decisive observation of PVS cells. Under these experimental conditions using PVS slice preparation (Choi et al., 2011; Han et al., 2010a), I was able to directly apply Hemacolor staining to intact live PVS cells (Figure 8a).

The WBCs in the PVS were similar to those of typical WBCs and myeloid precursors, which are composed of neutrophils, plasma cells, eosinophils, and lymphocytes (Figure 8F) (Eroschenko, 2008; Ross and Pawlina, 2005). The WBCs were consistent with the small round cells, which were further categorized into four types based on their current-voltage (I-V) relations recorded from cells in live PN slices in the previous electrophysiological study

(Choi et al., 2011). The presence of small clusters of RBCs in the PVS was previously reported (Han et al., 2010). In this study, I identified the RBCs in live PVS slice preparation as well as in isolation as single RBCs after Hemacolor staining. The RBCs were similar to the normal mature rat RBCs in terms of the following properties: size (6–8 μm), biconcave (flat) disk-shaped, non-nucleated cells with a central region of pallor appearing in middle of cytoplasm (Eroschenko, 2008; Ross and Pawlina, 2005). The putative MCs in the PVS appeared most outstanding in the images of Hemacolor-stained PVS and were more densely populated at the edges than other parts of the PVS. I confirmed the putative MCs in terms of their morphology, such as their large cell body of purple color, typical granules, and staining properties using toluidine blue, a dye commonly used for the staining of MCs (Cerri et al., 2010). These observation is consistent with previous reports (Lee et al., 2007). In the two types of rodent MCs, connective tissue and mucosal MCs (Metcalfe et al., 1997), the putative MCs of PVS are similar to those in connective tissues because of their large size (12–20 μm) and staining properties resulting from toluidine blue (Figure 8e).

In this study, I recorded the movement of granules both within cells and/or in isolation. The fact that one can observe granule movement indicates that the physiological conditions for putative MCs (Mizuno et al., 2007) are reasonably well preserved under my experimental conditions in live PVS slices. In addition, the granules of putative MCs of the PVS and isolated granules are similar in morphology to the primo-microcells (Sanal), which are spherical or oval in shape and have a diameter of 1–2 μm (Figure 9A) (Kim, 1965a; Kim,

1965b; Soh, 2009). However, as the granules of the putative MCs and the primo-microcells were stained green (denoting RNA) and red (denoting DNA), respectively, by acridine orange, their components differed (Figures 3C and 8d) (Jia et al., 2011; Ogay et al., 2006). The critical issue of whether the granules in the putative MCs or in isolation in the PVS tissue are the primo-microcells still need to be studied further.

It is unusual for any tissue to have such a high proportion of immune cells as in the PVS: WBCs (90.3%), RBCs (5.9%), and putative MCs (3.8%). The present study is an attempt to determine the relative composition of the PVS cells. Recently, the proportion of MCs is 20% of the whole immune cell population in the organ surface PVS (Kwon et al., 2012), which indicates that the proportion of MCs is different between two studies, 20% vs. 4.0%. The discrepancy may arise from the differences in the methods and experimental conditions and need to be studied further. Since the cellular composition of the PVS is different from that of blood (RBC of over 90%), bone marrow (MC of 2.6% ± 0.5%), and spleen (majority of lymphocytes) (Jamur et al., 2010; Sung et al., 2008), such a unique cellular composition could be a useful hallmark for the identification and comparison of the PVS in future studies.

In relation to the function of the PVS, the most salient point of the present observation is that Hemacolor staining of the PVS revealed a realistic integrated image of the PVS composed of the sinuses and the ductules reported previous studies (Lee et al., 2007; Ogay et al., 2009a). The PVS sinuses (varying in size) and the ductules (~10 μm) observed in this study are likely to function as circulatory pathways (Soh, 2009) since 1) the sinuses are channel-

like structures throughout PNs and PVs, 2) the sinuses contain three major types of PVS cells and granules with random arrangements, and 3) the ductules are well developed in PVs and contain lineally aligned single cells or granules. Thus, the primary function of the PVS can be thought of as a pathway for the cells, such as putative MCs, WBCs, and RBCs. In this study, the immune cells, such as MCs, neutrophils, eosinophils, and lymphocytes, accounted for the vast majority of the whole PVS cell population (~94%). The results strongly support that PVS may have a crucial role in the initiation and/or maintenance of immunological functions (Kwon et al., 2012; Lee et al., 2007; Ogay et al., 2009a; Sung et al., 2010). I found the degranulation of putative MCs in the sinuses of PVs, indicating that the MCs were preferentially activated in the sinuses in PVs rather than in PNs (Figure 2F). It is also known that MCs are rich at the acupoints (Hwang, 1992; Wang et al., 2010; Zhang et al., 2008), and the effects of acupuncture are related to MCs (He and Chen, 2010; Zhang et al., 2008). Although both the PVS and the classical acupuncture meridian system are known to be associated with MC as described above, there is a lack of sufficient evidence to directly connect them in the current stage of research, and therefore additional research is necessary.

CONCLUSION

This study shows that Hemacolor staining is useful in identifying as well as in characterizing cellular and structural properties of the PVS by confirming typical morphological features of PVs and PNs with a simple light microscope in a short time period. These results provide two pieces of morphological evidence supporting the circulatory nature of the PVS and its roles in relation to immune functioning. 1) There are two major channel structures in the PVS: sinuses and ductules. 2) The PVS is unique in its large population of immune cells, including a cellular composition of 90.3% WBCs, 5.9% RBCs, and 3.8% putative MCs. Of note, the MC population is high, and RBCs are present in PNs. These findings and the experimental approaches used in this study may help to elucidate the structure and function of the PVS in normal and disease states in future studies.

CHAPTER II

Identification of primo-vascular system in abdominal subcutaneous tissue layer of rats

ABSTRACT

The primo-vascular system (PVS) is a novel network identified in various animal tissues. However, the PVS in subcutaneous tissue has not been well identified. Here, I examined the putative PVS on the surface of abdominal subcutaneous tissue in rats. Hemacolor staining revealed dark blue threadlike structures consisting of nodes and vessels, which were frequently observed bundled with blood vessels. The structure was filled with various immune cells including mast cells and WBCs. In the structure, there were inner spaces (20–60 μm) with low cellularity. Electron microscopy revealed a bundle structure and typical cytology common with the well-established organ surface PVS, which were different from those of the lymphatic vessel. Among several subcutaneous (sc) PVS tissues identified on the rat abdominal space, the most outstanding was the scPVS aligned along the ventral midline. The distribution pattern of nodes and vessels in the scPVS closely resembled that of the conception vessel meridian and its acupoints. In conclusion, the results newly revealed that the PVS is present in the abdominal subcutaneous tissue layer, and indicate that the scPVS tissues are closely correlated with acupuncture meridians. These findings will help to characterize the PVS in the other superficial tissues and its physiological roles.

INTRODUCTION

The primo-vascular system (PVS) is a novel vascular network that was first reported in the 1960s by Bong-Han Kim, who claimed that the tissue corresponded with the acupuncture meridians (Kim, 1963). This tissue was therefore named "Bonghan tissue" after its discoverer. More recently, the tissue has been re-identified by Dr. Kwang-Sup Soh and colleagues (Soh, 2009); it was subsequently re-named the "primo-vascular system" at an international conference in Jecheon, South Korea (Kang, 2013a). The PVS is composed of primo-vessels (PVs, or Bonghan ducts) that connect primo-nodes (PNs, or Bonghan corpuscles), which are relatively thicker than the PVs (Soh, 2009). The PVS tissue has been identified in various sites, such as internal organs (Choi, J.H., 2011; Lee et al., 2009a; Lim et al., 2013; Shin et al., 2005), brain ventricles (Lee et al., 2008), and blood and lymphatic vessels (Jia et al., 2011; Lee et al., 2004; Lee et al., 2006) in several animal species (Jia et al., 2011; Lee et al., 2007). Various techniques have been used to visualize the PVS, including trypan blue, through which many important anatomical features of the PVS have been elucidated (An et al., 2010; Soh, 2009), and Hemacolor utilized in recent research (Lim et al., 2013).

PVS studies in the past 10 years have identified the following hallmarks of PVS. First, the PVS primarily consists of vessel parts (PVs) and node parts (PNs), and the vessels are often sub-branched from each node (Lee et al., 2009a; Shin et al., 2005; Soh, 2009). Second, rod-shaped nuclei (revealed by DNA-

specific staining) are linearly aligned along the longitudinal axis of the PVS (Jia et al., 2011; Lee et al., 2006; Shin et al., 2005). Third, the PVS contains various immune cells, including mast cells (MCs) and white blood cells (WBCs), such as eosinophils, neutrophils, and lymphocytes, and it has a unique cellular composition (Kwon et al., 2012; Lim et al., 2013; Ogay et al., 2009a) and a high number of MCs and WBCs. Fourth, the PVS is composed of a bundle of several small subducts or ductules (10–50 μm) containing immune cells (Kwon et al., 2012; Lim et al., 2013; Ogay et al., 2009a). This bundle structure is morphologically different from that of a lymphatic vessel, which only has a single lumen (Kwon et al., 2012; Shin et al., 2005).

Based on Bong-Han Kim's claim in the 1960s that the PVS is a reality of acupuncture meridians (Kim, 1963), more recent research has sought to identify the PVS in the skin or hypodermis, where the putative acupoints are located. For example, a series of blood plexuses at the putative acupoints along the left and right kidney meridian lines was showed in the abdominal skin of rats using a diffusive light illumination technique (Ogay et al., 2009b). In addition, a trypan blue-stained structure along the skin skeletal muscles was revealed in the hypodermal layer of a rat (Lee et al., 2010). In these studies, the locations of the putative PVS tissue appeared to correspond to the acupuncture meridians in the subcutaneous area. However, clear evidence that these putative PVS tissues have the established hallmarks of the existing PVS is missing.

Therefore, in this study, the gross morphological features of putative PVS in rat abdominal subcutaneous tissue was first examined using the Hemacolor reagents, which comprise a rapid staining system that is commonly

used in hematological and clinical specimens (Keisari et al., 1992; Walter et al., 2011), and has been effectively used to characterize organ surface PVS (osPVS) *in vitro* (Lim et al., 2013). Then, I confirmed the putative PVS is distinct from the lymphatic vessel by scanning and transmitting electron microscopy. Finally, I also examined the relationships between the subcutaneous PVS (scPVS) and the acupuncture meridians of the abdominal area.

MATERIALS AND METHODS

Animal Preparation

Male Sprague-Dawley rats weighing 120–150 g (4–5 week; n = 23; Orient Bio Inc., Gyeonggi-do, Korea) were used for this study. The rats were housed in a temperate (20–26℃), relatively humid (40–70%), light-controlled (12-hour light/dark cycle; with the light coming on at 9:00 AM) environment. They were allowed open access to water and standard rodent chow *ad libitum*. The rats were allowed to adjust to this environment for 3–4 days before the experiments were conducted. All animal experiments were conducted in accordance with the Guide for the Laboratory Animal Care Advisory Committee of Seoul National University and were approved by the Institute of Laboratory Animal Resources of Seoul National University (SNU-140926-2). All surgical procedures were performed under general anesthesia.

Identification of osPVS and scPVS in vivo

Under deep anesthesia induced with an anesthetic cocktail (Zoletil, 25 mg/kg; xylazine, 10 mg/kg) administered intramuscularly into the right femoral regions, two types of PVS samples were collected according to the following procedures.

For the first procedure, the osPVS was identified on the surface of the abdominal organs using the trypan blue or Hemacolor staining method. The Hemacolor dyes were comprised of a three-solution system (Solution 1, absolute methyl alcohol for primary fixation; Solution 2, buffered eosin with sodium for eosin staining; Solution 3, phosphate-buffered thiazine for methylene blue staining) (Keisari et al., 1992; Walter et al., 2011). These solution (1 mL each) were applied to the surface of the internal organs, such as the intestines and the liver, in the cut abdominal cavity for 5 sec. After application of Solution 3, the dye solutions were washed out using the Krebs solution (NaCl, 120.35 mM; $NaHCO_3$, 15.5 mM; glucose, 11.5 mM; KCl, 5.9 mM; $CaCl_2$, 2.5 mM; NaH_2PO_4, 1.2mM; and $MgSO_4$, 1.2mM) (Choi et al., 2011). After the Hemacolor staining, the revealed osPVS tissues were immediately sampled for additional staining under a stereomicroscope. For the second procedure, scPVS tissue was identified in the subcutaneous tissue layer using Hemacolor staining. Solution 1 (1 mL) was first applied to the hypodermis region of interest for 5 sec, and then Solutions 2 and 3 (1 mL each) were applied to the same region one by one. Then, Solution 3 had been applied for 5 sec; the region was washed out with a 0.9% saline solution and observed under a stereomicroscope (~1,000x).

Staining methods for the identification of scPVS in vitro

For the characterization of gross morphology, the identified scPVS was isolated from the abdominal hypodermis region using a micro-scissor (blade 5 mm) and transferred into a drop of Hank's balanced salt solution (Sigma, St. Louis, MO, USA) on a slide glass. After the sample was completely air-dried at room temperature for 1–3 min, the slide glass was immersed 10 times in and taken out of dye Solution 1 for 10 sec (~1/sec). Additional staining with Solutions 2 and 3 was repeated using the same process. The sample was then placed in a drop of phosphate buffer solution (pH 7.2) for 20 sec, washed by shaking it 10 times in distilled water for 20 sec, air-dried for 3–5 min, and finally mounted with Canada balsam (Sigma). The PVS slice preparation was performed according to the previous method (Lim et al., 2013). To confirm the DNA and RNA contents of the scPVS, the sample was kept immersed in a 0.1% acridine orange solution for 15 min, and a digital photograph was then taken using a confocal laser-scanning microscope at the wavelength of the acridine orange (Lee et al., 2013a). To verify the MCs in the scPVS, the sample was immersed in a 1% toluidine blue solution for 3 min (Cerri et al., 2010).

Electron microscopy of scPVS and the lymphatic vessel

For the scanning electron microscopy (SEM), scPVS and lymphatic vessels were collected from the rats. The procedure for harvesting the scPVS tissue was same as that used in the sampling by Hemacolor staining. The harvesting procedure for the lymphatic vessel was as follows: Under deep anesthesia, the abdomen of the rat was incised, and the lymphatic vessel was sampled under a stereomicroscope around the kidney by reference to the previous report (Jung et al., 2013). The scPVS attached hypodermis layer (Figure 3A) was isolated from the area of umbilicus on the rat abdominal middle line (Figures 2A and 11A). The sampled scPVS and lymphatic vessels were kept in 2% paraformaldehyde for 24 hr and primary-fixed by Karnovsky's fixation for 2 hr. After washing them with 0.05M sodium cacodylate buffer 3 times for a total of 10 min, the samples were post-fixed by 2% osmium tetroxide (1 mL) and 0.1M cacodylate buffer (1 mL) and washed twice using distilled water for 5 sec each. Dehydration was conducted using a series of ethanol of 30%, 50%, 70%, 90%, and 100% for 10 min each, and then the samples were dried using a critical point dryer (CPD 030, BAL-TEC) for 1 hr, coated by an sputter coater (EM ACE200, Leica), and observed under a field-emission SEM (SIGMA, Carl Zeiss, UK). For transmission electron microscopy (TEM), several procedures

were added to those of SEM: (1) After washing the samples with distilled water, en bloc staining was conducted with 0.5% uranyl acetate for 30 min; (2) after dehydration with ethanols, a transition procedure using propylene oxide was conducted twice for 10 min each; and (3) then the samples were embedded into Spurr's resin (2 ml), sectioned, and observed under a TEM (JEM1010, JEOL, Japan).

PVS cell counting and data analysis

The PVS cells were counted from 21 fields (100 × 100 μm) in an image of the Hemacolor staining of the PVS tissues (n = 7) at magnifications of 400 and 1000x. The sizes of the PNs, PVs, and resident cells were measured using image J software (developed at the U.S. National Institute of Health). All results are shown as mean ± standard errors, and the number of samples or cells was represented by n.

RESULTS

Gross morphological of the scPVS in vitro

The results of the present study were obtained from the examinations of subcutaneous PVS (scPVS) tissues in 14 rats and organ surface PVS (osPVS) tissues in 7 rats. The osPVS tissues (n = 17) were sampled mainly from the surfaces of the abdominal organs, including the large intestine (32%), the small intestine (38%), and the liver (17%). The scPVS tissues (n = 24) were sampled exclusively from the abdominal subcutaneous area. The osPVS tissues were identified without staining, whereas the scPVS tissues were identified with Hemacolor staining.

Previously, it has been shown that Hemacolor staining is effective in characterizing the gross morphology of the osPVS in isolation (Lim et al., 2013). In this study, Hemacolor dyes were directly applied to the PVS tissues on the surfaces of the abdominal organs to determine whether the osPVS could be stained *in vivo* as it is stained by trypan blue, which is a well-known dye that is used to identify PVS *in situ* (Soh, 2009). The Hemacolor staining revealed that the PVS was attached to the surface of the abdominal organ. Figures 1A and 1B show representative osPVS tissue composed of primo-nodes (PNs) and primo-

Figure 1. Identification of intact PVS tissue on the surface of abdominal organs in rats using Hemacolor and trypan blue staining. (A) PVS tissue on the surface of the small intestine stained by Hemacolor. **(B)** Magnified view of the organ surface PVS structure (square in (A)) composed of multiple-PNs (arrows), a PV (arrowhead), and a sub-branching point (dotted arrows). **(C)** PVS tissue on the surface of the large intestine stained by trypan blue. **(D)** Magnified view of the organ surface PVS structure (square in (C)) composed of two PNs (arrows) and a PV (arrowhead).

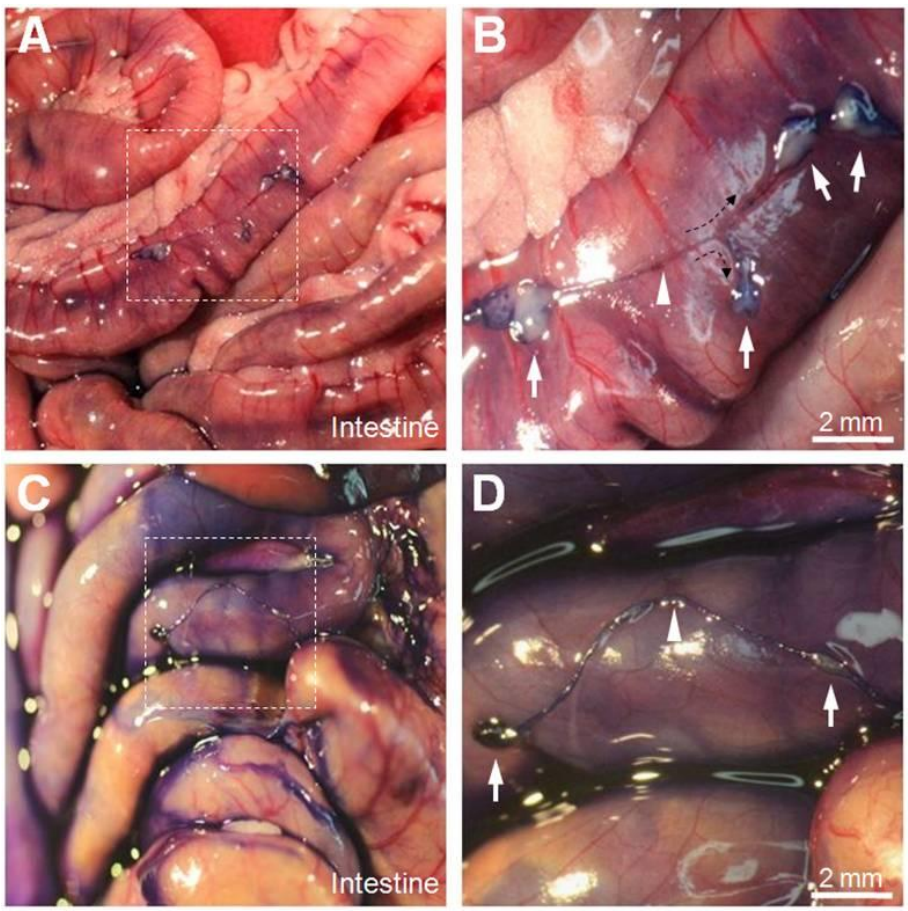
A
Intestine
B
2 mm
C
Intestine
D
2 mm

vessels (PVs) on the surface of the small intestines revealed by Hemacolor staining. The Hemacolor staining of the osPVS was comparable to the trypan blue staining (Figures 1C and 1D).

Figure 2 shows the appearance of the abdominal subcutaneous region after the applications of Solutions 1, 2, and 3 for the Hemacolor staining *in vivo*. After completion of the Hemacolor staining, dark blue threadlike structure was observed through the fascia in the stained area of the abdominal subcutaneous tissue layer (Figure 2D). Figure 3 shows the anatomical location of the Hemacolor stained-dark blue threadlike structure on the surface of the subcutaneous tissue layer identified by scanning electron microscopy (SEM). This threadlike structure was comprised of a bundle of subducts or small tubes; this morphology was characteristically different from that of the lymphatic and blood vessels, which consisted of a single tube.

Figure 4 shows a representative example of a dark blue-colored threadlike structure revealed by Hemacolor staining in the abdominal subcutaneous area. The vessels were divided into a vertically elongated type (yellow vertical arrow) along the abdominal middle line and a horizontally elongated type (yellow horizontal arrow) branched from each node form (Figure 4B). As shown in Figures 4B and 4C, the dark blue-colored multiple-branched

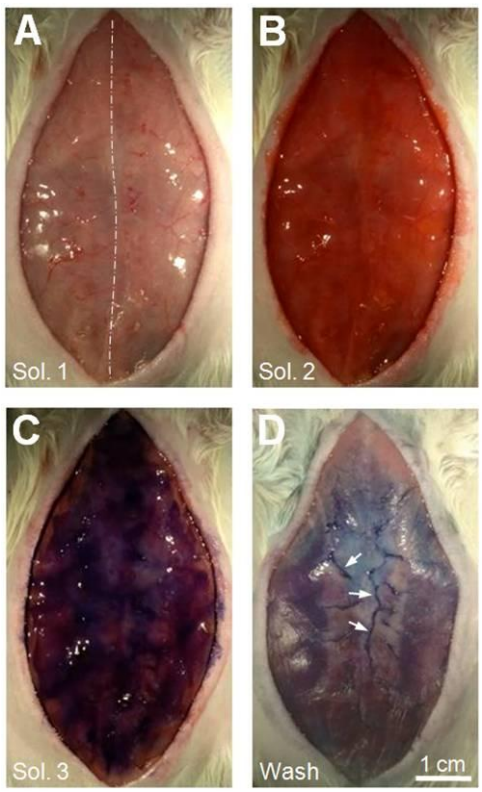

Figure 2. Identification of the threadlike structures in the rat abdominal subcutaneous tissue using Hemacolor staining. (A, B, and C) Appearance of the subcutaneous area after serial applications of three Hemacolor solutions: Solution 1 (methanol fixative, (A)), Solution 2 (eosin stain, (B)), and Solution 3 (methylene blue stain, (C)). Dotted line is the abdominal middle line. **(D)** Appearance of the subcutaneous area after wash-out of Hemacolor solutions. Note the dark blue threadlike structures (arrows). See the *Materials and Methods* sections for a description of the protocol.

Figure 3. The location of the threadlike structure in the rat abdominal tissue layer revealed by scanning electron microscopy. (A) Cross-section of tissue explant including the skin (s), subcutaneous tissue layer (st), and abdominal wall muscle (am). The explant is isolated from the near area of umbilicus on the abdominal middle line. Note that the threadlike structure (arrowheads) is located between the skin and subcutaneous tissue layer. **(B)** Magnified view of the threadlike structure (square in (A), arrowheads) on the surface of subcutaneous tissue layer. **(C)** Magnified view of the threadlike structure (square in (B)) showing a bundle structure of three subducts (arrowheads). Note that the rough surface of threadlike structure.

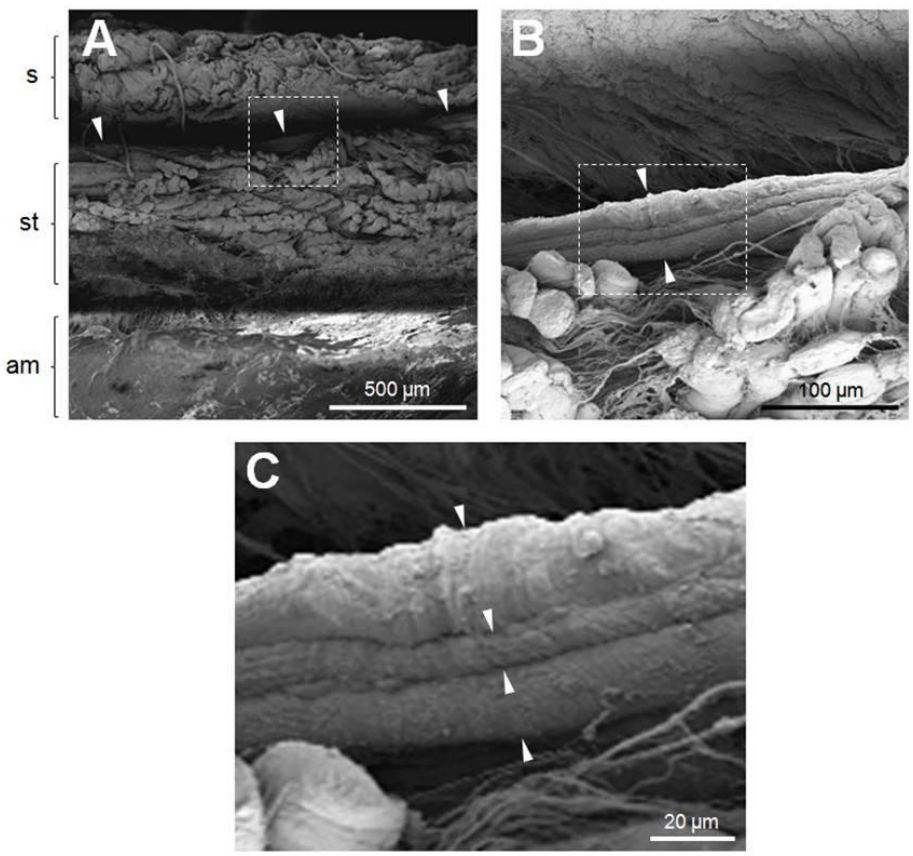
A
s
st
am
500 µm
B
100 µm
C
20 µm

threadlike structures (white arrows) were distributed across the surface of the subcutaneous tissue. In addition, some vessels were also distributed beneath the surface of the subcutaneous tissue (Figures 4B and 4C, two-way dotted white arrows and open arrowheads). The dark blue threadlike structures appeared to be interrupted where the structures were buried underneath the surface of the subcutaneous tissue layer. In addition, blood vessels were observed around the threadlike structures (Figures 4B and 4C, asterisks). The blood vessels were not stained dark blue like the threadlike structures by Hemacolor staining; rather, they maintained their original red colors. The average size of the nodes of the threadlike structures was 0.94 ± 0.14 mm (n = 12), and the average thickness of the vessels was 0.21 ± 0.05 mm (n = 15).

Cytomorphology of the scPVS in vitro

The threadlike structure was isolated and the tissue was re-stained *in vitro* to identify the cellular properties of the threadlike structure stained by Hemacolor. Figure 5A shows a sample on the slide glass of a threadlike structure composed of nodes and vessels connected by these nodes. Figure 5B is a representative stereoscopic image of the threadlike structure stained by Hemacolor. The Hemacolor-stained cells of the threadlike structure were mainly classified into

Figure 4. Hemacolor-stained threadlike structures in the rat abdominal subcutaneous tissue. (A) Typical example of the distribution of threadlike structures (white arrows) on the subcutaneous area stained by Hemacolor. **(B and C)** Threadlike structures (dotted squares marked as "(B)" and "(C)" in (A)) composed of the vessels (arrowheads) that connect the nodes (arrows). Note that the node structures are multi-branched (white arrows) from the nodes, and the vessel structures are distributed either on or beneath the subcutaneous surface (two-way dotted white arrows and open arrowheads). Note that the blood vessels (BVs, asterisks) maintain their red color; and that threadlike structures are aligned in either a vertical or horizontal direction (yellow arrows). Note the blood vessels around the branching points of the threadlike structures (asterisks).

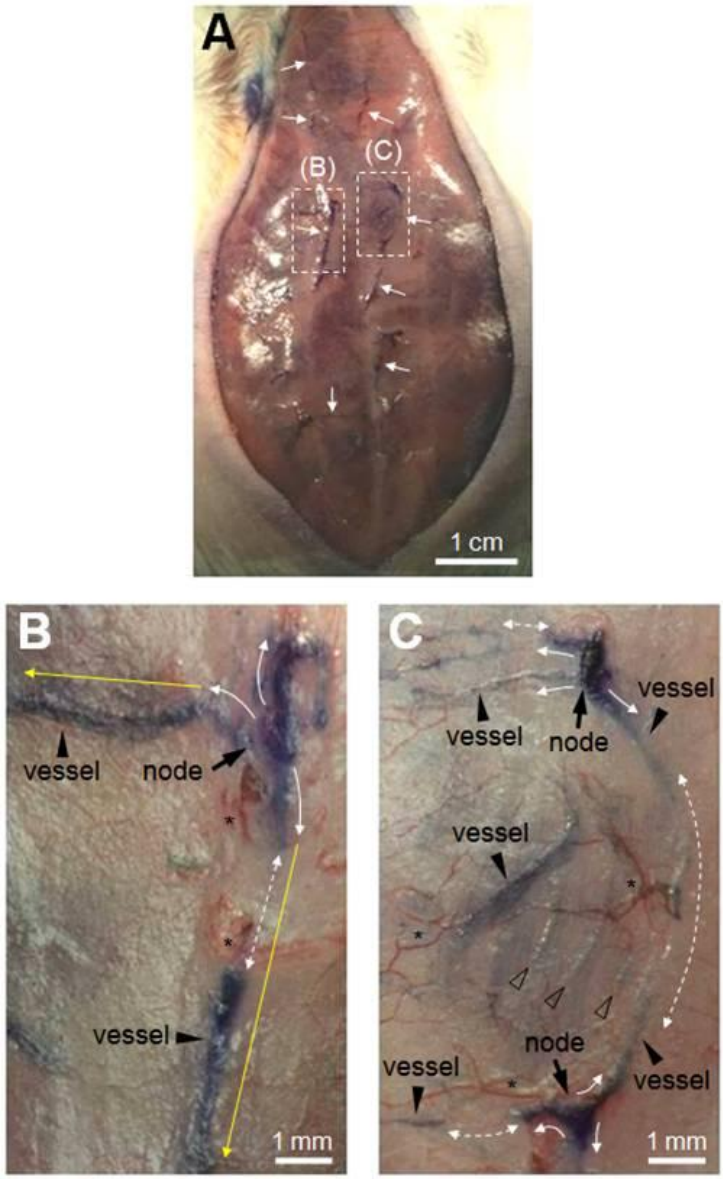
A
(B)
(C)
1 cm
B
vessel
node
vessel
1 mm
C
vessel
vessel
node
vessel
node
vessel
vessel
1 mm

two groups based on their morphologies: small round cells (~10 μm) and large granular cells (10–20 μm). The cells in the vessels and nodes differed in shape and distribution. The cells within a node were mostly round in shape and were dispersed unsystematically (Figure 5C). In contrast, the cells within a vessel were elliptical and linearly aligned along the longitudinal axis of the vessel (Figure 5D). Figure 5E shows the image of the cells of the threadlike structure revealed by toluidine blue staining, which is widely used to stain selectively MCs (Cerri et al., 2010). In previous studies, the PVS has been found to contain a variety of immune cells, including MCs and WBCs (Lim et al., 2013; Walter., 2011); therefore, in this study, toluidine blue staining was performed. The granules within large granular cells showed the typical metachromatic staining property of toluidine blue staining, indicating that the large granular cells in the threadlike structure were MCs (Figure 5E) (Cerri et al., 2013). The threadlike structure was also stained with acridine orange staining to determine DNA (revealed green) and RNA (revealed red) components for the further characterization of the cellular properties of the threadlike structure (Lee et al., 2013). Figure 6A illustrates the threadlike structure consisting of one node and connecting vessel stained by acridine orange. The majority of cells in the threadlike structure were stained a green color, as shown in Figure 6. The nuclei

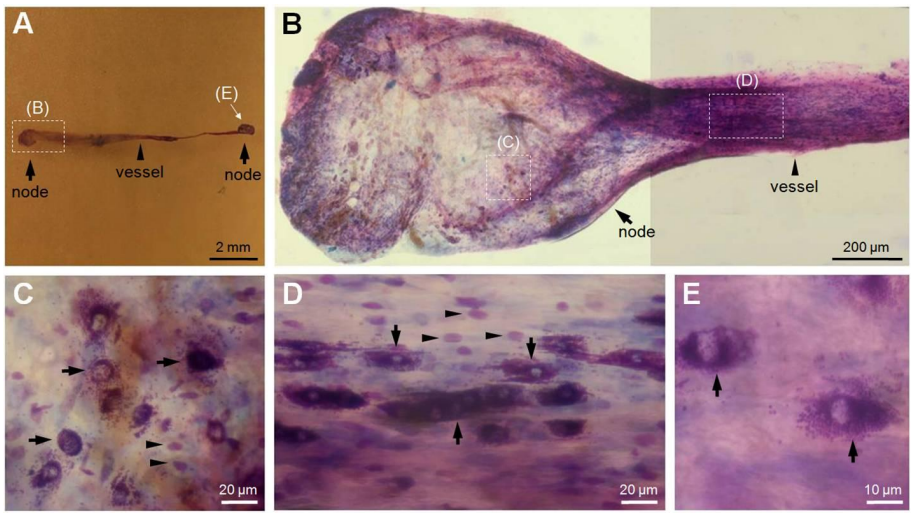

Figure 5. Hemacolor staining of the threadlike structure isolated from the rat abdominal subcutaneous tissue. (A) Threadlike structure isolated from the Hemacolor-stained layer of the subcutaneous tissue. **(B)** Typical longitudinal image of a whole threadlike structure (marked as "(B)" in (A)). **(C and D)** Two major types of cells in the threadlike structure: large granular (arrows) or small round cells (arrowheads). Note that the cells in the node (C) and in the vessel (D) are aligned differently. **(E)** Toluidine blue staining of the large granular cells (arrows).

of the small round cells were stained green (Figures 6B and 6C, arrowheads), whereas the large granular cells were stained green and red in the nuclei and surrounding granules, respectively (Figures 6B and 6C, arrows). The shape and distribution of the acridine orange-stained cells were similar to those of the Hemacolor staining, as shown in Figure 5. Most cells in the vessel were aligned along the long axis of the vessel (Bottom inset in Figure 6A and Figure 6C). In contrast, the cells in the node were randomly distributed without any clear direction (Figure 6B).

Structural properties of the scPVS in vitro

The inner regions of the vessel of the threadlike structure revealed by Hemacolor staining appeared as white space, indicating a lower cellularity (Figure 7). The inner space was linearly continuous along the longitudinal axis of the vessel (Figures 7A and 7B). The diameters of the inner space were 20–60 μm. The inner space structures contained various cells, such as large granular cells (Figure 7B, arrowheads), granules (Figure 7B, dotted circle), and small round cells (Figure 7D, arrowheads). Figure 7C shows a bundle-like structure revealed by Hemacolor staining as shown in Figure 3 by scanning electron microscopy. In addition, a cross-sectioned slice (200 μm) of the threadlike

Figure 6. Confocal laser-scanning microscopic image of the cells in the threadlike structure stained by acridine orange. (A) Typical longitudinal image of the whole threadlike structure. Note that the cells (arrowheads in bottom inset) in the vessel are linearly aligned along the longitudinal axis of the vessel. **(B)** Acridine orange-stained cells in the node (marked as "(B)" in (A)) showing the small round cells with green nuclei (arrowheads) and large cells with green nuclei and red granules (arrows). **(C)** Acridine orange-stained cells in the vessel (marked as "(C)" in (A)). Note that the density and alignment of resident cells are different in the node (B) and in the vessel (C).

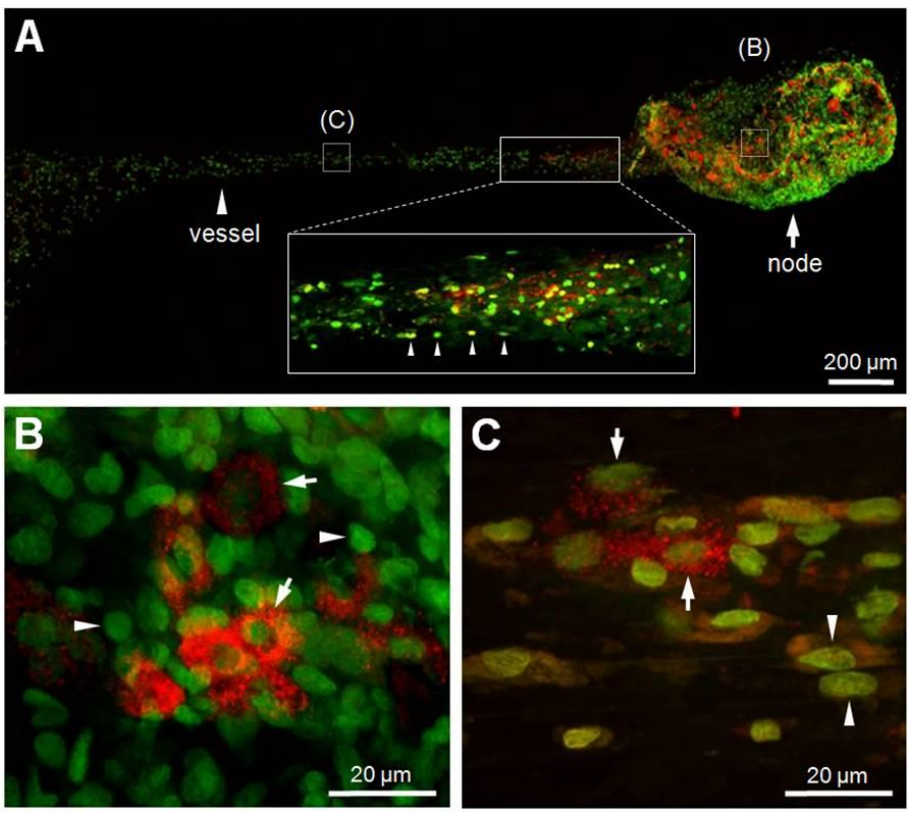
A
(B)
(C)
vessel
node
200 µm
B
20 µm
C
20 µm

structure was stained, and the small and large granular cells were observed in the whole threadlike structures. As shown in Figures 7E and 7F, there was a sinus (~60 μm) that contained granules (~1 μm).

Comparison of the ultrastructural features between the scPVS and lymphatic vessel

Scanning electron microscopy was used to show differences between the threadlike structure and the lymphatic vessel in isolation (Figure 8). The threadlike structure was comprised of a bundle structure of several subducts (Figure 8A), whereas the lymphatic vessel did not appear to have bundle structure (Figure 8C). At a higher magnification view, I observed the round cells (Figure 8B, asterisks) and fine fiber structures on the surface of the threadlike structure. In contrast, in the lymphatic vessel, such cells were not found and the fiber structures were more extensive than those of threadlike structure (Figures 8B and 8D). Figure 9 shows the major resident cells of the threadlike structure and the lymphatic vessel revealed by transmission electron microscopy. As can be seen, the threadlike structure contains various immune cells, including MCs, eosinophil, and granules (Figure 9A), whereas the lymphatic vessel is mostly comprised of lymphocytes (Figure 9B). Thus, there

Figure 7. The inner space structure containing cells along the inside of the subcutaneous threadlike structure. (A) Continuous inner space (arrows) along the longitudinal axis of a threadlike structure revealed by Hemacolor staining. **(B)** Distribution of the cells (large granular cells, arrowheads; granules, dotted circle) in the inner space (marked as "(B)" in (A), 20–30 μm) of the vessel. **(C)** Large inner space structure (> 50 μm) inside the threadlike structure showing low cellularity. **(D)** Distribution of the cells (small round cells, arrowheads) in the inner space (marked as "(D)" in (C)) of the vessel. **(E)** Cross-sectional image (200 μm) showing an inner space (dotted square, > 50 μm) of a threadlike structure revealed by Hemacolor staining. **(F)** Inner space (marked as "(F)" in (E)) within a vessel slice containing granules (about 1 μm, inset). Note that the inner space contains the resident cells of the threadlike structure.

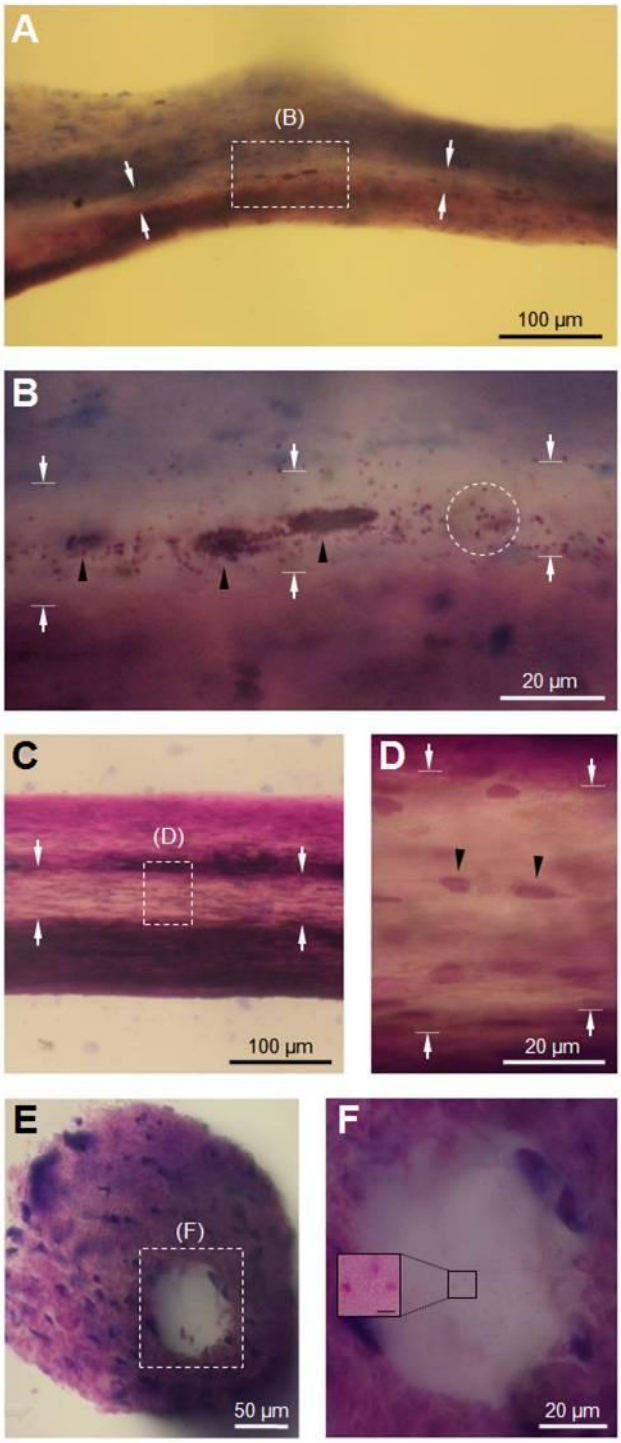
A
(B)
100 µm
B
20 µm
C
(D)
100 µm
D
20 µm
E
(F)
50 µm
F
20 µm

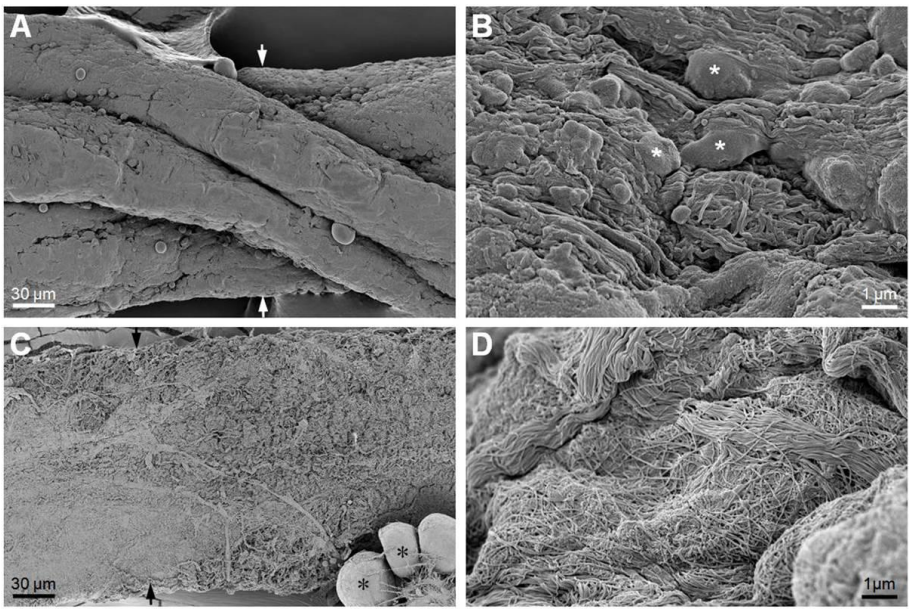

Figure 8. Comparison of the subcutaneous threadlike structure and lymphatic vessel using scanning electron microscopy. (A and C) Typical longitudinal images of the threadlike structure and lymphatic vessel. Asterisks are an adipocyte attached to the lymphatic vessel. **(B and D)** The surfaces of the threadlike structure and lymphatic vessel at higher magnification. Asterisks are the cells on the surface of the threadlike structure. Note that the threadlike structure and lymphatic vessel are different in terms of the presence or absence of the bundle structure of several subducts and cells.

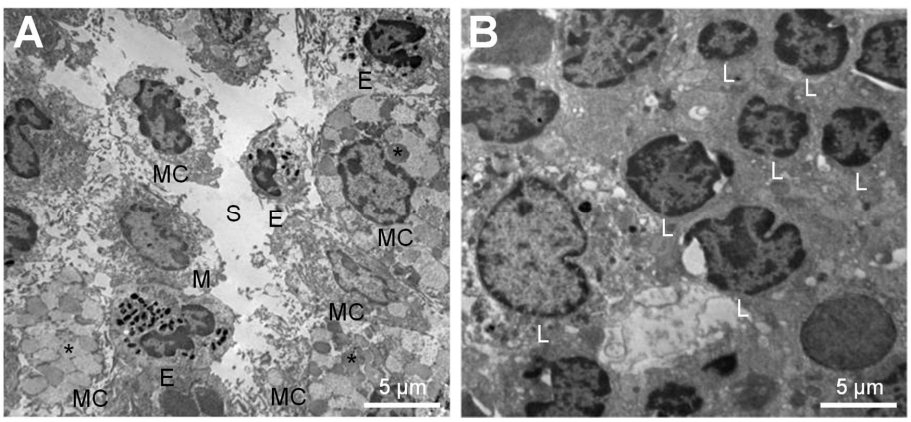

Figure 9. Comparison of the subcutaneous threadlike structure and lymphatic vessel using transmission electron microscopy. (A) Threadlike structure containing a sinus structure (S), mast cell (MC) and its granules (asterisks), monocyte (M), eosinophil (E). **(B)** Lymphatic vessel containing mostly lymphocytes (L). Note that there is the difference in the major resident cells between the threadlike structure and the lymphatic vessel.

are the clear differences between the threadlike structure and lymphatic vessel in terms of the presence or absence of the bundle structures and the types of resident cells.

Comparison of the MC density between the scPVS and the osPVS

The above results regarding gross morphology, cytomorphology, and structural properties have many features in common with the well-established PVS (Lim et al., 2013; Shin et al., 2005; Soh, 2009); thus, the subcutaneous threadlike structure, vessel, and node part were identified as the scPVS, the PV, and the PN, respectively. In addition, the large granular cells and small round cells of the threadlike structure were also identified as the MCs and WBCs of the PVS reported previously in the osPVS (Lim et al., 2013). Figure 10 shows a comparison of the density and degranulation ratios of the MCs in the scPVS and osPVS tissues stained by Hemacolor. The cell densities of the MCs in the scPVS were lower than that of the osPVS (Figures 10A and 10B), and the degranulation ratio of the MCs in the scPVS was higher than the ratio in the osPVS (Figures 10C and 10D), which indicates that the scPVS is different from the osPVS in MC activation.

Figure 10. Comparison of the density and degranulation ratio of MCs identified in Hemacolor-stained scPVS and osPVS tissue. (A and B). Representative photomicrographs showing the distribution of MCs in the PNs of scPVS and osPVS stained with Hemacolor. **(C and D)** Summary bar graphs showing the number of MCs (c) and the degranulation ratio of these MCs in the scPVS and osPVS tissue (d). PVS cells counted from 21 fields (100 × 100 μm) in an image of the Hemacolor staining of the PVS tissue (n = 7) at magnifications of 400x and 1000x.

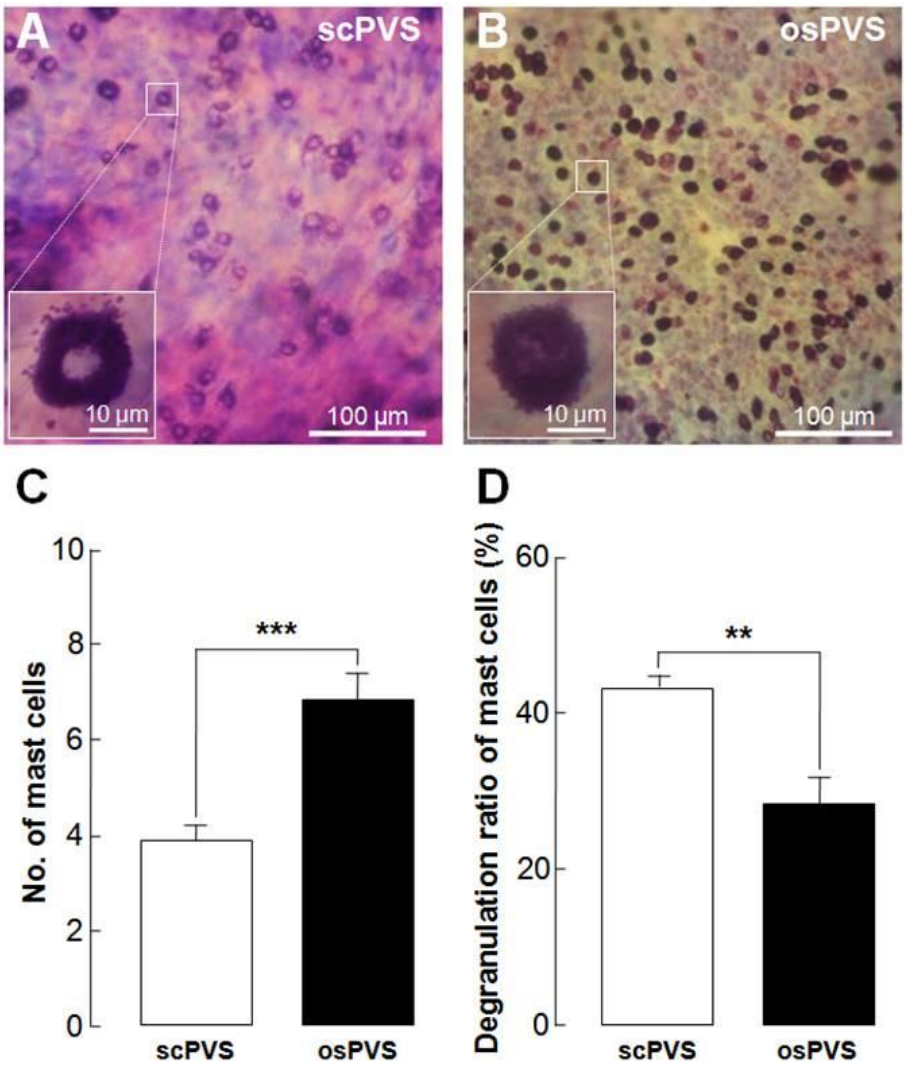
A
scPVS
10 μm
100 μm
B
osPVS
10 μm
100 μm
C
No. of mast cells
10
8
6
4
2
0
***
scPVS
osPVS
D
Degranulation ratio of mast cells (%)
60
40
20
0
**
scPVS
osPVS

Relationship between the scPVS and Acupuncture Meridians

Hemacolor staining of the abdominal subcutaneous tissue revealed that there were multiple scPVS tissues over the whole abdominal space, as shown in Figures 2 and 4. Among these, the most consistently observed tissue was the scPVS tissue, which was located on the abdominal middle area (Figure 11). Since the conception vessel (CV) meridian is also known to be located at the ventral midline connecting the umbilicus to the sternum (Yin et al., 2008), the correlation between the positions of the scPVS present in the ventral midline and the CV meridian was also examined. The CV meridian and acupoints are illustrated in Figures 11A and 11B. Figure 11C shows a typical example of scPVS tissue in the abdominal subcutaneous tissue visualized by Hemacolor staining. The most notable observation is that the scPVS is mainly distributed along the ventral midline, which consists of the vessels connected by nodes. The nodes appear to correspond to the CV acupoints (i.e., CV13, CV10, and CV8). For example, the node corresponding to CV13 appears to be enlarged and located near the blood vessel (Figure 11D). The node corresponding to CV10 appears to be sub-branched and connected another node of the scPVS (Figure 11E, open arrow) located in the right lateral area. A dark blue structure, scPVS was also noted that appeared to be mixed with bloods/plexus (Figure 11E,

Figure 11. The distribution of scPVS in the abdominal subcutaneous tissue in a rat. (A and B) Locations of the conception vessel (CV) acupuncture meridian in a rat (L1, L6, and T13; lumbar 1, lumbar 6, and thoracic 13 vertebrae, respectively). **(C)** Typical example of the scPVS tissue (dotted square marked as "(C)" in (B)) on the abdominal subcutaneous tissue layer in relation to the CV meridian and the acupoints. Note other abdominal scPVS tissue away from the CV meridian line (white arrows and dotted circles). **(D)** scPVS corresponding to putative CV 12 and 13 (dotted square marked as "(D)" in (C)) comprised of a PN (arrow) and a PV (arrowheads). **(E)** scPVS corresponding to putative CV 9 and 10 (dotted square marked as "(E)" in (C)) comprised of a PN (arrow) and PVs (arrowheads). Note that there are three direction-branched PVs (white arrows) from a branching point of a PN, and two branches are connected to one vessel (dotted arrows); there is another vessel away from the vessel located at the ventral midline (open arrow). Note the blood vessels around the scPVS tissue (asterisks in (D) and (C)).

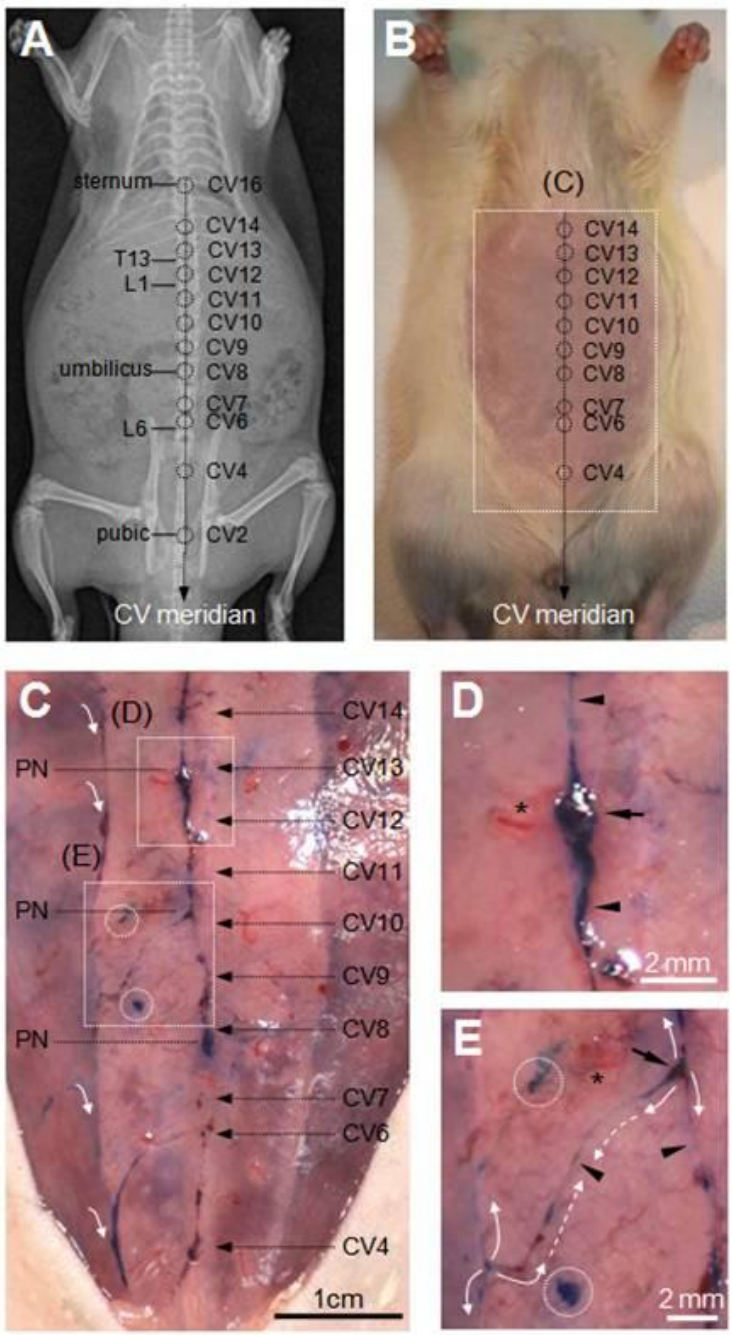
A
sternum
CV16
CV14
T13
CV13
L1
CV12
CV11
CV10
CV9
umbilicus
CV8
CV7
L6
CV6
CV4
pubic
CV2
CV meridian
B
(C)
CV14
CV13
CV12
CV11
CV10
CV9
CV8
CV7
CV6
CV4
CV meridian
C
(D)
PN
(E)
PN
PN
CV14
CV13
CV12
CV11
CV10
CV9
CV8
CV7
CV6
CV4
1cm
D
2 mm
E
2 mm

arrow). Collectively, these observations indicate that the scPVS in the middle of the abdominal subcutaneous tissue layer is likely to correspond to the CV acupuncture meridian. In addition to scPVS in the ventral midline, scPVS tissue was also located laterally, at about 6 mm (Figure 11C, dotted circles) and 9 mm from the midline (Figure 11C, white arrows). A connection between each scPVS was also noted (Figure 11E, dotted arrows).

DISCUSSION

In this study, I identified the PVS in the abdominal subcutaneous tissues in rats using various staining techniques. The scPVS consisted of vessels that connect the node parts and that the vessels were frequently sub-branched. In the Hemacolor-stained whole scPVS tissue in isolation, the cells of the scPVS were found to be composed of WBC-like small round cells and MC-like large granular cells. The cell distributions differed among the nodes (showing a random distribution of round-shaped cells) and the vessels (showing a linear arrangement of elliptical-shaped cells along the long axis of the vessel). Acridine orange staining showed green-stained WBC nuclei (denoting DNA) and green-stained MC nuclei with red-stained granules (denoting RNA). In addition, the inner space-channel (20–60 μm) structure containing WBCs and MCs along the inside of a vessel of the scPVS was identified. Electron microcopy revealed that the threadlike structure has a bundle structure of subducts and round cells on the surface and that these were not found in the lymphatic vessel. The distribution pattern of scPVS tissues in the ventral midline was similar to the route of the CV meridian. Collectively, these finding indicate that the PVS is also present on the subcutaneous layer and that the

scPVS is likely to be closely related to the acupuncture meridians in the subcutaneous tissue layer.

Compared with the unique characteristics of well-established PVS tissue, the putative scPVS of the present study had several features in common with the existing PVS, which is primarily composed of PVs and PNs that are often branched into multiple vessels (Lee et al., 2009a; Shin et al., 2005; Soh, 2009). As shown in Figure 4, the scPVS also has vessels that connect the nodes, and there are well-developed branches that form each node. The rod-shaped nuclei (10–20 μm) of the existing PVS were revealed by DNA-specific fluorescent staining, including acridine orange, 4',6-diamidino-2-phenylindole (DAPI), and the Feulgen reaction (Lee et al., 2004; Lee et al., 2006; Shin et al., 2005). The scPVS revealed that the rod-shaped nuclei were aligned along the longitudinal axis of the vessel stained by acridine orange (Figure 6). The PVS is also known to contain various immune cells (Kwon et al., 2012; Lee et al., 2007; Lim et al., 2013), and in this study, the scPVS showed many WBCs and MCs (Figures 5 and 9). In terms of the internal structure of the PVS, a bundle structure and diverse subducts (~10 or 20–50 μm) that pass through a vessel or node containing the WBCs, MCs, and granules of about 1 μm in diameter were noted (Lee et al., 2007; Lim et al., 2013; Shin et al., 2005). Figures 7, 8, and 9

demonstrate a bundle structure, subducts, and sinus within the vessels of the long axis or a cross-section of the scPVS, including WBCs, MCs, and granules. These findings indicate that the newly identified scPVS belongs to the existing PVS group. However, there were a few different characteristics between the scPVS and the existing PVS. For example, one can differentiate the osPVS tissue from the surrounding organ tissue because it is semi-transparent, freely movable, and present on the surfaces of the internal organs (Choi et al., 2011; Lee et al., 2009a; Lim et al., 2013; shin et al., 2005). That is, it is possible to identify the osPVS without any staining. In contrast, the scPVS tissue, which is located in the interior regions as well as on the surface of the hypodermis, is not easily identified in adjacent subcutaneous tissues; thus, it is necessary to stain the hypodermis region to distinguish the scPVS from the surrounding tissue. In addition, the vessels of the scPVS are more elastic than of the osPVS, and they are often bent during the process of scPVS sampling.

The presence of enriched MCs in osPVS has been confirmed in previous studies, and they have been the considered to be the major resident cells of osPVS (Kwon et al., 2012; Lim et al., 2013). MCs have primarily been viewed as effectors of allergic/inflammatory reactions (Ma et al., 1984). The results of the present study indicate that the scPVS also contains MCs, but they are

different from those in osPVS in terms of density and their degranulation ratio, which are significant parameters that are widely used in studies on MCs. In this study, the MC density was higher in the osPVS than in the scPVS; however, the granulation ratio was higher in the scPVS than in the osPVS (Figure 10), indicating that the MCs in the scPVS are preferentially activated compared to the MCs in the osPVS. Thus, the scPVS could be more exposed to immune disorders, including physical agents, products of diverse pathogens, and many innate danger signals than osPVS. This idea is consistent with a recent hypothesis on the PVS (Stefanov et al., 2013). In the hypothesis, the external PVS such as scPVS functions as a receiving PVS that transforms the external stimuli in to a type of PVS signals, whereas the internal PVS such as a osPVS functions as communicating PVS that transmits the PVS signals among different PVS. This may explain the higher level of MC activation in the scPVS. It is well-known that MC degranulation is remarkably increased by acupuncture on the acupoints of skin tissue (Zhang et al., 2008). Thus, it is conceivable that in this study, the MCs were more activated when associated with the position of the CV meridian and its acupoints in the scPVS than in the osPVS.

One of the primary objectives of this work was to correlate the scPVS and acupuncture meridians, which are known to be present in the skin (Stefanov

et al., 2013; Yin et al., 2008). The present study provides experimental evidences supporting for the close correlation between the scPVS and meridians in the abdominal subcutaneous tissue. Firstly, the PNs revealed by Hemacolor staining showed key features of the Bonghan corpuscle. In the early 1960s, Bong-Han Kim reported that the Bonghan corpuscles (denoting PNs) corresponding to acupuncture meridians/acupoints was present in the subcutaneous tissue layer and was connected by a bundle of blood vessels and Bonghan ducts (denoting PVs) (Kim, 1963; Soh, 2009). Recently, a series of blood vessel plexuses at the putative acupuncture points along the left and right kidney meridians was observed in the abdominal subcutaneous tissue layer of rats by using a diffusive light illumination of the region of skin (Ogay et al., 2009). This report elucidated the morphometric scales of the blood vessel plexus at the kidney and stomach meridians, which are 4–5 mm and 2 cm from the conception vessel meridian in rats by 6–12 weeks. However, they were not able to conclude that the blood plexuses are the anatomical structures of subcutaneous Bonghan corpuscles because the PNs or PVs were not found with the bundle of the blood vessels. The findings in the present study are consistent with the Bong-Han Kim's claim that the scPVS composed of PNs and PVs are frequently bundled with the blood vessels (Figures 4 and 11). This study also

found that the PVS tissue in the subcutaneous layer contains MCs (Figures 5 and 9). This observation is consistent with previous studies that MCs are rich at the various acupuncture points (Chen et al., 2008; Zhang et al., 2008). The scPVS located on the ventral midline of the abdominal space appears similar to the CV meridian. As shown in Figure 11, the distribution of the nodes, vessels, and sub-branches of the scPVS is in good agreement with the known features of the CV meridian.

The Hemacolor staining mainly used this experiment is a commercially available tool for rapid blood smears that permits good morphological judgment of cells, such as lymphocytes, monocytes, and neutrophilic granulocytes. The total process takes less than 10 min and can be done with prepared dyes without technical assistance (He and Chen, 2010). In this study, Hemacolor staining was used as a major diagnostic tool for the PVS because it was possible to identify the PVS *in situ* as well as its cellular properties and structures. In the case of trypan blue, which is a well-known dye that is widely used to identify PVS *in situ*, its use for elucidating detailed information about the cytology and anatomical structure of PVS is somewhat limited although it is easy and simple to use (Lim e al., 2013).

One of the limitation of this study is that scPVS was not always detected

as a uniform pattern or continuous threadlike structure after Hemacolor staining (Figures 4 and 11). This could have been due to differences in the depth of the scPVS from the surface of the abdominal subcutaneous tissue layer (Figures 4B and 4C, two-way dotted white arrows and open arrows). Alternatively, it could also have been be due to variations in the individual rat's genetic or health states. In addition, the sinus structure (Figures 7E and 7F) in the cross sectioned slice of the scPVS vessel was confirmed twice during the 11th attempt. This could have been due to differences in the vessel structures and the morphological denaturalization during the tissue sectioning and staining. Further studies are needed to fully understand these variations and detailed experimental conditions.

In this study, I showed that the PVS is present on the subcutaneous tissue layer, which is likely to be target sites or area of acupuncture stimulations. It is first to show that the scPVS can be identified in a specific region of the body, namely the abdominal midline in the subcutaneous tissue layer, and will help further study on the function of PVS in the body. For example, a selected part of a specific PVS could be damaged and then monitored for changes in physiological functions, and changes in the PVS in relation to changes in body states could be investigated (Wang et al., 2013), or the effect of specific acupuncture stimulation in relation to the changes in the selected PVS tissues

could be monitored. In addition, this study will also provide a base for the study on the role of PVS in innate immunity since MCs, rich in the PVS, are important in innate immune system phenotypic and function (Galli et al., 2011).

CONCLUSION

In this study, the presence of scPVS in abdominal subcutaneous tissue has been identified for the first time using the Hemacolor staining technique. The scPVS has major features in common with the well-established PVS tissue (i.e., osPVS) in terms of gross morphology and cellular/structural characteristics. The scPVS present on the midline of the abdominal subcutaneous tissue layer was also found to overlap with the CV meridian and its acupoints. This study is the first to show the presence of the PVS on the superficial tissues of the body. These findings may help to identify other scPVS tissues in the body and further elucidate their pathophysiological roles in healthy and disease states.

CHAPTER III

Ultrastructure of the subcutaneous primo-vascular system in rat abdomen

ABSTRACT

Recently, I identified the primo-vascular system (PVS), a novel vascular network, in rat subcutaneous tissues. Little is known about the subcutaneous PVS (scPVS). Here, I examined the ultrastructure of the scPVS in the hypodermis at the rat abdominal midline by electron microscopy. On the surface of scPVS, I observed three types of cells: microcells (5–6 μm), large elliptical cells (> 20 μm), and erythrocyte (3–4 μm). The inside of the scPVS was filled with numerous cells, which can be classified into three major groups: leucocytes, mast cells, and erythrocytes. The dense leucocytes and mast cells were easily noticed. The extracellular matrix of the scPVS was mainly composed of extensive fibers (79 ± 6.5 nm) tightly covered by micro- (0.5–2 μm) and nanoparticles (10–100 nm). In conclusion, the ultrastructural features, such as the resident cells on and in the scPVS and fiber meshwork covered by particles, indicate that scPVS might act as a circulatory channel for the flow and delivery of numerous cells and particles. These findings will help understand the nature of various scPVS beneath-the-skin layers and how they relate to acupuncture meridians.

INTRODUCTION

The primo-vascular system (PVS), which consists of primo-vessel (PV) and primo-node (PN), is a newly-discovered vascular tissue reported by Bong-Han Kim in the 1960s to be the classical acupuncture meridians. However, Kim's findings have not been reproduced until recently, mainly because the detailed experimental methods were not available. In the early 2000s, Dr. Soh's group rediscovered the part of the findings using dyes, such as alcian blue (Han et al., 2009; Huh et al., 2013; Lee et al., 2012) and trypan blue (Lim et al., 2009; Yoo et al., 2009), to visualize the PVS.

The PVS was confirmed in various tissues including the surface of abdominal organs (i.e., small intestine, large intestine, and liver) (Bae et al., 2013; Kim et al., 2011; Lee et al., 2013a), and blood vessels (Lee et al., 2004; Yoo et al., 2008), and lymphatic vessels (Jung et al., 2012). The organ surface PVS (osPVS) in the abdominal cavity of rats has been most extensively studied, because it is semitransparent, freely movable, and possible to recognize under a stereoscope (10–20x). The PVS afloat in the lymphatic vessels is not visible *in vivo* without a suitable staining dye (Lee at el., 2006). The osPVS has a bundle structure of several subducts, different from that of an lymphatic vessel with a

single tube (Lee et al., 2007; Shin et al., 2005). In addition, it has a unique cellular composition, high density of leucocytes and mast cells (MCs) (Kwon et al., 2012; Lee et al., 2007; Lim et al., 2013).

A recent study revealed that the PVS also exists in the abdominal subcutaneous tissue layer of rats using Hemacolor staining (Lim et al., 2015). The subcutaneous PVS (scPVS) was distributed at the conception vessel (CV) meridian and its acupoints (Lim et al., 2015), which are known to be located at the ventral midline connecting the umbilicus to the sternum (Yin et al., 2008). The scPVS had the morphological properties in common with the well-established osPVS tissue, which is composed of PVs and PNs that are frequently multiple-branched from each node form (Lee et al., 2009a; Shin et al., 2005; Soh, 2009). These findings correspond to Kim's initial report that the PVS in the skin is the anatomical entity of the acupuncture meridians (Kim, 1963). However, the understanding of the detailed structure and function of the scPVS tissue is limited.

Therefore, I investigated the various resident cells and extracellular matrix (ECM) of scPVS identified in the ventral midline of the hypodermis of rats by scanning and transmission electron microscopy. In addition, I compared the ultrastructural characteristics of the sc/osPVS and lymphatic vessel.

MATERIALS AND METHODS

Animal preparation

This study was performed on twelve Male Sprague-Dawley rats (5–7 weeks), which were purchased from Orient Bio Inc (Gyeonggi-do, Korea). The rats were kept in an isolator maintained at a constant temperature-controlled environment (22–26 °C) with atmospheric humidity range of 40–60% under a 12:12-h light-dark cycle (light on at 9:00 AM). All of the rats had *ad libitum* access to water and standard rodent chow until sacrifice. Every effort was conducted to minimize the number of rats and their suffering. All the experiments were performed in accordance with the Guide for the Laboratory Animal Care Advisory Committee of Seoul National University and approved by the Institute of Laboratory Animal Resource of Seoul National University (SNU-140926-2).

Isolation of osPVS and scPVS

For the surgical procedure, anesthesia of rats was induced by an anesthetic cocktail (Zoletil, 25 mg/kg; xylazine, 10 mg/kg) administered intramuscularly

to their right femoral regions. All surgical operations were performed under general anesthesia. With the rats under general anesthesia, after abdominal hair was removed with a razor blade, abdominal skin layer of each rat was incised along the linea alba. Then, three kinds of samples, scPVS, osPVS, and lymphatic vessels were harvested according to the following procedure. scPVS was revealed on the abdominal subcutaneous tissue layer using Hemacolor staining *in vivo* (Lim et al., 2015). Hemacolor dyes, a staining set widely used in blood smear for microscopy, consist of a three-solution system (Solution 1, methanol fixative; Solution 2, red-colored reagent for eosin staining; Solution 3, blue-colored reagent for methylene blue staining). Solution 1 was applied to the ventral hypodermis region of interest for 5 sec, and then Solutions 2 and 3 also applied to the same region one by one. After application of Solution 3, the dye solution were washed out using a 0.9% saline solution and I identified the dark blue-colored scPVS tissue. The observation of the osPVS were performed above the abdominal organs under a stereomicroscope (OSM-1, Dongwon, Korea). The osPVS is milky-colored, semitransparent, and freely movable (Lee et al., 2009a; Lim et al., 2013; Shin et al., 2005). Kreb solution (NaCl, 120.35 mM; $NaHCO_3$, 15.5 mM; glucose, 11.5 mM; KCl, 5.9 mM; $CaCl_2$, 2.5 mM; NaH_2PO_4, 1.2mM; and $MgSO_4$, 1.2mM) was added into the abdominal cavity to

prevent drying out of internal organs using a 1 mL syringe during the surgical procedure (Choi et al., 2011). Lymphatic vessels were collected around the caudal vena cava of a rats (Lee et al., 2006).

Scanning electron microscopy

For scanning electron microscopy (SEM), three kinds of isolated samples, scPVS, osPVS, and lymphatic vessels were maintained in paraformaldehyde for 1–2 days and primary fixated with Karnovsky's fixation at 4 °C for 2–4 hr. The samples were washed at 4 °C with 0.05M sodium cacodylate buffer three times for 10 min each, and post fixated at 4 °C with a mixture of 2% osmium tetroxide (1 mL) and 0.1M cacodylate buffer (1 mL) for 2 hr. After washing them with distilled water twice for 5 sec each, dehydration procedures is done in a graded series of ethanol starting at 30% then going to 50, 70, 80, 90, and 100% for 10 min each at room temperature. The samples were completely dried in a critical point dryer (CPD 030, BAL-TEC) for 30–60 min and the surfaces were coated with a sputter coater (EM ACE200, Leica). The resulting specimens were then observed under a field-emission SEM (SIGMA, Carl Zeiss, UK).

Transmission electron microscopy

For transmission electron microscopy (TEM), samples was treated in the same manner until the primary- and post fixation procedures of the SEM. After washing the samples with distilled water twice for 5 sec each, en bloc staining was performed with 0.5% uranyl acetate for 30 min at room temperature. Dehydration were carried out with a graded ethanol series (30–90% ethanol for 10 min each; 100% ethanol three times for 10 min each), and transition procedure was conducted with propylene oxide twice for 10 min each at room temperature. The samples were infiltrated with a mixture of propylene oxide (1 mL) and Spurr's resin (1 mL; ERL, vinyl cyclohexene dioxide; DER, diglycidyl ether polypropylene glycol; NSA, nonenyl succinic anhydride; DMAE, dimethylamino ethanol) for 2 hr, and then polymerized in a Spurr's resin (2 mL) at 70 °C for 24 hr on a rotator. The resulting specimens were sectioned per slice and observed under a TEM (JEM1010, JEOL, Japan) at 80 kV of acceleration voltage. The diameters of cells, fibers, and micro- and nanoparticles of the sc- and osPVS tissues were measured by ImageJ software (developed at the US National Institute of Health). All experimental data values are presented as mean ± standard errors.

RESULTS

General characteristics

The results of this study were obtained from the evaluation of the subcutaneous primo-vascular system (scPVS) from the abdominal hypodermis region and organ surface primo-vascular system (osPVS) on the serosal surface of internal organs (i.e., large intestine, small intestine, and liver) in the peritoneal cavity of rats. The scPVS was identified by Hemacolor staining *in vivo* (Lim et al., 2015), and osPVS was identified without staining (Lee et al., 2007; Lim et al., 2013). The sc- and osPVS isolated from surrounding tissues were used to investigate their ultrastructural characteristics by scanning and transmission electron microscopy.

The surface structure of the scPVS

Scanning electron microscopy (SEM) revealed the cytomorphology of the surface of the scPVS. The scPVS consisted of a subcutaneous primo-node (scPN) (Figure 1A, arrowhead) and a primo-vessel (scPV) (Figure 1D, arrow) part comprised of a bundle structure of several subducts or small tubes (Figure 1D, asterisks). Figure 1G illustrates the bundle structure (asterisks) of organ

Figure 1. SEM micrographs of resident cells on the subcutaneous PVS. (A, D, and G) Macroscopic structure of the scPN revealed by scanning electron microscopy ((A), 489.3 × 429.5 μm), scPV ((D), 212.1 μm), and osPV ((G), 207.6 μm). Note the bundle structure composed of subducts (asterisks) and large cells (open arrowheads). **(B, E, and H)** Magnified views (marked as squares in (A), (D), and (G)) of scPN (B), scPV (E), and osPV (H). Note the microcells (the majority, asterisks) and large elliptical cell (open arrowhead) on the surface of the scPN. **(C, F, and I)** Major resident cells on the surface of PVS including an elliptical cell ((C), open arrowhead, 28.1 × 19.2 μm), erythrocytes ((C), circle), and microcells ((F), arrow, 6.2 μm; (I), arrow, 5.1 μm). Note the fibers (arrowheads) and fluidic structures (asterisks) around the microcells.

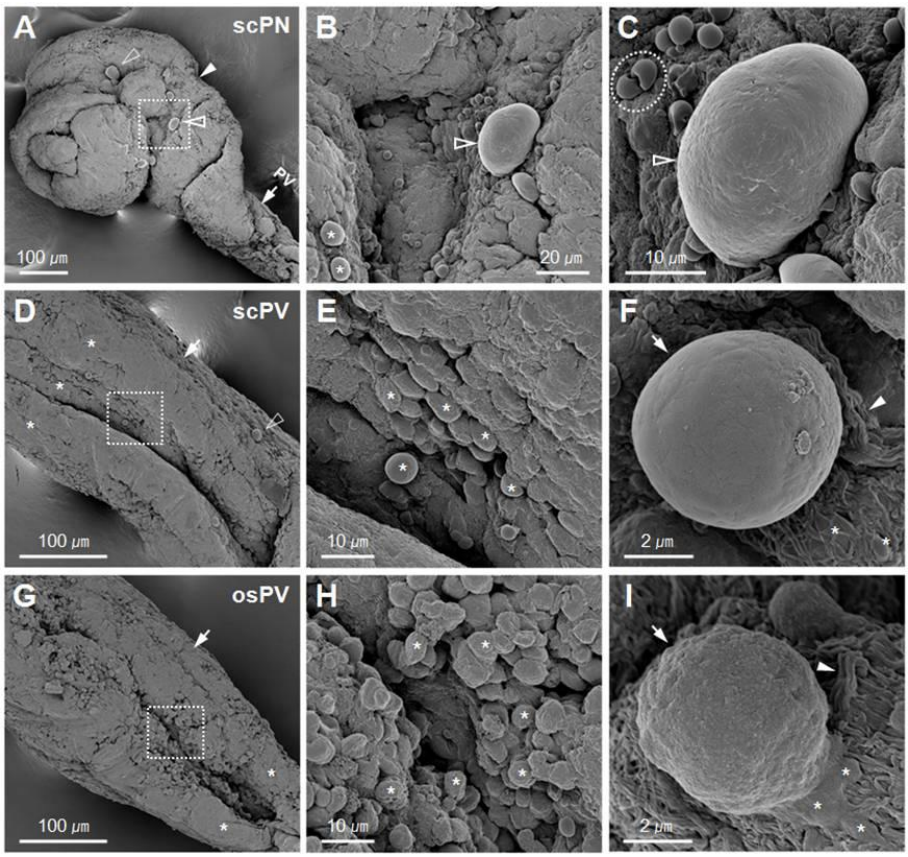
A
scPN
PV
100 μm
B
20 μm
C
10 μm
D
scPV
100 μm
E
10 μm
F
2 μm
G
osPV
100 μm
H
10 μm
I
2 μm

surface primo-vessel (osPV) revealed by SEM. The most abundant cells on the surface of the scPN and scPV were round microcells of 5–6 μm (Figures 1B and 1E, asterisks), which were also existed on the surface of the osPV (Figure 1H, asterisks). There were elliptical cells on the surface of the scPN, which are relatively larger than the microcells (Figure 1B, arrowhead). In addition, at a higher magnification view, I observed the biconcave disk-shaped erythrocytes (Figure 1C, dotted circle) on the surface of the scPN. Most of the resident cells on the surface of the scPVS belonged to one of three types: microcells, large elliptical cells (> 20 μm), and erythrocytes (3–4 μm). The surface texture of the scPV microcells was generally smooth (Figure 1F, arrow), whereas the osPV microcells were rough (Figure 1I, arrow). The fibers and fluidic structures were well developed at the bottom of the microcells in the extracellular matrix (ECM) of the sc- and osPV (Figures 1F and 1I, arrows and asterisks).

The cytomorphology inside the scPVS

To further confirm the cytomorphological features inside the scPVS, the tissue samples were cross-sectioned and observed by transmission electron microscopy (TEM). As shown in Figure 2A, the TEM revealed the composition of resident cells within the scPVS, which were mainly categorized into three

Figure 2. TEM micrographs of resident cells inside the subcutaneous PVS. **(A)** Typical example of resident cells inside scPV revealed by transmission electron microscopy. Note the leucocytes (arrows), mast cells (dotted lines), erythrocytes (asterisks), and secreted vesicles (arrowheads). **(B)** Normal mast cell with central nucleus (N) and surrounding uniform electron-dense granules (G). **(C)** Degranulated mast cell. Note that vesicles (V) swelled and became grainy. **(D)** Normal erythrocyte without a nucleus. **(E)** Neutrophil with three lobes of nucleus (N). **(F)** Eosinophil with two lobes of nucleus (N). **(G)** Lymphocyte with a nucleus (N) and nucleolus (Nu).

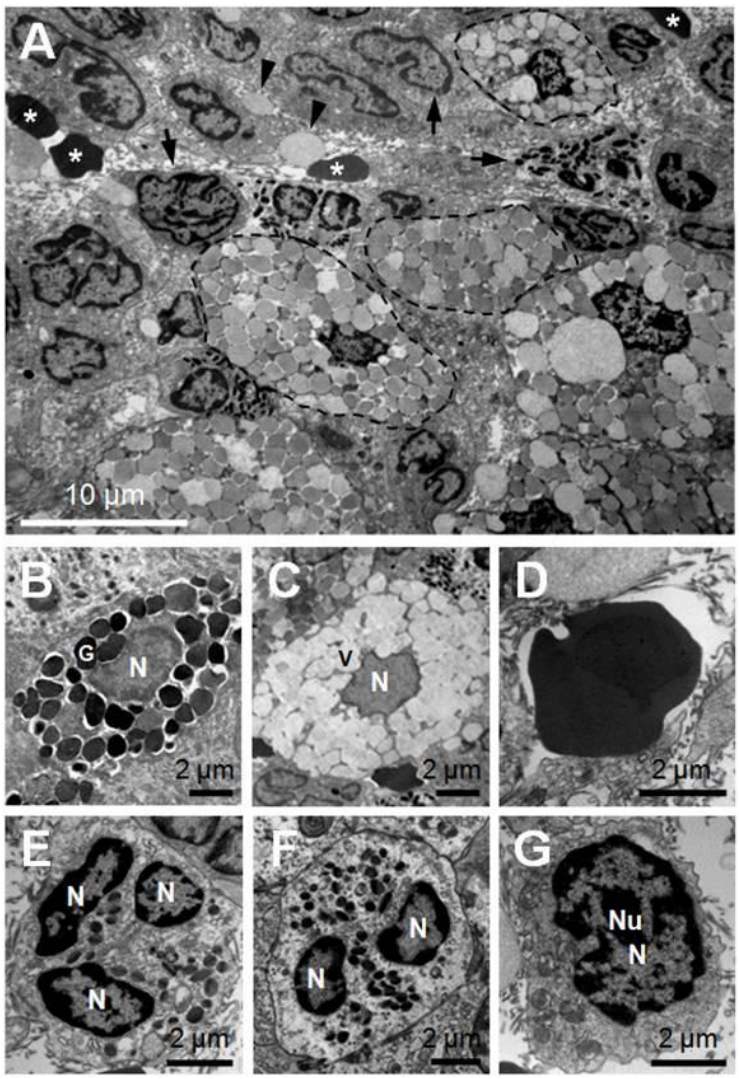
A
10 µm
B
G
N
2 µm
C
V
N
2 µm
D
2 µm
E
N
N
N
2 µm
F
N
N
2 µm
G
Nu
N
2 µm

groups based on their morphologies: mast cells (MCs, dotted lines), erythrocytes (asterisks), and leucocytes (arrowheads). The most abundant was the leucocyte group including neutrophils (Figure 2E) with multilobed nuclei, eosinophils (Figure 2F) with eosinophilic cytoplasmic granules, and lymphocytes (Figure 2G) with one nucleus and sparse cytoplasm. MCs were also rich, although less abundant than leucocyte group at PN slices. The MCs inside the scPVS were elliptical or elongated as are those observed in skin and muscle tissues (Căruntu et al., 2014; Zhang et al., 2008). Most MCs of the scPVS appeared degranulated (Figures 2A and 2C), whereas normal MCs with uniform electron-dense granules were also observed (Figure 2B).

The structure on extracellular matrix of the scPVS

To identify the ECM of the scPVS, I conducted high-magnified SEM. As shown in Figure 3, the ECM of scPVs consists of extensive and winding fiber structures and microparticles range of 0.5–2 μm (Figure 3A, asterisks), which were similar to those of the osPVs (Figure 3B). The microparticles appeared to sprout from inside the sc- and osPVs (Figures 4A and 4C, asterisks). The surface of the fiber structures and microparticles were tightly covered by nanoparticles (10–100 nm, Figures 4B and 4D, asterisks). There were round or

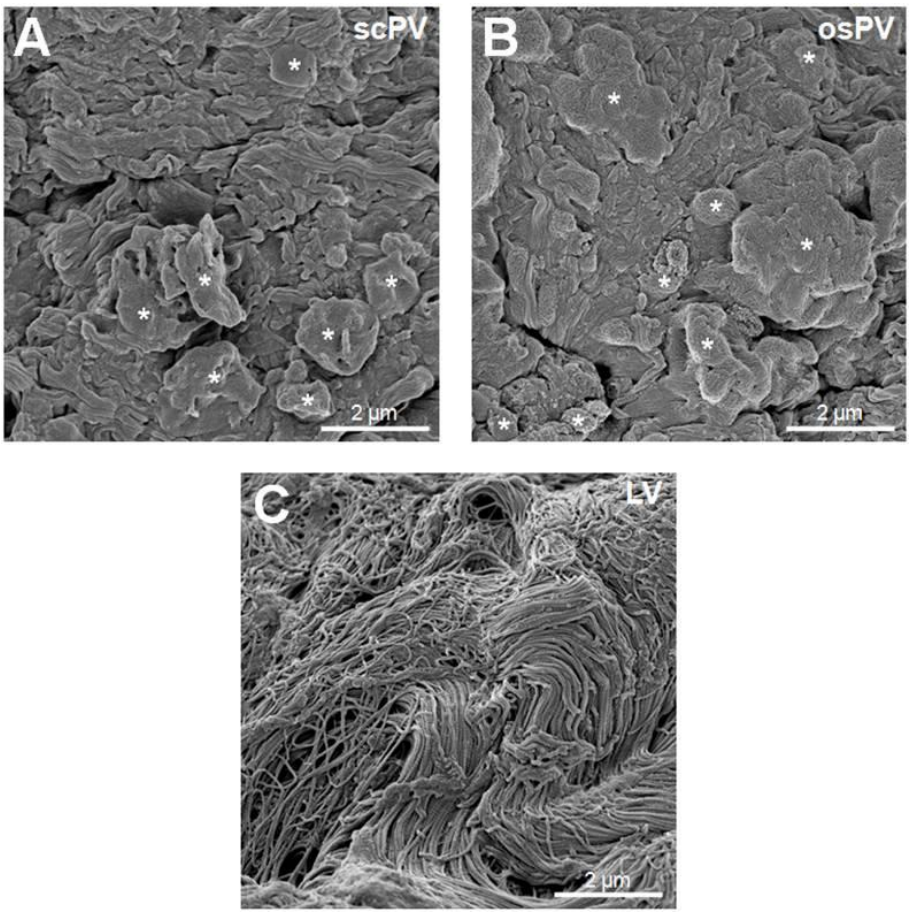

Figure 3. SEM micrographs of microparticles of the subcutaneous PV, organ surface PV, and lymphatic vessel. (A and B). Low magnification view on the surface of an scPV (A) and osPV (B). Note the dense fibrous structures that are randomly oriented in multiple directions and microparticles (0.5–2 µm; asterisks) covering the surface on the sc- and osPV. **(C)** Typical example of the fibrous structure on the surface of the lymphatic vessel.

Figure 4. SEM micrographs of extracellular matrix of the subcutaneous PV, organ surface PV, and lymphatic vessel. (A, C, and E) Comparison of fibrous structure on the scPV (A), osPV (C), and lymphatic vessel (LV, (E)). **(B, D, and F)** Magnified views (marked as squares in (A), (C), and (E)) of the fiber appearance on the scPV (B), osPV (D), and LV (E). Note that the diameters of the fibers within extracellular matrix in the scPV ((B), arrows, 76.4 nm) and the osPV ((D), arrows, 81.4 nm) are thicker than those of the LV ((F), arrows, 46.5 nm). Note also the regular stripes on the fibrous structure in the LV. The fiber structure of the scPV and the osPV have irregular surfaces containing nanoparticles (10–100 nm, (B) and (D), asterisks). There are openings in the fiber meshwork. ((B) and (F), circles).

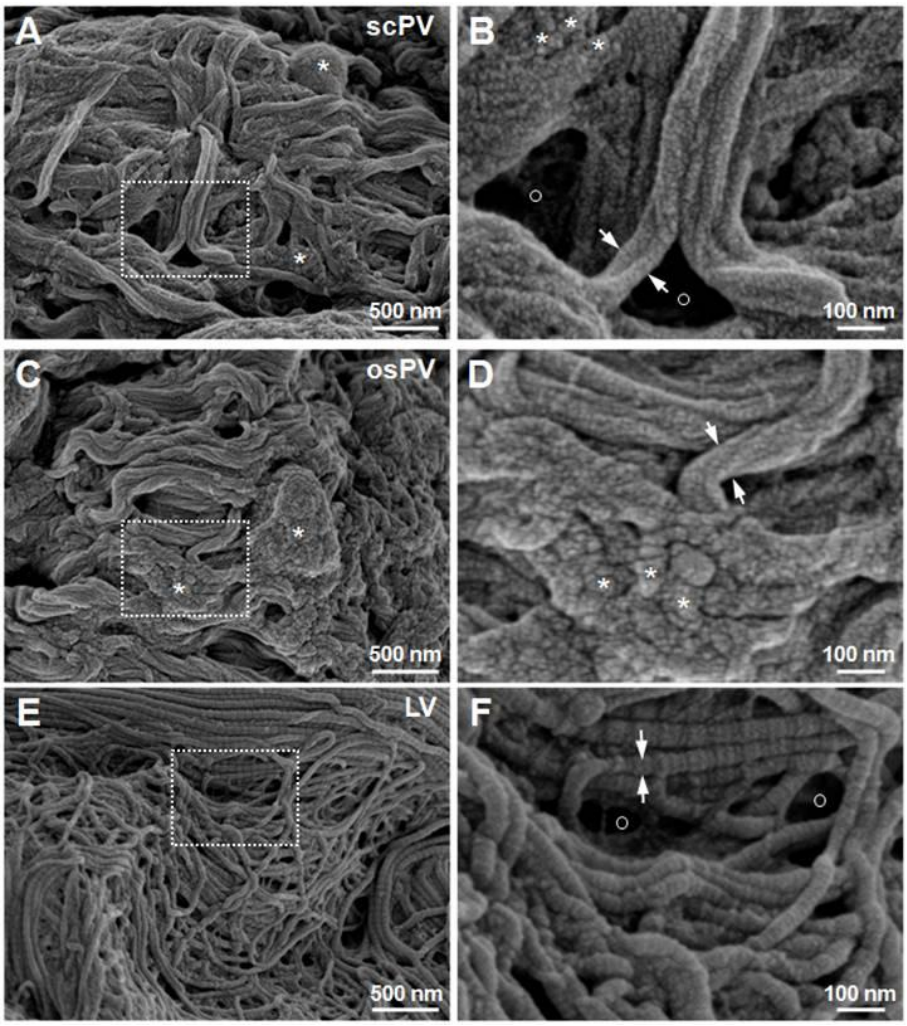
A
scPV
500 nm
B
100 nm
C
osPV
500 nm
D
100 nm
E
LV
500 nm
F
100 nm

triangular openings structures (~300 nm) in fiber meshwork in the sc- and osPVs. Lymphatic vessels also showed dense fibers and opening structures, but the micro- and nanoparticles were not well developed (Figures 3C, 4E, and 4F). The fiber diameter of the lymphatic vessels were smaller than those of PVs (scPVs, 79 ± 6.5 nm; osPVs, 83 ± 7.0 nm vs. lymphatic vessel, 48 ± 2.3 nm; n = 3; $p < 0.001$), and showed a periodic striped pattern (Figure 4F, arrows), whereas such a pattern was much less evident in PVs.

DISCUSSION

The major findings of this study are as follows: 1) the resident cells on the surface of the scPVS were mainly composed of the microcells (the majority), elliptical cells, and erythrocytes; 2) the resident cells inside the scPVS could be grouped into three types: mast cells, erythrocytes and leucocytes including the neutrophils, eosinophils, and lymphocytes; and 3) the ECM structure of the scPVS showed the fibers and microparticles (0.5–2 μm) covered with nanoparticles (10–100 nm). The above results regarding the ultrastructural characteristics of scPVS have many features in common with the existing osPVS, which were different from those of the lymphatic vessels.

This study newly revealed that there are at least three types of resident cells on the scPVS, and the cells are attached on the surface of the fibrous structure of the ECM. Among these, erythrocytes were easily identified by their size (3–4 μm) and concave form (Potter et al., 1997). Some microcells are likely to be stem cells, because similar microcells (3–5 μm) of the PVS inside the lymphatic vessels were recently identified as adult stem cells (Hwang et al., 2014; Lee et al., 2014). The detailed properties of other microcells remain to be studied further. The nature of the elliptical cells is presently unknown, although

they are similar to mast cells in elliptical shape and size (> 20 μm) (Lim et al., 2013).

The cell composition in the scPVS is in good agreement with previous reports (Lee et al., 2007; Lim et al., 2013; Lim et al., 2015). The presence of abundant leucocytes and mast cells indicates that the scPVS may play an important role in immune reaction. In addition, the scPVS seems to be related to a conception vessel meridian, the acupuncture meridian located at the ventral midline and midpoints in hypodermal region, in terms of the location and resident cells. They are both linearly distributed along the ventral midline in the hypodermis and contain high-density mast cells (Lim et al., 2015).

Other novel findings of the scPVS are the extensive fibrous structures and micro- and nanoparticles that appeared to have "sprouted" from the ECM of scPVs (Figures 3 and 4). These features were markedly different from those of lymphatic vessels, which are part of another circulating system. For example, the lymphatic vessels did not present the microparticles, and were less variable in the fiber diameter and more prominent in the fiber stripes. In this study, the scPVS was visible only after Hemacolor staining, which was successful in ~20% of the rats tested. Further study is needed to improve the reproducibility of sampling of scPVS tissue.

Taken together, the results demonstrate that ultrastructural features of the scPVS are similar to those of the osPVS, but different from lymphatic vessels. These findings indicate that the scPVS can function as a circulatory channel for the flow and delivery of various types of cells and particles to the body.

CONCLUSION

This study newly showed the ultrastructural characteristics of the scPVS in the subcutaneous tissue layer in rat abdomen using electron microscopy. Fibrous structures containing micro/nanoparticles and resident cells on the surface of and inside the scPVS are in good agreement with the known features of the osPVS, but different from those of the lymphatic vessels. In addition, microcells inside the scPVS are morphologically similar to the stem cells of the osPVS. This study help to confirm the unique properties among PVS group at the level of the extracellular matrix.

CHAPTER IV

Potential erythropoiesis in the primo-vascular system in heart failure

ABSTRACT

The primo-vascular system (PVS), composed of primo-nodes (PNs) and primo-vessels (PVs), has been identified in various animal models. However, little is known about its function. In this study, I investigated the changes in gross morphology and cellular composition of the organ surface PVS (osPVS) in rats with heart failure (HF) induced by myocardial infarction. The size of the PNs in rats with HF was larger than in Sham rats (1.87 vs. 0.80 mm^2; $P < 0.01$) and the density of osPVS per rat was greater for the HF rats (28 of 6 rats vs. 19 of 9 rats; $P < 0.01$). In addition, the osPVS number containing red chromophore was greater in HF rats ($P < 0.001$). The chromophore was identified as hemoglobin. Transmission electron microscopy and H&E staining revealed that the osPVS of HF rats possessed more red blood cells (RBCs) than that of the Sham rats ($P < 0.001$). In particular, the number of immature RBC increased in the HF rats (90.7 vs. 42.3%; $P < 0.001$). Altogether, the results showed that the osPVS in HF rats increased in its size, density, and the proportion of immature RBCs in the PNs, which may indicate that the PVS has erythropoietic activity. These study will help to elucidate the physiological roles of PVS in normal and disease states associated with HF.

INTRODUCTION

The primo-vascular system (PVS) was first reported in the 1960s by BH Kim as a novel vascular system corresponding to the acupuncture meridians (Kim, 1963). The PVS consists of primo-nodes (PNs) and primo-vessels (PVs). Its existence has been confirmed on the surface of abdominal organs (Kang et al., 2013b; Lee et al., 2013b; Tian et al., 2013), inside the lymphatic vessel (Jung et al., 2013; Lee et al., 2006), and in the subcutaneous tissue layer (Lim et al., 2015) in rats, mice, and rabbits (Lee et al., 2015; Park et al., 2015; Soh, 2009). Recently, the PVS was identified inside of a blood vessel in a human placenta (Lee et al., 2014a). In addition, various identification techniques were developed and applied to the PVS, such as the window chambers (Kim et al., 2016) and hollow gold nanospheres (Carlson et al., 2015).

The trend in PVS research over the past 5 years has focused mostly on developing new methods to visualize the PVS in lymphatic vessels (Jung et al., 2016; Kim et al., 2016), understanding the associations between PVS and acupuncture meridians (Jang et al., 2016; Lim et al., 2015), and identifying stem cells in the PVS (Hwang et al., 2014; Lee et al., 2014; Rai et al., 2015). These

studies were mainly performed on the PVS in normal, healthy rats. PVS was also examined in cancer animal models (Kang et al., 2013b; Yoo et al., 2010; Yoo et al., 2011); however, the changes in PVS under various disease conditions are not yet well understood. In this study, I aimed to study morphological changes in the osPVS of the rats with heart failure (HF). I chose the osPVS because it can be identified without staining, which is different from other PVS subtypes (Lim et al., 2013; Soh, 2009).

MATERIALS AND METHODS

Animal preparation

All animal experiments were performed in accordance with the Guide for the Laboratory Animal Care Advisory Committee of Seoul National University and approved by the Institute of Laboratory Animal Resource of Seoul National University (SNU-140926-2). Male Sprague-Dawley rats (5–7 weeks; n = 15, Orient Bio Inc., Gyeonggi-do, Korea) were used in this study and housed in an isolator (20–26 °C) under a 12-h light/dark schedule (light on at 9:00 AM) with water and food available *ad libitum* until sacrifice. Every effort was conducted to reduce the number of rats and their suffering during experimental periods.

Induction of heart failure

For the HF models, myocardial infarction was induced as described previously (Han et al., 2010b; Lee et al., 2013). Briefly, rats were anesthetized by intramuscular injection of an anesthetic cocktail (Zoletil, 25 mg/kg; xylazine, 10 mg/kg), and intubated for mechanical ventilation (Harvard Apparatus, Holliston, MA). After the left thoracotomy at the third intercostal space, the heart was exteriorized and the pericardium was carefully incised. The left descending

coronary artery was then ligated with 6-0 sterile silk suture at the level of tip of the auricle (Zhang et al., 2001). In the case of Sham models, the same surgical procedure was performed as the HF model except for the coronary artery ligation. The infarct size was measured as previously described (Han et al., 2010b; Lee et al., 2013). The rats with infarct size less than 30% were excluded from the analysis. In the three or four transverse sections (2 mm) of the heart, the infarct size was measured as ratio of the infarcted area to the mean left ventricular circumference with ImageJ software (developed at the National Institutes of Health) (Han et al., 2010b).

Identification of organ surface PVS

At 8 weeks after the surgery, osPVS was sampled under deep anesthesia. The rat abdomen was incised along the linea alba, and osPVS on the surface of abdominal organs, such as intestines, livers, and bladders, was sampled under a stereomicroscope (OSM-1, Dongwon, Korea) (Choi et al., 2011; Lim et al., 2013). I identified the osPVS from surrounding tissues according to the following criteria: milky-colored, semitransparent, and slightly flexible threadlike structure. In this study, I defined the PN as the part PVS tissue that is markedly thicker (> 1.7 folds) than that of PV connected (0.09–0.57 mm), and

excluded the tissue samples without a PN. The size of the PNs was estimated based on the area of the tissue image measured with ImageJ software.

Transmission electron microscopy and hematoxylin and eosin staining

For transmission electron microscopy (TEM), samples were primary- and post fixed, then underwent en bloc staining with 0.5% uranyl acetate for 30 min, and were then dehydrated with an ethanol series. The samples were kept in propylene oxide for 20 min, infiltrated with Spurr's resin overnight on a rotator, and observed by TEM (JEOL, JEM 1010, Japan) at 80 kV of acceleration voltage. The number of red blood cells (RBCs) was counted from 20 TEM images (90 × 70 μm) of the PNs at magnification of 400x. For the staining of cells in PNs, hematoxylin and eosin (H&E) staining was performed by conventional protocols. All data are expressed as mean ± standard error and the Student *t*-test or Fisher's test used to analyzed the data (GraphPad Prism version 5.0).

RESULTS

Comparison of the morphological properties of the osPVS from Sham and HF rats

The results were based on the 19 osPVS tissue samples from 9 Sham rats and 28 osPVS tissue samples from 6 HF rats. The mean infarct ratio of the heart was 38.0 ± 1.5% (n = 6) in the HF rats. As shown in Figure 1A, there was no difference in the detected location of the osPVS between Sham and HF rats. However, the total number of osPVS tissue samples per rat was increased by 2.2-times in the HF (n = 28) compared to the Sham rats (n = 19) (Figure 1B). Then, I investigated gross morphological changes of the osPVS tissues between the Sham and HF rats. Figure 2A shows a representative osPVS identified on the surface of the small intestine from Sham rats, which is composed of the primo vessel (PV) that connects the primo-nodes (PNs) of typical form. Figure 2B shows an enlarged PN attached to one end of a PV from the HF rats. The area of the PNs from the HF rats (1.87 ± 0.28 mm^2, n = 28) was significantly larger than the Sham rats (0.80 ± 0.09 mm^2, n = 19; $P < 0.01$) (Figure 2C). In addition, I often found a red chromophore inside some PNs and/or PVs. As illustrated in Figures 3A and 3B, when the osPVS tissues were considered in

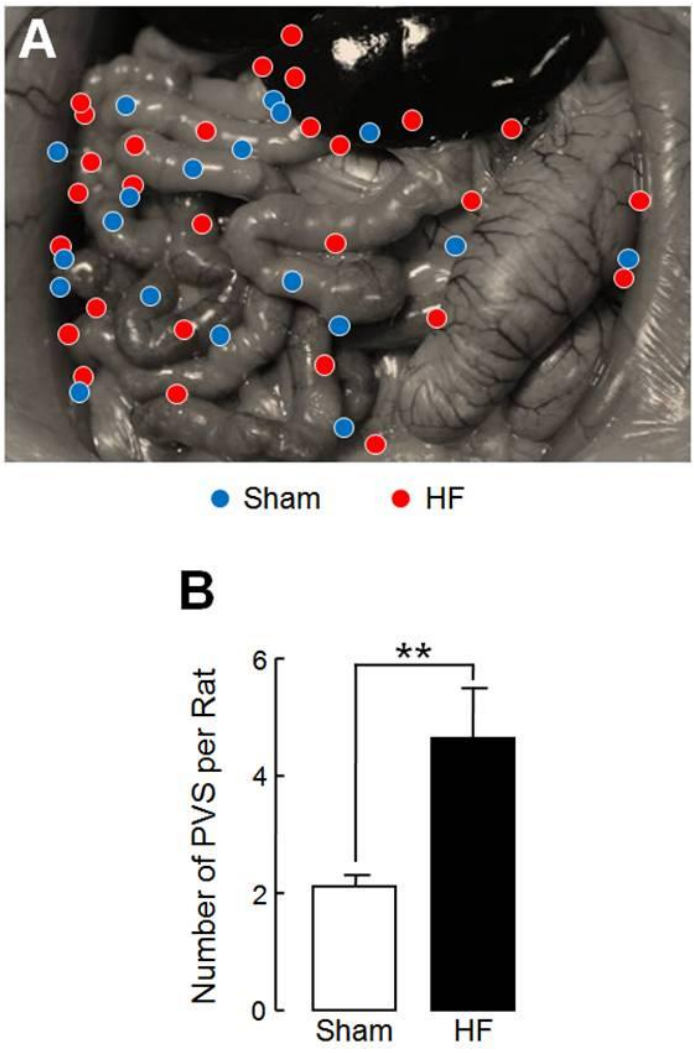

Figure 1. Comparison of the location and number of the osPVS of two groups from Sham and HF rats. (A) Detected locations of the osPVS tissues between Sham and HF rats. **(B)** Summary bar graph showing the mean number of osPVS tissues in Sham (n = 19 from 9 rats) and HF rats (n = 28 from 6 rats). Values are mean ± SEM. $^{**}P < 0.01$, by Student's t-test .

Figure 2. Comparison of the node size of the osPVS of two groups from Sham and HF rats. (A and B) Representative images of intact osPVS tissue composed of PNs (arrows) and PVs (arrowheads) identified on the surface of the intestines from Sham (A) and HF rats (B). Note the size of the primo-nodes ((A) and (B), insets) of Sham ((A), 0.91 × 0.77 mm) and HF rats ((B), 1.75 × 1.43 mm). Scale bars: 2 mm and 1 mm (insets). **(C)** Summary bar graph showing the area of PN in Sham (n = 19 from 9 rats) and HF rats (n = 28 from 6 rats). Values are mean ± SEM. $^{**}P < 0.01$, by Student's t-test .

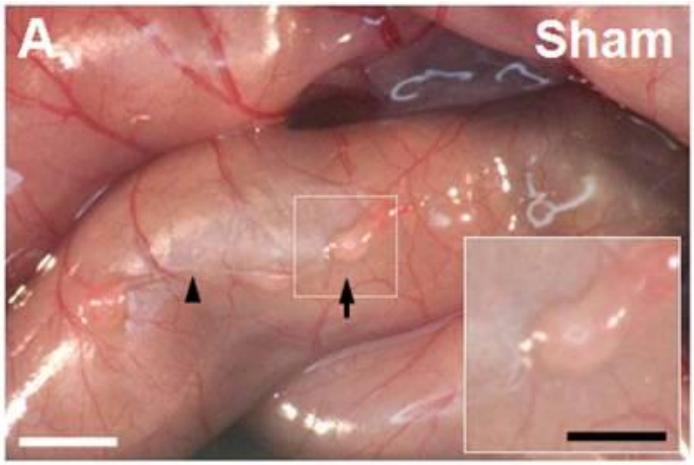
A
Sham

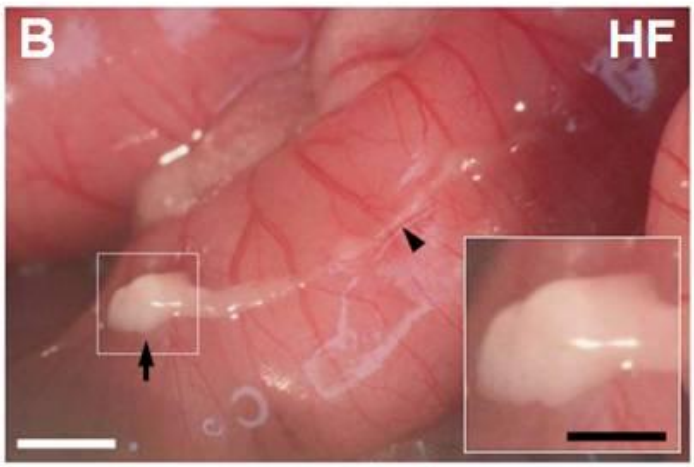
B
HF

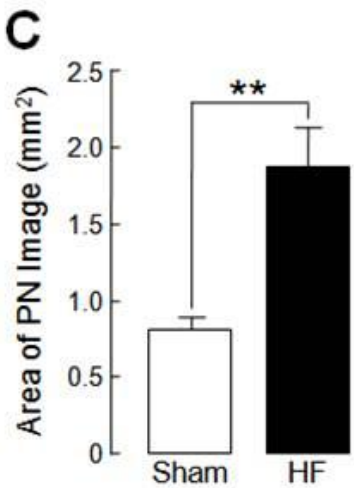
C
Area of PN Image (mm²)
2.5
2.0
1.5
1.0
0.5
0
**
Sham
HF

isolation, the osPVS number containing red chromophore was 4.0-times higher in the HF rats (n = 17, 60.7%) than Sham rats (n = 3, 15%) (Figure 3C). Figure 4 is the collection of all the PVS samples used in this study from Sham and HF rats .

Comparison of the cytological properties of the osPVS from Sham and HF rats

To further examine the red chromophore inside the PN and PV, I sectioned the PVS, stained with hematoxylin and eosin (H&E) dyes, and conducted transmission electron microscopy (TEM). Figures 5A and 5B illustrates typical examples of a PN slice (10 μm) stained with H&E. Inside of the PN of the HF rats, the cells with reddish cytoplasm were grouped together. The cell number and the red color intensity in the PN from the HF rats (Figure 5B, asterisks) were significantly greater than those of the Sham rats (Figure 5A, asterisks). As shown in Figures 6A and 6B, the TEM images showed many dark cells, which is typical for iron containing cells, such as erythrocytes and reticulocytes (asterisks). In the TEM images, mature and immature red blood cells (RBCs) displayed a rounded (Figures 6A and 6B, dotted circles) and a distorted shape (Figures 6A and 6B, dotted squares), respectively (Fukuta et al., 2007). The

Figure 3. Comparison of the red chromophore within the osPVS of two groups from Sham and HF rats. (A and B) Collection of isolated PVS specimens in saline solution from Sham (A) and HF rats (B). **(C)** Summary bar graphs showing the proportion of osPVS containing a red chromophore in Sham (n = 19 from 9 rats) and HF rats (n = 28 from 6 rats). Values are mean ± SEM. ***$P < 0.001$, by Fisher's test.

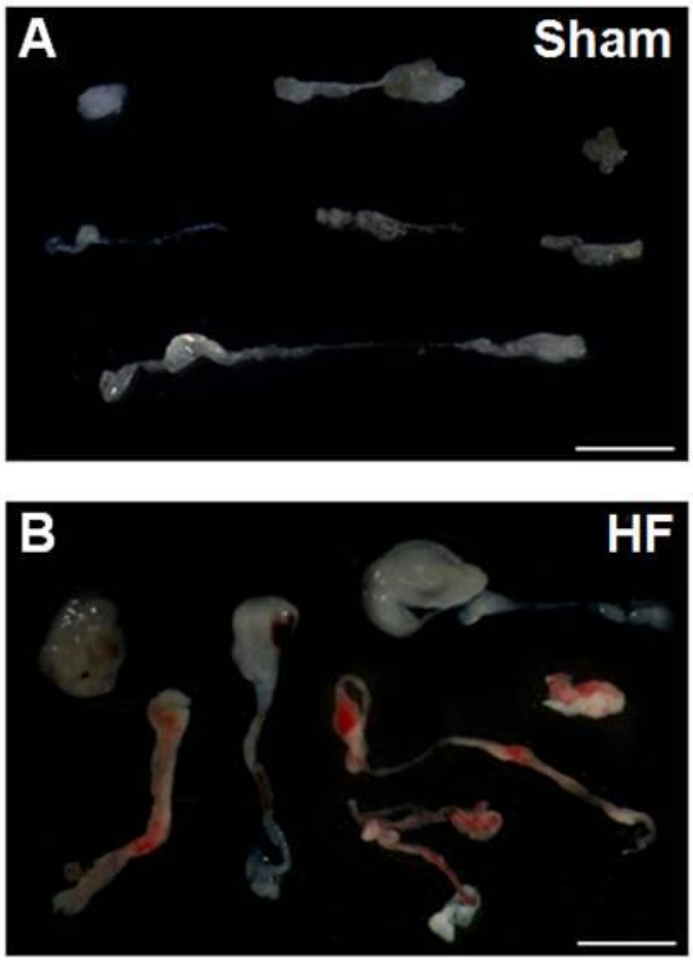
A
Sham
B
HF
C
Uncolored
Red-colored
***
Red-colored PVS (%)
100
80
60
40
20
0
Sham
HF

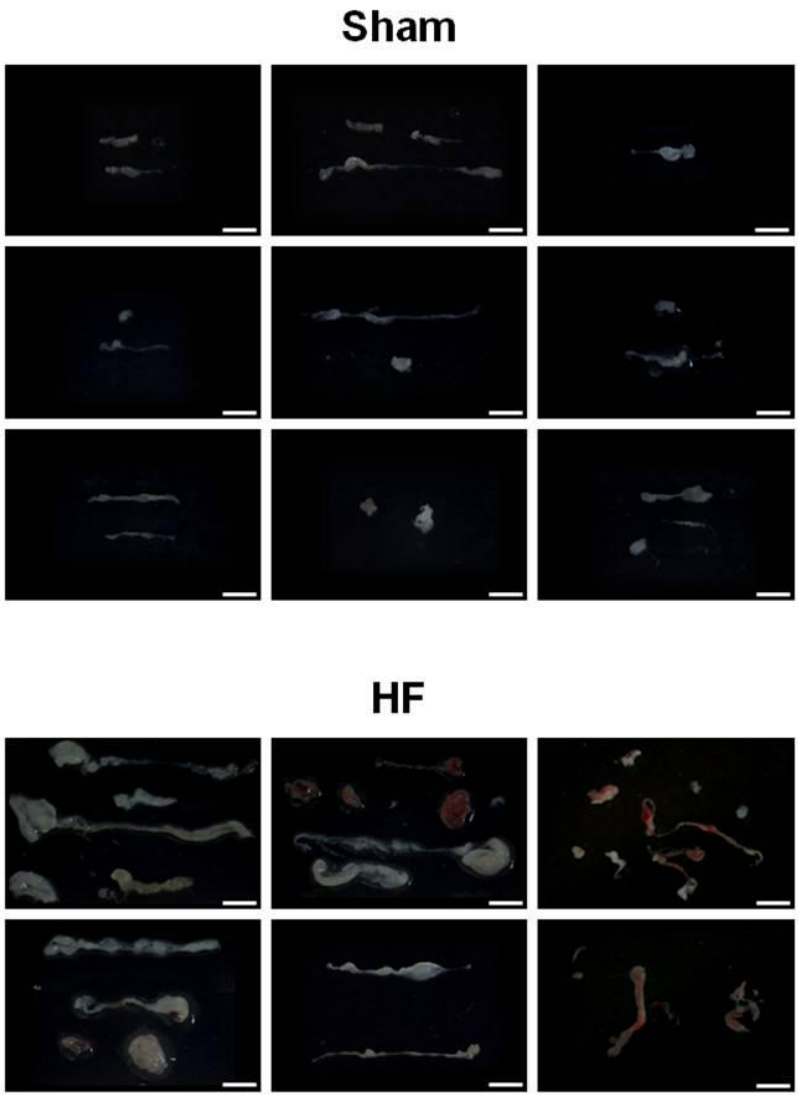

Figure 4. Collection of all the PVS samples isolated from Sham and HF rats.

Each image means PVS samples obtained from one rat. Scale bars: 2 mm.

Figure 5. Comparison of the H&E image of the osPVS between Sham and HF rats. (A and B) Representative images (400x) of the cross-sectioned PN slice (10 μm) stained by H&E from Sham (A) and HF rats (B). Insets in (A) and (B) represent whole PN slices at low magnification (40x). Note the intensity of red chromophore is more clearly revealed in the PN from HF rats ((B), asterisks) than Sham rats ((A), asterisks). Scale bars: 50 μm and 200 μm (insets). **(C)** Representative images of the isolated primo-vessel revealed by H&E staining from HF rats. Note the red chromophore is clearly revealed in the PV part (asterisks). Scale bars: 100 μm.

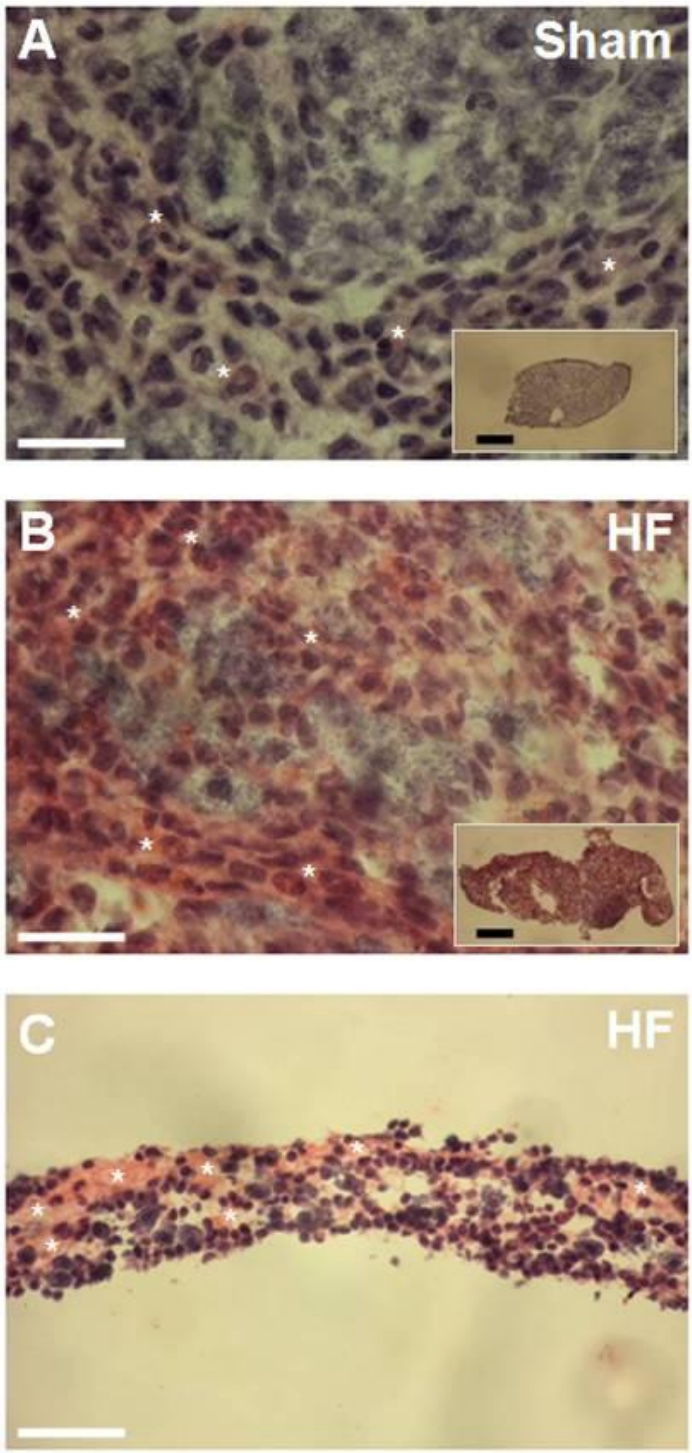
A
Sham
B
HF
C
HF

number of mature and immature RBCs per osPVS of the HF rats was increased by 12.6-times of those of Sham rats (Figure 6C). Such difference was largely due to the increased number of immature RBCs in the HF rats (Sham, 42.3% vs. HF, 90.7%; $P < 0.001$) (Figure 6D).

Figure 6. Comparison of the number and proportion of the RBC in the osPVS between Sham and HF rats. (A and B) Representative TEM images of a PN slice showing RBCs (asterisks), mast cells (arrows), and white blood cells (arrowheads) from Sham (A) and HF rats (B). RBCs in dotted circles are mature RBCs and RBCs in dotted squares are immature RBCs. Scale bars: 10 μm. **(C)** Summary bar graphs showing the mean number of RBC in osPVS in Sham (n = 3 from 3 rats) and HF rats (n = 3 from 3 rats). Individual RBCs in osPVS were counted from 20 rectangular fields (90 × 70 μm) in a TEM micrograph of the osPVS tissues. **(D)** Summary bar graphs showing the proportion of mature and immature RBCs in osPVS from Sham and HF rats. Values are mean ± SEM. ***$P < 0.001$, by Student's t-test or Fisher's test.

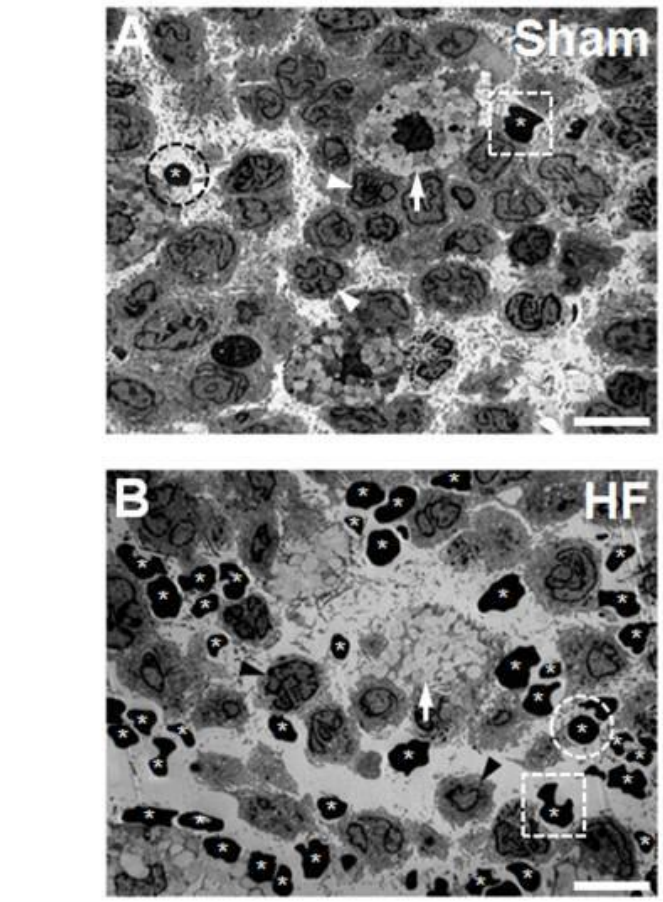
A
Sham
B
HF

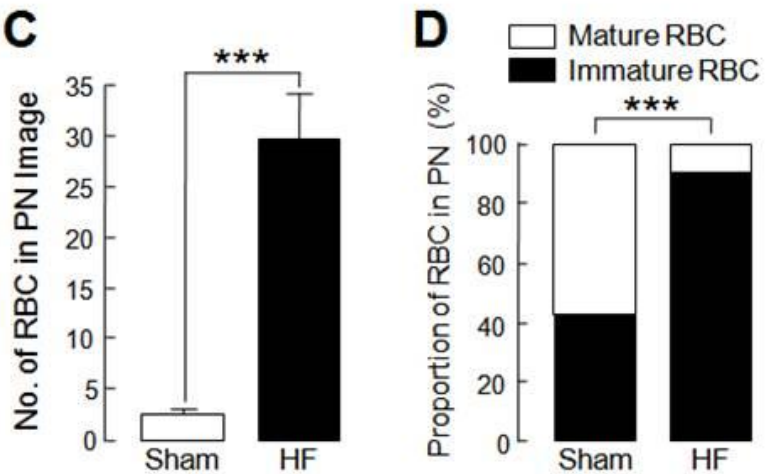
C
No. of RBC in PN Image
35
30
25
20
15
10
5
0
***
Sham
HF
D
Mature RBC
Immature RBC
Proportion of RBC in PN (%)
100
80
60
40
20
0
***
Sham
HF

DISCUSSION

Major findings of this study can be summarized as follows: the osPVS in the HF rats showed increases in the following parameters, 1) the PN size (in terms of the area): 2.1-times, 2) osPVS number per rat: 2.2-times, 3) total RBC number: 12.6-times, and 4) ratio of immature to mature RBCs: 2.1-times. These morphological and cytological changes indicate that significant erythropoiesis occurred inside the PN and PV of osPVS from the HF rats.

It is well-known that HF predisposes an individual to infections and anemia due to decreased hematopoiesis in bone marrow (Iversen et al., 2002). Chronic anemia or heart failure potentially precipitates extramedullary hematopoiesis, which occurs in the liver, spleen, lymph nodes, and hearts in HF (Goldman et al., 2001; Orphanidou-Vlachou et al., 2014). Therefore, it may suggest that the erythropoiesis inside the PN and PV in HF rats also resulted from the compensatory extramedullary hematopoiesis.

The existence of erythrocytes in the PVS of healthy rats was shown in my previous study (Lim et al., 2013). The present study further demonstrates that PVS contains reticulocytes, which normally constitute approximately 1% of the total number of circulating erythrocytes (Junqueira and carneiro, 2003). The

high percentage of reticulocytes (42.3% in Sham rats) is a unique feature of the osPVS. These observations are in agreement with BH Kim's report, in that PNs inside the blood vessels increased in its size (1.5–2-times), density, and the number of mature and immature RBCs in the anemic rabbits (Kim, 1965b). In the anemia model, Soh (2009) also stated that the PVS became thicker and easier to detect. Recently, Kwon et al. (2015) showed the presence of hematopoietic progenitor cells in the PVS. These findings strongly suggest that the PVS can function as a hematopoietic organ, which was claimed by BH Kim in 1965. More studies are required to further understand detailed mechanisms of the changes in the osPVS in HF and the role of the PVS in erythropoiesis in normal and disease states.

CONCLUSION

This study demonstrated for the first time the morphological and cytological changes of the PN and PV of the osPVS from a rat model of HF. There are distinct increase in the proportion of mature and immature erythrocytes in osPVS as well as size and density of osPVS in HF rats. Understanding the mechanism of HF-induced erythropoiesis changes in the PVS may help further elucidate the pathophysiology of the diseases associated with HF.

GENERAL CONCLUSION

The majority of studies thus far have mainly focused on aspects of observing PVS in various sites in the body, and little has been confirmed about detailed structure and functions of PVS. In this study, my findings showed that Hemacolor staining is useful to rapidly identify the morphological and cytological properties of PVS (Chapter I). Newly identified PVS in the subcutaneous rat abdomen tissue layers provides good agreement with the known features of the acupuncture points and meridians (i.e., the conception vessel) in terms of its distribution and the abundance of degranulated mast cells (Chapter II). The extracellular matrix of the PVS was mainly composed of extensive fibers tightly covered by micro- and nanoparticles in a characteristically different form to that of lymphatic vessels (Chapter III). In addition, the PVS showed larger values in its size (in terms of area), density, and the number of mature/immature RBC in heart failure rats compared to Sham rats, indicating the occurrence of erythropoiesis in the PVS tissue (Chapter IV).

In conclusion, the present study provides various useful experimental approaches for the identification and characterization of the hallmarks and functions of PVS, and it can be applied in a variety of PVS subtypes. These findings will help to further elucidate the potential physiological roles of PVS in the body.

REFERENCES

An, P., Dai, J., Su, Z., Yoo, J.S., Qu, R., Lee, S.W., Eom, K.H., Bae, K.H., Luo, H., Soh, K.S., 2010. Putative primo-vascular system in mesentery of rats. J Acupunct Meridian Stud. 3, 232-240.

Bae, K.H., Park, S.H., Lee, B.C., Nam, M.H., Yoon, J.W., Kwon, H.M., Yoon, S.Z., 2013. Novel threadlike structures may be present on the large animal organ surface: evidence in Swine model. Evid Based Complement Alternat Med. 5 pages Article ID 758763.

Baik, K.Y., Ogay, V., Jeoung, S.C., Soh, K.S., 2009. Visualization of Bonghan microcells by electron and atomic force microscopy. J Acupunct Meridian Stud. 2, 124-129.

Carlson, E., Perez-Abadia, G., Adams, S., Zhang, J.Z., Kang, K.A., Maldonado, C., 2015. A Novel Technique for Visualizing the Intralymphatic Primo Vascular System by Using Hollow Gold Nanospheres. J Acupunct Meridian Stud. 8, 294-300.

Căruntu, C., Boda, D., Musat, S., Căruntu, A., Mandache, E., 2014. Stress-induced mast cell activation in glabrous and hairy skin. Mediators Inflamm. 9 pages Article ID 105950.

Cerri, P.S., Pereira-Júnior, J.A., Biselli, N.B., Sasso-Cerri, E., 2010. Mast cells and MMP-9 in the lamina propria during eruption of rat molars: quantitative and immunohistochemical evaluation. J Anat. 217, 116-125.

Chen, H.N., Lin, J.G., Yang, A.D., Chang, S.K., 2008. Safe depth of abdominal acupoints in pediatric patients. Complement Ther Med. 16, 331-335.

Choi, J.H., Lim, C.J., Han, T.H., Lee, S.K., Lee, S.Y., Ryu, P.D., 2011. TEA-sensitive currents contribute to membrane potential of organ surface primo-node cells in rats. J Membr Biol. 239, 167-175.

Darzynkiewicz, Z., Kapuscinski, J., Traganos, F., Crissman, H.A., 1987. Application of pyronin Y(G) in cytochemistry of nucleic acids. Cytometry. 8, 138-145.

Eroschenko, V.P., 2008. DiFiore's atlas of histology with functional correlations. Lippincott Williams & Wilkins, 11th edition.

Fukuta, K., Orui, T., Tanaka, K., 2007. Novel erythrocyte pits in the small tropical ruminant, lesser mouse deer. Anat Histol Embryol. 36, 424-427.

Galli, S.J., Borregaard, N., Wynn, T.A., 2011. Phenotypic and functional plasticity of cells of innate immunity: macrophages, mast cells and neutrophils. Nat Immunol. 12, 1035-1044.

Goldman, B.I., Wurzel, J., 2001. Hematopoiesis/erythropoiesis in myocardial infarcts. Mod Pathol. 14, 589-594.

Goudy, S., Law, A., Sanchez, G., Baldwin, H.S., Brown, C., 2010. Tbx1 is necessary for palatal elongation and elevation. Mech Dev. 127, 292-300.

Han, H.J., Ogay, V., Park, S.J., Lee, B.C., Kim, K.W., Lee, Y.W., Lee, J.K., Soh, K.S., 2010. Primo-vessels as new flow paths for intratesticular injected dye in rats. J Acupunct Meridian Stud. 3, 81-88.

Han, H.J., Sung, B., Ogay, V., Soh, K.S., 2009. The flow path of alcian blue from the acupoint BL23 to the surface of abdominal organs. J Acupunct Meridian Stud. 2, 182-189.

Han, T.H., Lim, C.J., Choi, J.H., Lee, S.Y., Ryu, P.D., 2010a. Viability assessment of primo-node slices from organ surface primo-vascular tissues in rats. J Acupunct Meridian Stud. 3, 241-248.

Han, T.H., Lee, K., Park, J.B., Ahn, D., Park, J.H., Kim, D.Y., Stern, J.E., Lee, S.Y., Ryu, P.D., 2010b. Reduction in synaptic GABA release contributes to target-selective elevation of PVN neuronal activity in rats with myocardial infarction. Am J Physiol Regul Integr Comp Physiol. 299, R129-R139.

He, T.F., Chen, Y.F., 2010. Advances in studies on the correlation between acupuncture-moxibustion treatment and mast cells. Zhongguo Zhen Jiu. 30, 84-87.

Huh, H., Lee, B.C., Park, S.H., Yoon, J.W., Lee, S.J., Cho, E.J., Yoon, S.Z., 2013. Composition of the extracellular matrix of lymphatic novel

threadlike structures: is it keratin? Evid Based Complement Alternat Med. 6 pages Article ID 195631.

Hwang, S., Lee, S.J., Park, S.H., Chitteti, B.R., Srour, E.F., Cooper, S., Hangoc, G., Broxmeyer, H.E., Kwon, B.S., 2014. Nonmarrow hematopoiesis occurs in a hyaluronic-acid-rich node and duct system in mice. Stem Cells Dev. 23, 2661-2671.

Hwang, Y.C., 1992. Anatomy and classification of acupoints. Probl Vet Med. 4, 12-15.

Iversen, P.O., Woldbaek, P.R., Tønnessen, T., 2002. Decreased hematopoiesis in bone marrow of mice with congestive heart failure. Am J Physiol Regul Integr Comp Physiol. 282, R166-172.

Jamur, M.C., Moreno, A.N., Mello, L.F., Souza Júnior, D.A., Campos, M.R., Pastor, M.V., Grodzki, A.C., Silva, D.C., Oliver, C., 2010. Mast cell repopulation of the peritoneal cavity: contribution of mast cell progenitors versus bone marrow derived committed mast cell precursors. BMC Immunol.

Jang, H., Yoon, J., Gil, H., Jung, S.J., Kim, M.S., Lee, J.K., Kim, Y.J., Soh, K.S., 2016. Observation of a Flowing Duct in the Abdominal Wall by Using Nanoparticles. PLoS One. 11, e0150423.

Jia, Z.F., Soh, K.S., Zhou, Q., Dong, B., Yu, W.H., 2011. Study of novel threadlike structures on the intestinal fascia of dogs. J Acupunct Meridian Stud. 4, 98-101.

Jones, J.S., 1987. Pathology of the mesothelium. London: Springer-Verlag.

Jung, S.J., Bae, K.H., Nam, M.H., Kwon, H.M., Song, Y.K., Soh, K.S., 2013. Primo vascular system floating in lymph ducts of rats. J Acupunct Meridian Stud. 6, 306-318.

Jung, S.J., Cho, S.Y., Bae, K.H., Hwang, S.H., Lee, B.C., Kim, S., Kwon, B.S., Kwon, H.M., Song, Y.K., Soh, K.S., 2012. Protocol for the observation of the primo vascular system in the lymph vessels of rabbits. J Acupunct Meridian Stud. 5, 234-240.

Jung, S.J., Gil, H., Kim, D.H., Kim, H.L., Kim, S., Soh, K.S., 2016. Ultrastructure of a Mobile Threadlike Tissue Floating in a Lymph Vessel. Evid Based Complement Alternat Med. 5 pages Article ID 3064072.

Junqueira, L.C., Carneiro, J., 2003. Basic histology. 10th edition. Lange medical books McGraw-Hill.

Kang, K.A., 2013a. Historical observations on the half-century freeze in research between the Bonghan system and the primo vascular system. J Acupunct Meridian Stud. 6, 285-292.

Kang, K.A., Maldonado, C., Perez-Aradia, G., An, P., Soh, K.S., 2013b. Primo vascular system and its potential role in cancer metastasis. Adv Exp Med Biol. 789, 289-296.

Keisari, Y., 1992. A colorimetric microtiter assay for the quantitation of cytokine activity on adherent cells in tissue culture. J Immunol Methods. 146, 155-161.

Kim, B.H., 1962. Study on the reality of acupuncture meridians. J Acad Med Sci DPR Korea. 9, 5-13.

Kim, B.H., 1963. On the kyungrak system. J Acad Med Sci DPR Korea. 108, 1-41.

Kim, B.H., 1965a. Sanal theroy. J Acad Med Sci DPR Korea. 108, 39-62

Kim, B.H., 1965b. Sanal and hematopoiesis. J Acad Med Sci DPR Korea. 108, 1-6.

Kim, J., Kim, D.H., Jung, S.J., Gil, H.J., Yoon, S.Z., Kim, Y.I., Soh, K.S., 2016. Monitoring the primo vascular system in lymphatic vessels by using window chambers. Biomed Opt Express. 7, 1251-1259.

Kim, S.R., Lee, S.K., Jang, S.H., Choi, J.H., Lee, B.C., Hwang, I.K., Lee, S.Y., Ryu, P.D., 2011. Expression of keratin 10 in rat organ surface primo-vascular tissues. J Acupunct Meridian Stud. 4, 102-106.

Kwon, B.S., Ha, C.M., Yu, S., Lee, B.C., Ro, J.Y., Hwang, S., 2012. Microscopic nodes and ducts inside lymphatics and on the surface of

internal organs are rich in granulocytes and secretory granules. Cytokine. 60, 587-592.

Lee, B.C., Baik, K.Y., Johng, H.M., Nam, T.J., Lee, J., Sung, B., Choi, C., Park, W.H., Park, E.S., Park, D.H., Yoon, Y.S., Soh, K.S., 2004. Acridine orange staining method to reveal the characteristic features of an intravascular threadlike structure. Anat Rec B New Anat. 278, 27-30.

Lee, B.C., Jhang, S.U., Choi, J.H., Lee, S.Y., Ryu, P.D., Soh, K.S., 2009a. DiI staining of fine branches of Bonghan ducts on surface of rat abdominal organs. J Acupunct Meridian Stud. 2, 301-305.

Lee, B.C., Kim, K.W., Soh, K.S., 2009b. Visualizing the network of Bonghan ducts in the omentum and peritoneum by using Trypan blue. J Acupunct Meridian Stud. 2, 66-70.

Lee, B.C., Kim, S., Soh, K.S., 2008. Novel anatomic structures in the brain and spinal cord of rabbit that may belong to the Bonghan system of potential acupuncture meridians. J Acupunct Meridian Stud. 1, 29-35.

Lee, B.C., Lee, H.S., Yun, J.E., Kim, H.A., 2013a. Evidence for the fusion of extracellular vesicles with/without DNA to form specific structures in fertilized chicken eggs, mice and rats. Micron. 44, 468-474.

Lee, B.C., Soh, K.S., 2010. Visualization of acupuncture meridians in the hypodermis of rat using Trypan blue. J Acupunct Meridian Stud. 3, 49-52.

Lee, B.C., Sung, B., Eom, K.H., Park, E.S., Kim, M.S., Kim, S.H., Ogay, V., Kim, K.W., Ryu, Y., Yoon, Y.S., Soh, K.S., 2013b. Novel threadlike structures on the surfaces of mammalian abdominal organs are loose bundles of fibrous stroma with microchannels embedded with fibroblasts and inflammatory cells. Connect Tissue Res. 54, 94-100.

Lee, B.C., Yoo, J.S., Ogay, V., Kim, K.W., Dobberstein, H., Soh, K.S., Chang, B.S., 2007. Electron microscopic study of novel threadlike structures on the surfaces of mammalian organs. Microsc Res Tech. 70, 34-43.

Lee, B.S., Lee, B.C., Park, J.E., Choi, H.K., Choi, S.J., Soh, K.S., 2014a. Primo vascular system in human umbilical cord and placenta. J Acupunct Meridian Stud. 7, 291-297.

Lee, C., Seol, S.K., Lee, B.C., Hong, Y.K., Je, J.H., Soh, K.S., 2006. Alcian blue staining method to visualize Bonghan threads inside large caliber lymphatic vessels and x-ray microtomography to reveal their microchannels. Lymphat Res Biol. 4, 181-190.

Lee, H.R., Rho, M.S., Hong, Y.J., Ha, Y.E., Kim, J.Y., Noh, Y.I., Park, D.Y., Kim, C.K., Kim, E.J., Jang, I.H., Kang, S.Y., Lee, S.S., 2015. Primo Vessel Stressed by Lipopolysaccharide in Rabbits. J Acupunct Meridian Stud. 8, 301-306.

Lee, H.S., Lee, B.S., 2012. Visualization of the network of primo vessels and primo nodes above the pia mater of the brain and spine of rats by using Alcian blue. J Acupunct Meridian Stud. 5, 218-225.

Lee, H.W., Han, T.H., Yi, K.J., Choi, M.C., Lee, S.Y., Ryu, P.D., 2013. Time course of diurnal rhythm disturbances in autonomic function of rats with myocardial infarction. Auton Neurosci. 179, 28-36.

Lee, S.J., Park, S.H., Kim, Y.I., Hwang, S., Kwon, P.M., Han, I.S., Kwon, B.S., 2014. Adult stem cells from the hyaluronic acid-rich node and duct system differentiate into neuronal cells and repair brain injury. Stem Cells Dev. 23, 2831-2840.

Lim, C.J., Lee, S.Y., Ryu, P.D., 2015. Identification of Primo-Vascular System in Abdominal Subcutaneous Tissue Layer of Rats. Evid Based Complement Alternat Med. 13 pages Article ID 751937.

Lim, C.J., Yoo, J.H., Kim, Y., Lee, S.Y., Ryu, P.D., 2013. Gross morphological features of the organ surface primo-vascular system revealed by hemacolor staining. Evid Based Complement Alternat Med. 13 pages Article ID 350815.

Lim, J., Chae, M., Kim, J., Sohn, J., Soh, K.S., 2009. Development of a laparoscopic system for in vivo observation of the Bonghan structure. J Acupunct Meridian Stud. 2, 248-252.

Lim, J., Jung, J.H., Lee, S., Su, Z., Qiang, Z., Cha, J.M., Lee, J.K., Soh, K.S., 2011. Estimating the density of fluorescent nanoparticles in the primo vessels in the fourth ventricle and the spinal cord of a rat. J Biomed Opt.

Lua, I., Asahina, K., 2016. The Role of Mesothelial Cells in Liver Development, Injury, and Regeneration. Gut Liver. 10, 166-176.

Ma, P., Villanueva, T.G., Kaufman, D., Gillooley, J.F., 1984. Respiratory cryptosporidiosis in the acquired immune deficiency syndrome. Use of modified cold Kinyoun and Hemacolor stains for rapid diagnoses. JAMA. 252, 1298-1301.

Metcalfe, D.D., Baram, D., Mekori, Y.A., 1997. Mast cells. Physiol Rev. 77, 1033-79.

Mizuno, K., Tolmachova, T., Ushakov, D.S., Romao, M., Abrink, M., Ferenczi, M.A., Raposo, G., Seabra, M.C., 2007. Rab27b regulates mast cell granule dynamics and secretion. Traffic. 8, 883-892.

Moon, S.H., Cha, R., Lee, G.L., Lim, J.K., Soh, K.S., 2013. Primo vascular system in the subarachnoid space of a mouse brain. Evid Based Complement Alternat Med. 7 pages Article AD 280418.

Moon, SH., Cha, R., Lee, M., Kim, S., Soh, K.S., 2012. Primo vascular system in the subarachnoid space of the spinal cord of a pig. J Acupunct Meridian Stud. 5, 226-233.

Ogay, V., Baik, K.Y., Lee, B.C., Soh, K.S., 2006. Characterization of DNA-containing granules flowing through the meridian-like system on the internal organs of rabbits. Acupunct Electrother Res. 31, 13-31.

Ogay, V., Bae, K.H., Kim, K.W., Soh, K.S., 2009a. Comparison of the characteristic features of Bonghan ducts, blood and lymphatic capillaries. J Acupunct Meridian Stud. 2, 107-117.

Ogay, V., Min, F., Kim, K., Kim, J., Bae, K.H., Han, S.C., Soh, K.S., 2009b. Observation of coiled blood plexus in rat skin with diffusive light illumination. J Acupunct Meridian Stud. 2, 56-65.

Okuthe, G.E., 2013. DNA and RNA pattern of staining during oogenesis in zebrafish (Danio rerio): a confocal microscopy study. Acta Histochem. 115, 178-184.

Orphanidou-Vlachou, E., Tziakouri-Shiakalli, C., Georgiades, C.S., 2014. Extramedullary hemopoiesis. Semin Ultrasound CT MR. 35, 255-262.

Park, S.Y., Jung, S.J., Bae, K.H., Soh, K.S., 2015. Protocol for Detecting the Primo Vascular System in the Lymph Ducts of Mice. J Acupunct Meridian Stud. 8, 321-328.

Potter, M.D., Shinpock, S.G., Popp, R.A., Godfrey, V., Carpenter, D.A., Bernstein, A., Johnson, D.K., Rinchik, E.M., 1997. Mutations in the murine fitness 1 gene result in defective hematopoiesis. Blood. 90, 1850-1857.

Rai, R., Chandra, V., Kwon, B.S., 2015. A Hyaluronic Acid-Rich Node and Duct System in Which Pluripotent Adult Stem Cells Circulate. Stem Cells Dev. 24, 2243-2258.

Ross, M.H., Pawlina, W., 2005. Histology: A text and atlas. Lippincott Williams & Wilkins, 5th editoin.

Shin, H.S., Johng, H.M., Lee, B.C., Cho, S.I., Baik, K.Y., Yoo, J.S., Soh, K.S., 2005. Feulgen reaction study of novel threadlike structures (Bonghan ducts) on the surfaces of mammalian organs. Anat Rec B New Anat. 284, 35-40.

Simionescu, M., Simionescu, N., 1977. Organization of cell junctions in the peritoneal mesothelium. J Cell Biol. 98-110.

Soh, K.S., 2009. Bonghan circulatory system as an extension of acupuncture meridians. J Acupunct Meridian Stud. 2, 93-106.

Spencer, N.J., Hennig, G.W., Dickson, E., Smith, T.K., 2005. Synchronization of enteric neuronal firing during the murine colonic MMC. J Physiol. 564, 829-847.

Stefanov, M., Kim, J., 2012. Primo vascular system as a new morphofunctional integrated system. 5, 193-200.

Stefanov, M., Potroz, M., Kim, J., Lim, J., Cha, R., Nam, M.H., 2013. The primo vascular system as a new anatomical system. J Acupunct Meridian Stud. 6, 331-338.

Sung, B., Kim, M.S., Lee, B.C., Yoo, J.S., Lee, S.H., Kim, Y.J., Kim, K.W., Soh, K.S., 2008. Measurement of flow speed in the channels of novel threadlike structures on the surfaces of mammalian organs. 95, 117-124.

Tian, Y.Y., Jing, X.H., Guo, S.G., Jia, S.Y., Zhang, Y.Q., Zhou, W.T., Huang, T., Zhang, W.B., 2013. Study on the Formation of Novel Threadlike Structure through Intravenous Injection of Heparin in Rats and Refined Observation in Minipigs. Evid Based Complement Alternat Med. 6 pages Article ID 731518.

Walter, J., Klein, C., Wehrend, A., 2011. Comparison of eosin-thiazin and Papanicolaou-Shorr staining for endometrial cytologies of broodmares. Tierarztl Prax Ausg G Grosstiere Nutztiere. 39, 358-362.

Wang, G.J., Ayati, M.H., Zhang, W.B., 2010. Meridian studies in China: a systematic review. J Acupunct Meridian Stud. 3, 1-9.

Wang, X., Shi, H., Cui, J., Bai, W., He, W., Shang, H., Su, Y., Xin, J., Jing, X., Zhu, B., 2013. Preliminary Research of Relationship between Acute Peritonitis and Celiac Primo Vessels. Evid Based Complement Alternat Med. 8 pages Article ID 569161.

Yin, C.S., Jeong, H.S., Park, H.J., Baik, Y., Yoon, M.H., Choi, C.B., Koh, H.G., 2008. A proposed transpositional acupoint system in a mouse and rat model. Res Vet Sci. 84, 159-165.

Yoo, J.S., Ayati, M.H., Kim, H.B., Zhang, W.B., Soh, K.S., 2010. Characterization of the primo-vascular system in the abdominal cavity of lung cancer mouse model and its differences from the lymphatic system. PLoS One. 5, e9940.

Yoo, J.S., Kim, H.B., Ogay, V., Lee, B.C., Ahn, S., Soh, K.S., 2009. Bonghan ducts as possible pathways for cancer metastasis. J Acupunct Meridian Stud. 2, 118-123.

Yoo, J.S., Kim, H.B., Won, N., Bang, J., Kim, S., Ahn, S., Lee, B.C., Soh, K.S., 2011. Evidence for an additional metastatic route: in vivo imaging of cancer cells in the primo-vascular system around tumors and organs. Mol Imaging Biol. 13, 471-480.

Yoo, J.S., Kim, M.S., Ogay, V., Soh, K.S., 2008. In vivo visualization of Bonghan ducts inside blood vessels of mice by using an Alcian blue staining method. Indian J Exp Biol. 46, 336-339.

Young, B., Heath, J.W., 2002. Functional histology. Third edition. Churchill livingstone.

Yung, S., Chan, T.M., 2012. Pathophysiological changes to the peritoneal membrane during PD-related peritonitis: the role of mesothelial cells. Mediators Inflamm. 21 pages Article ID 484167.

Zhang, D., Ding, G., Shen, X., Yao, W., Zhang, Z., Zhang, Y., Lin, J., Gu, Q., 2008. Role of mast cells in acupuncture effect: a pilot study. Explore (NY). 4, 170-177.

Zhang, K., Li, Y.F., Patel, K.P., 2001. Blunted nitric oxide-mediated inhibition of renal nerve discharge within PVN of rats with heart failure. Am J Physiol Heart Circ Physiol. 281, H995-1004.

ABSTRACT IN KOREAN

국문초록

최근 발견된 조직인 프리모 순환계통의 형태학적 특성

임채정

서울대학교 대학원

수의학과 수의생명과학 전공

(수의약리학)

(지도교수: 류판동)

프리모순환계는 1960년대 김봉한 박사에 의해서 경락경혈의 해부학적 구조물로 보고 된 새로운 관 형태의 조직이다. 그러나, 이후 타 연구자에 의하여 관련 후속연구가 이루어지지 않았다. 2000년대 초, 소광섭 교수와 동료들에 의해서 여러 동물 종의 조직상에서 재발견되었다. 그러나, 프리모 조직의 세부적인 형태 및 기능, 그리고 경락경혈과의 연관성은 아직 잘 밝혀져 있지 않다. 본 연구에서는 Hemacolor

염료를 프리모 조직 연구에 새롭게 적용하여 장기표면 프리모 조직의 형태학적 특성과 기능을 조사하고자 하였다. 또한, 이 Hemacolor 염료를 통하여 경락경혈과 위치적으로 관련이 있을 것으로 여겨지는 피하 프리모 조직, 즉 피하에도 프리모 조직이 존재하는 지를 확인하고자 하였다.

본 연구의 주요 결과들은 다음과 같다. (1) 소체와 관 구조물로 구성된 장기표면 프리모 조직은 내부에 소관 (20–50 μm)과 고유한 세포조성 (90.3%의 백혈구, 5.9%의 적혈구, 3.8%의 비만세포)을 가진다. (2) 심부전 랫드의 장기표면 프리모 조직에서, 조직의 면적 (2.1배), 발견빈도 (2.2배), 그리고, 미성숙 적혈구의 비율 (2.1배)이 증가했으며, 이것은 프리모 조직 내에서 적혈구생성이 발생했음을 의미한다. (3) Hemacolor 염색을 통하여 새로이 복부 피하층에 존재하는 프리모 조직을 확인했으며, 이는 기존의 프리모 조직과 형태, 구조 및 세포측면에서 유사함을 나타내었다. (4) 피하 및 장기표면 프리모 조직의 세포외 기질부분은 나노 크기의 입자들로 덮여있는 광범위하게 펼쳐진 섬유구조 및 마이크로 크기의 입자들로 구성되며, 이러한 특징들은 기존의 림프관과는 차이가 있었다.

종합적으로, 이 연구결과들을 통하여 Hemacolor 염료가 프리모 조직 연구에 유용하고, 피하에도 프리모 조직이 있으며 기존의 프리모 조직의 특성을 가진다는 것을 확인하였다. 또한, 피하 및 장기표면 프리모 조직의 초 미세구조는 서로 유사하고 림프관과는 차이가 있으며, 장기표면 프리모 조직의 조혈기관으로서의 가능성 등을 최초로 밝혀 내었다. 본 연구에서 확립된 Hemacolor 염색법과 프리모 조직의 형태 및 기능적인 측면에 대한 연구결과는 향후 프리모 조직 연구에 대한 기반을 제공하고, 체내에서 프리모 조직의 생리학적인 역할을 이해하는데 도움을 줄 것이다.

주요어: Hemacolor 염색, 피하층, 비만세포, 적혈구, 세포외 기질, 심부전, 조혈작용

학번: 2010-21651